EFFECTS OF KEY PARAMETERS ON THE PERFORMANCE OF CONCRETE MASONRY SHEAR WALLS UNDER IN-PLANE LOADING

By

JACOB DEAN SHERMAN

A thesis submitted in partial fulfillment of
the requirements for the degree of

MASTER OF SCIENCE IN CIVIL ENGINEERING

WASHINGTON STATE UNIVERSITY
Department of Civil and Environmental Engineering

December 2011

To the Faculty of Washington State University:

The members of the Committee appointed to examine the thesis of JACOB DEAN SHERMAN find it satisfactory and recommend that it be accepted.

David I. McLean, Ph. D., Chair

James D. Dolan, Ph. D.

William F. Cofer, Ph. D.

ACKNOWLEDGMENTS

I would like to acknowledge the financial support provided by the National Institute of Standards and Technology (NIST). I would also like to acknowledge The Masonry Society for the Clayford T. Grimm Scholarship and The Eastern Washington Masonry Promotion Group for the Fraser Graduate Fellowship, and Mutual Materials and Central Pre-Mix for the donated materials.

I would like to thank Dr. David McLean for serving as my committee chair and for giving me the opportunity to work on this project. His patience, encouragement, guidance, and support are greatly appreciated for the entirety of my master's program at Washington State University. My gratitude is also extended to Dr. Dan Dolan and Dr. Bill Cofer for serving as committee members and offering me invaluable knowledge that I will use in my future career. The assistance and guidance from the other groups involved with the project, specifically Dr. Benson Shing, Dr. Richard Klingner, and Farhad Ahmadi, is appreciated. A special thanks to my colleagues, Will Cyrier and Christina Kapoi, for the countless hours they spent helping me construct and test my walls.

I would also like to thank the staff of the Composite Materials and Engineering Center, especially Bob Duncan and Scott Lewis, for their patience, assistance, time, and an unforgettable experience. I greatly appreciate all of the people who helped me construct and test my walls: Kyle Spangenberg, Alex Kirk, Kyle Barker, Louis de Fontenay, and Drew Mills. I would also like to thank Vicki Ruddick, Cyndi Whitmore, Lola Gillespie, and Glenda Rogers in the Department of Civil and Environmental Engineering for all their help. Thanks to Dr. David Pollock for assisting me in the design of various steel components used in my research.

Finally I would like to acknowledge all of my family and friends who encouraged and prayed for me during my time here at WSU. Your love and support are appreciated more than words could express. To the love of my life, Alicia, thank you for your respect, support, encouragement, patience, love, time, and all that you've made me to be. I couldn't have made it through this without you. Lastly, I would like to thank my Lord and Savior, for the provisions, blessings, and unconditional love that have shaped me to be the man that I am; my life would be empty without you.

EFFECTS OF KEY PARAMETERS ON THE PERFORMANCE OF CONCRETE MASONRY SHEAR WALLS UNDER IN-PLANE LOADING

Abstract

By Jacob Dean Sherman, M.S.
Washington State University
December 2011

Chair: David I. McLean

The primary objective of this research is to evaluate the effects that key design and wall parameters have on the performance of concrete masonry shear walls under in-plane loading. The parameters evaluated include aspect ratio, axial compressive stress, and amount of reinforcement. A secondary objective is to evaluate the effects that splicing of the vertical reinforcement has on wall performance.

Eight, fully grouted, reinforced concrete masonry shear walls were designed in accordance with the 2008 MSJC *Building Code Requirements for Masonry Structures*. The walls were tested as cantilever specimens and subjected to cyclic, in-plane lateral loads under varying levels of axial load. Wall aspect ratios of 0.78, 1.0, and 2.0 were evaluated along with varying axial compressive stress ratios of 0.0, 0.0625, and 0.125 of the masonry compressive strength. Two pairs of walls evaluated the effects of lap splices in the vertical reinforcement with varying vertical reinforcement ratios.

The performance of the walls was established from the test results considering predicted load capacities, wall drift, displacement ductility, plastic hinging, and energy dissipation. Increasing wall aspect ratios cause an increase in yield displacements but reduce the sliding deformations and displacement ductilities. Sliding and shear deformations are larger with lower

axial compressive loads. The extent of plastic hinging is reduced by larger axial loads and by larger vertical reinforcement ratios. Larger reinforcement ratios also cause reductions in displacement ductility and an increase in the contributions from sliding and shear deformations. Drift levels at actual wall failure were significantly higher than those associated with the code-specified failure point. This indicates that larger drift capacities can be achieved at actual wall failure than is implied by the MSJC Code. Lap splices in the vertical reinforcement cause a reduction in wall performance. Further evaluations should be conducted on the effects of lap splices considering additional design and wall parameters beyond those considered in this study.

TABLE OF CONTENTS

LIST OF TABLES

LIST OF FIGURES

CHAPTER 1

INTRODUCTION

1.1 Background

Masonry construction is commonly used for low-rise structures because it offers durability and fast construction at a relatively low cost. As recently as a century ago, masonry structures were unreinforced and did not account for seismic forces. Seismic design for lateral loads was slowly introduced into masonry structures when engineers observed that buildings designed for wind forces performed better during significant earthquakes (Priestley et al., 2007).

Shear walls are the main component in masonry structures that resist lateral and axial loads. Lateral loads from earthquakes are transferred into horizontal diaphragms comprised of the floor and roof systems and then into shear walls by adequate connections to the diaphragms. Axial loads from floor or roof loads are also transferred through the shear walls and into the foundation.

The manner in which a shear wall fails is an important characteristic of wall behavior. One such failure mechanism is a shear failure that generally produces a brittle response, or the inability for the wall to deform inelastically, causing rapid strength degradation of the structure. Another failure mechanism is a flexure failure that generally produces a ductile response, or the ability for the wall to deform inelastically without fracture. The level of ductility is dependent on axial compressive load, vertical and horizontal reinforcement ratios, and the wall geometry. However, masonry shear walls are currently designed based largely on the assumption that the elastic behavior of a shear wall accounts for the inelastic behavior as well; this is an unrealistic representation of a structure's behavior (Priestley, 1993).

Masonry shear walls have traditionally been designed based primarily on force levels for convenience and because this is how other actions (e.g., dead and live loads) are designed. Over the last 20 years, a new approach has been introduced that is based on providing a desired performance, typically displacement capacity, in a structure. This new approach, *performance-based design*, was developed due to numerous shortcomings of the current *force-based design*. One such shortcoming involves the required iterations for an adequate design—specifically those associated with correct representation of member stiffness. The member stiffness must be initially estimated in design to determine the period and force distribution within the system. Once the design is complete, the stiffness must be checked with the initial estimate and the member possibly redesigned if the stiffness values do not coincide. Another inadequacy of initial stiffness estimation is that all structural elements are assumed to yield simultaneously (Priestley et al., 2007); this is not a realistic seismic response of a structure.

The use of a performance-based design has gained favor due to the realization that displacement capacity is often a more important parameter than force capacity. This design process has not only been introduced to overcome the shortcomings of force-based design but also to produce more economical designs. Current design standards for masonry shear walls are given in the Masonry Standards Joint Committee (MSJC) *Building Code Requirements and Specifications for Masonry Structures* (MSJC, 2008). The MSJC Code requirements incorporate minimum levels of assumed ductility for varying shear wall types. The code requirements do not account for the displacement capacity of the structure, only the specified wall types (ordinary, intermediate, or special). Current codes assume that special shear walls will be flexure-dominated and ductile. This may not be possible for certain wall configurations.

Performance-based design provides predictable and consistent seismic performance of masonry shear walls based on design and wall parameters as well as a more realistic representation of the behavior of shear walls under seismic loads. The intent of this research is to evaluate the performance of walls designed in accordance with the current code provisions to support the implementation of performance-based design for masonry structures.

1.2 Scope and Objectives

This research was conducted in collaboration with researchers from the University of California at San Diego and the University of Texas at Austin and was funded by the National Institute of Standards and Technology (NIST). The objective of the broader project is to quantify the seismic performance of reinforced masonry shear-wall structures for use in developing improved design procedures. The research presented in this thesis will increase the current database for reinforced masonry shear walls to better understand their seismic performance.

The primary objective of this research is to evaluate the effect that key design and wall parameters have on the performance of concrete masonry shear walls designed in accordance with the current MSJC Code. Eight concrete masonry shear walls with varying parameters including aspect ratio, axial compressive stress, and amounts of reinforcement were subjected to cyclic, in-plane loads. A secondary objective of this research is to evaluate the effects that lap splices of vertical reinforcement located in the plastic hinge zone have on wall performance. Performance measures considered in this study include strength, drift, ductility, curvature, plastic hinging, and energy dissipation.

CHAPTER 2

LITERATURE REVIEW

2.1 Introduction

Recent research efforts have been directed at obtaining an improved understanding of the response of masonry structures under seismic loading for the purpose of developing performance-based design procedures. Numerous experimental and theoretical studies have been conducted to characterize the performance of masonry shear walls. This chapter provides a review of the various failure modes of masonry shear walls as well as previous experimental studies investigating their performance under in-plane loads. A review of the seismic design provisions of the 2008 MSJC *Building Code Requirements for Masonry Structures* (MSJC, 2008) is also provided.

2.2 Masonry Shear Wall Failure Modes

Numerous experimental and theoretical studies have been conducted to evaluate the performance of masonry shear walls in high seismic events. The seismic performance of masonry shear walls can be deduced by applying static, non-linear lateral loads through use of a hydraulic jack with predetermined displacements. Loads such as out-of-plane lateral and axial loads should also be considered for a realistic representation. Axial loads, along with wall aspect ratios and the percentage of reinforcement, influence the behavior of masonry shear walls.

The manner in which a shear wall fails is an important characteristic of wall behavior. Four commonly recognized failure modes of masonry shear walls include shear, flexure, rocking, and sliding (Paulay & Priestley, 1992), shown in Figure 2.1. However, if a shear wall has sufficient anchorage into the foundation, then shear and flexural failures will become dominant. Flexure failures generally produce a ductile response, or the ability for the wall to deform

inelastically without fracture. Shear failures generally produce a brittle response, or the inability for the wall to deform inelastically, causing rapid strength degradation of the structure. As a result, it is more desirable to have masonry shear walls fail in flexure.

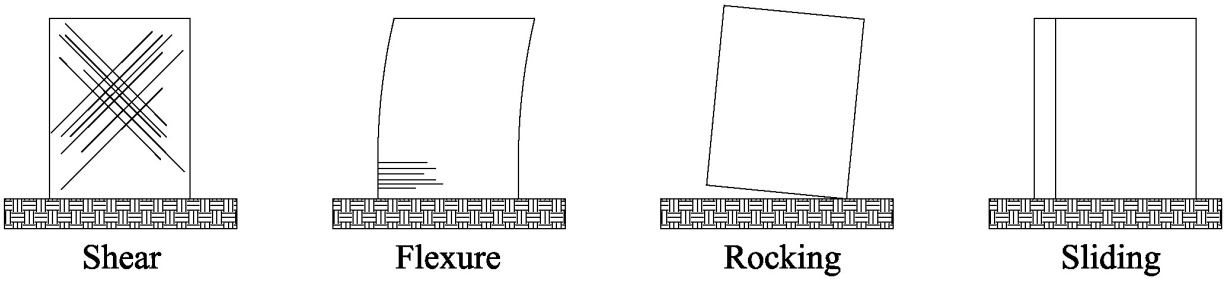

Figure 2.1 Shear Wall Failure Mechanisms (adapted from Eikanas, 2003)

Although flexural failure is the more preferred mechanism, shear failure may be difficult to avoid, especially for squat shear walls. Squat walls are structural walls that have a height-to-length (aspect) ratio less than 2.0 (Paulay & Priestley, 1992). These particular types of shear walls are most common in low-rise masonry construction, but they can also be found in some high-rise structures. Shear failures, which are characterized by diagonal tension cracking (idealized at a 45° angle), cause a brittle failure and a rapid decrease in strength (Shing et al., 1990; Shing et al., 1990). Shear failures may also occur in walls with significant amounts of vertical (flexural) reinforcement.

Ductile walls, typically associated with a flexure failure, can withstand larger displacements without significant loss in strength. Ductile flexural failure is characterized by the tensile yielding of flexural reinforcement, plastic hinge formation, and compression crushing at critical sections (Paulay & Priestley, 1992; Shing et al., 1990). Compression crushing at the extreme edges of the walls, commonly referred to as toe crushing, may not be detected until well beyond the code-specified masonry crushing strain of 0.0025 (Eikanas, 2003). Plastic hinges are typically formed at the base of the shear walls and are characterized by the plastic yielding of

flexural reinforcement. The plastic hinge length (l_p) may be related to the ductility (μ) of the structure by the following equation given by Paulay and Priestley (1992):

$$\mu_{\Delta} = 1 + 3(\mu_{\phi} - 1)\left(\frac{l_p}{l}\right)\left(1 - 0.5\frac{l_p}{l}\right) \qquad \text{(Eqn. 2.1)}$$

In Equation 2.1, μ_{Δ} is the displacement ductility, μ_{φ} is the curvature ductility, and l is the height of the wall. The displacement ductility (μ_{Δ}), is defined as the ratio of the ultimate displacement (Δ_u) to the yield displacement associated with yielding of the outermost flexural bar (Δ_y) and is the most frequently used representation of a structure's ductility capacity. However, there is currently no consensus on the definition of the yield and ultimate displacements (Priestley et al., 2007; Shedid et al., 2010). Priestley (1986) concluded in his studies that the displacement ductility of a shear wall is dependent upon the axial load ratio [$P/(f'_m A_g)$], the reinforcement ratio (ρ), and the compressive strength of the masonry (f'_m).

2.3 MSJC Code Provisions (2008)

The Masonry Standards Joint Committee (MSJC) *Building Code Requirements and Specifications for Masonry Structures* (MSJC, 2008) provides seismic provisions for concrete masonry shear walls. Section 1.17.3.2 requires that a seismic force-resisting system be specified for every structure. Twelve types of masonry shear walls, each with a different capacity for inelastic response and energy dissipation, are defined in the MSJC Code. Each shear wall type is distinguished by their response modification factor (R), the Seismic Design Category (SDC) they are permitted in, requirements for the reinforcement size and spacing, and requirements for the masonry materials. This section presents a summary of the relevant seismic design provisions of the MSJC Code, including prescriptive minimum requirements for the reinforcement, shear capacity, and maximum permitted reinforcement. Two design methodologies for masonry shear

walls, strength design and allowable stress design, are compared in this section. The allowable stress design of reinforced masonry shear walls is given in Section 2.3 of the MSJC Code, and the strength design of reinforced masonry shear walls is given in Section 3.3.

One provision required by the MSJC Code is the minimum reinforcement requirement of Section 1.17.3.2 to ensure a minimum level of assumed inelastic ductility. Table 2.1 lists the minimum reinforcement requirements for ordinary, intermediate, and special reinforced masonry shear walls. Ordinary reinforced walls, which would be expected to withstand somewhat larger deformations than unreinforced walls, are used in low to moderate seismic areas (Seismic Design Categories A, B, and C). Intermediate reinforced shear walls are similar to ordinary walls except that they have a higher response modification factor and additional requirements. Special reinforced walls, which would be expected to perform the best in all SDC categories, consist of additional requirements beyond those for ordinary and intermediate walls.

Table 2.1 2008 MSJC Prescriptive Reinforcement Requirements

Wall Type	Prescriptive Reinforcement Requirements			
	Vertical		Horizontal	
	Minimum Area	Maximum Spacing	Minimum Area	Maximum Spacing
Ordinary	0.2 in^2	120 in.	0.2 in^2	120 in.
Intermediate	0.2 in^2	48 in.	0.2 in^2	120 in.
Special	1/3 of required shear reinforcement	Smallest of: (1/3)L, (1/3)H, or 48 in.	0.2 in^2	Smallest of: (1/3)L, (1/3)H, or 48 in.

L: Wall Length; H: Wall Height

To improve the ductility of a special reinforced wall, the MSJC Code specifies additional reinforcement requirements that provide a minimum level of in-plane shear and are given in Sections 1.17.3.2.6(a) through 1.17.3.2.6(e). The individual reinforcement ratios (ρ) in the vertical and horizontal direction cannot be less than 0.0007 multiplied by the gross cross-

sectional area of the wall. The sum of both the horizontal and vertical reinforcement ratios must also be greater than 0.002 multiplied by the gross cross-sectional area of the wall. The minimum reinforcement provisions apply for both strength design and allowable stress design methods.

Current code provisions require a shear design capacity check for special reinforced masonry shear walls in accordance with Section 1.17.3.2.6.1 of the MSJC Code. These provisions increase the ductility of a wall by reducing the likelihood of shear failures preceding inelastic flexural behavior. For special walls being designed with strength design, the design shear strength shall exceed the shear corresponding to the development of 1.25 times the nominal flexural strength. However, the nominal shear strength need not exceed 2.5 times the required shear strength to carry the applicable loads. For strength design, the shear capacity check is given in Section 3.3 of the code. In allowable stress design, the shear stress caused by in-plane seismic loads on shear walls shall be multiplied by a factor of 1.5; this requirement is given in Section 2.2 of the MSJC Code.

The flexural reinforcement of masonry shear walls is limited by a maximum permitted area in Sections 2.3.3.4 and 3.3.3.5 of the 2008 MSJC Code. These provisions are used to keep the compressive zone from crushing before yielding of the flexural reinforcement. The maximum reinforcement ratio for allowable stress design is:

$$\rho_{\max} = \frac{nf'_m}{2f_y\left(n + \frac{f_y}{f'_m}\right)} \qquad \text{(Eqn. 2.2)}$$

For strength design, the maximum reinforcement ratio is:

$$\rho_{\max} = \frac{0.64 f_m^{'}\left(\dfrac{\varepsilon_{mu}}{\varepsilon_{mu} + \alpha\varepsilon_y}\right) - \sigma}{f_y\left(\dfrac{\alpha\varepsilon_y - \varepsilon_{mu}}{\varepsilon_{mu} + \alpha\varepsilon_y}\right)} \qquad \text{(Eqn. 2.2)}$$

where n is the ratio of the modulus of elasticity of steel over masonry, f'_m is the compressive strength of masonry, f_y is the yield strength of the reinforcement, ε_{mu} is the maximum compressive strain of masonry (0.0025 for concrete masonry), ε_y is the yield strain of steel, and α is a tension strain factor. The tension strain factor varies with each wall type: intermediate walls are assigned a strain factor of 3, and special walls are assigned a strain factor of 4. The maximum reinforcement in a wall is limited by the tensile strain, which is equal to the factor times the yield strain ($\alpha\varepsilon_y$) that develops in the extreme flexural reinforcement located at the wall edge.

This study also investigated the effects of lap splices, which are used to facilitate the construction process, in masonry shear walls. The required development length is identical for allowable stress design and strength design. From Section 2.1.9.3 and 3.3.3.3 of the 2008 MSJC Code, the development length is:

$$l_d = \frac{0.13 d_b^2 f_y \gamma}{K\sqrt{f_m^{'}}} \qquad \text{(Eqn. 2.3)}$$

where d_b is the diameter of the flexural reinforcement; γ is 1.0 for No. 3 to No. 5 bars, 1.3 for No. 6 to No. 7 bars, and 1.3 for No. 8 to No. 11 bars; and K is the smallest of the minimum masonry clear cover, the clear spacing between adjacent splices, or $5d_b$. The MSJC Code also specifies a minimum splice length of 12 in.

2.4 Cyclic In-Plane Masonry Shear Walls

Numerous previous studies have been conducted on the performance of masonry shear walls under in-plane lateral loads. This section includes a summary of several experimental studies that have contributed to the development of performance-based design criteria for masonry walls.

2.4.1 Priestley

Priestley (1986) analyzed two previous experimental studies on concrete masonry shear walls that were subjected to cyclic, in-plane loading. Priestley identified shortcomings of current design procedures and suggested improvements. Current design methods are based on the elastic behavior of masonry structures and are intended to account for inelastic behavior. Priestley concluded that this is invalid and that masonry design should be based on the ultimate strength of the structure. A more realistic assumption would be to design for the ultimate capacity so that the structure can sustain the required ductility without rapid loss in strength.

Priestley first examined a previous experimental study that focused on masonry shear walls with low aspect ratios, which are expected to fail in shear rather than flexure. The study included six heavily reinforced shear walls with an aspect ratio of 0.75. These walls were subjected to a gradual increase in the displacement level. There was a noticeable amount of sliding along the top of the foundation beam near the end of the cycles, which caused significant loss in load and stiffness. However, the ultimate strength was obtained again upon increasing the displacement. Priestley concluded that although flexural failure modes could be achieved, the base slip limited the energy absorption within the structure.

The second experimental study summarized by Priestley was of two 6-m (approximately 3 stories) tall slender walls that were constructed with 140-mm wide fully grouted concrete

masonry blocks (Figure 2.2). One of the walls (Wall 1) was unconfined while the other wall (Wall 2) had confining plates that were placed in the bottom seven-mortar courses. The confining plates, which were 600 mm long and 3 mm thick steel plates, were used to inhibit vertical splitting in the extreme ends of the walls and to increase ductility capacity. A hydraulic jack, located at the tops of the walls, applied a cyclic, in-plane load until failure. This test investigated the effects of high aspect ratios (slender) on the ductility of structural walls. The test also examined the influence of axial load levels on seismic response and lateral buckling in the plastic hinge zones.

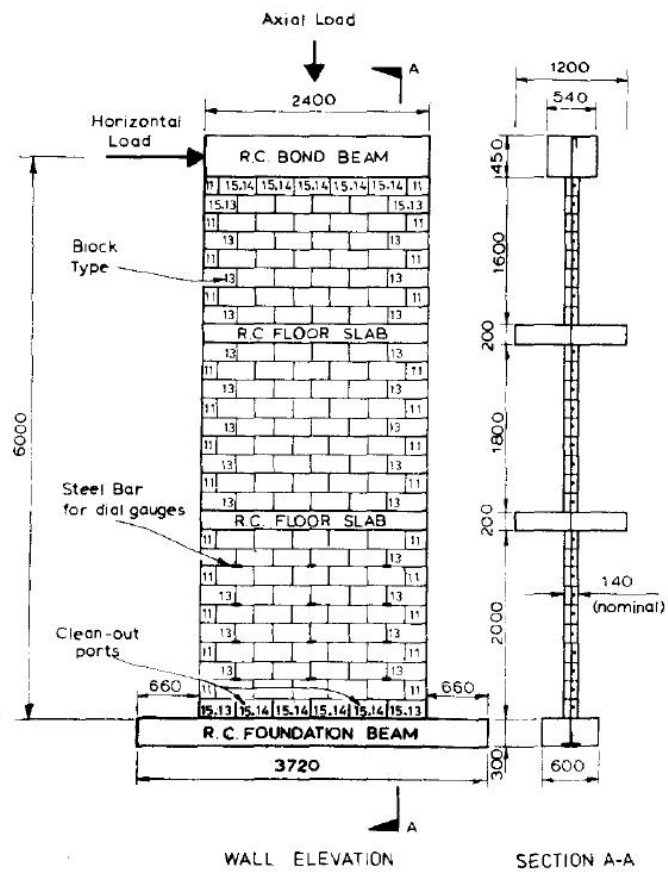

Figure 2.2 Priestley – Test Specimen

Wall 2 performed significantly better than Wall 1 in regard to seismic performance. The test for Wall 1 was abandoned after significant physical damage occurred when increasing the

displacement to a displacement ductility factor of 3.91. Wall 2 exceeded the theoretical ultimate strength for each peak displacement. At high ductilities, poor bond conditions were evident at the lap splices, which were located in the plastic hinge zones. Therefore, Priestley recommended avoiding lapping flexural reinforcement in plastic hinge zones. There was no observed lateral buckling in the plastic hinges at high values of ductility. Lastly, the study confirmed one of Priestley's hypotheses that ductility reduces with increasing aspect ratios.

2.4.2 Shing et al.

Shing et al. (1990) tested 22 masonry shear walls to enhance the knowledge of the strength and ductility of reinforced masonry shear walls. The walls were constructed from either 6x8x16 in. hollow concrete blocks or 6x4x16 in. hollow clay brick and were 72 in. high and 72 in. long. The specimens were fully grouted with distributed vertical and horizontal reinforcement. Each wall was subjected to cyclic, in-plane loading with a gradual increase of displacement. The test setup is given in Figure 2.3. All failure mechanisms were dominated by either flexural or shear.

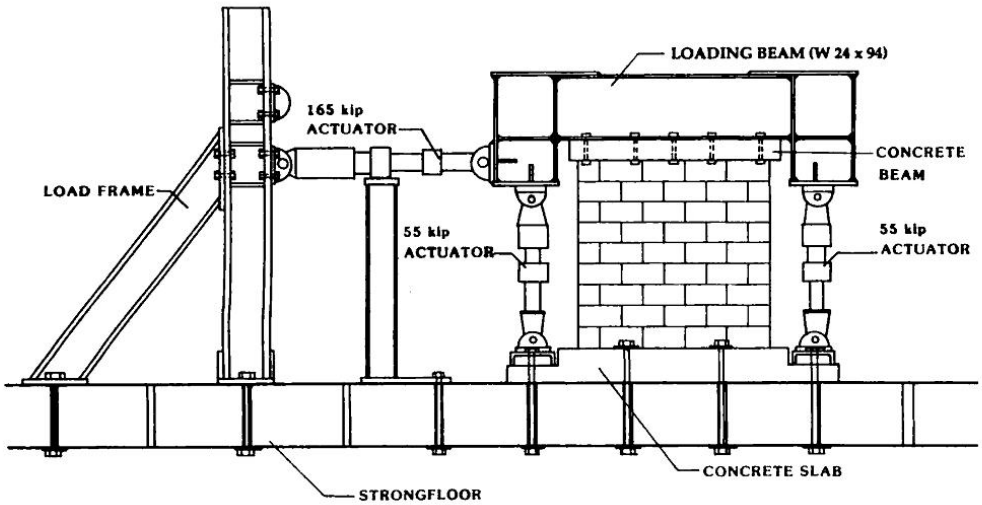

Figure 2.3 Shing et al. – Test Setup

The flexural strengths of the walls were evaluated by two different methods. The first method is based on the computer program UNCOLA, which is a fiber model that splits the cross-sectional area of the specimen into a number of longitudinal elements. The UNCOLA analysis was comparable to the actual test data because it used similar cyclic loads. However, the authors observed a 20% overestimate of the moment capacity at a zero axial load. The second method was a simple formula based on the rectangular stress-block assumption and the perfectly elasto-plastic behavior of flexural steel. This method showed an underestimation of the moment capacity at all axial load levels. Therefore, the authors concluded that the second method (simple flexure theory) accurately evaluated the flexural strength and ductility of a squat reinforced masonry wall.

The flexural responses of the specimens were summarized in terms of their flexural deformation and ductility. The two methods produced similar yield and ultimate displacements to that of the actual data. The ultimate curvature (i.e., bending), displacement, and ductility for each specimen decreased as the axial load increased. Although previous studies have shown a rapid decrease in ductility with an increase in flexural steel, this study showed that ductility was not dependent to the amount of flexural reinforcement. Low ductility is a characterization of a shear-dominated wall, but can be avoided with additional horizontal reinforcement.

The shear strength and shear deformation of all the specimens were compared in this study. There was an increase in the shear strength due to an increase in the amount of flexural reinforcement and axial load. The shear deformation (i.e., shear stiffness) was increased by a reduction in the crack openings, which was influenced by an increase in the horizontal and vertical steel and/or the axial load. The residual strengths of the masonry walls were not reliable once diagonal cracking began.

2.4.3 Eikanas

Eikanas (2003) examined the effects of varying wall aspect ratios and the amount of flexural reinforcement on concrete masonry shear walls. Eikanas also compared his observations to the assumed reinforcement limits of the 2000 International Building Code (IBC). Seven fully-grouted cantilever concrete masonry shear walls were tested in this study. Each wall was subjected to cyclic, in-plane lateral loads and three constant axial loads of 27 psi at the top. The wall aspect ratios varied from 0.72, 0.93, 1.5, and 2.1. The flexural reinforcement consisted of No. 5 bars spaced every 8 or 16 in., and the shear reinforcement consisted of No. 4 bars spaced every 16 in. Four of the tested walls contained flexural reinforcement ratios that were equivalent to the maximum reinforcement ratio (ρ_{max} = 0.0026) of the IBC. The other three walls contained flexural reinforcement ratios that were approximately twice the IBC maximum.

Eikanas evaluated the performance of the walls based on testing observations, load-displacement measurements, drift ratios, ultimate displacement ductility, and curvature measurements. The testing observations gave a brief summary of how the walls performed under the loading, including a visualization of any significant cracking, toe crushing, or unexpected response modes. Using a data analysis system, the load-displacement measurements were recorded and plotted into a hysteresis curve. This study used a load-displacement hysteresis to compare with the IBC provisions and to determine the rate of degradation following toe crushing. Figure 2.4 represents the hysteresis curve for one of the walls tested by Eikanas. A load-displacement hysteresis shows the various limit states of the masonry shear walls and can be seen in the upper right key in the figure below. The drift values were calculated by the ratio of the in-plane lateral displacement to the overall wall height. The displacement ductility of each specimen was the ratio of the ultimate displacement, found at the 20% load degradation limit

state, to the yield displacement. The wall curvatures were measured by string potentiometers placed at five different locations along the wall height.

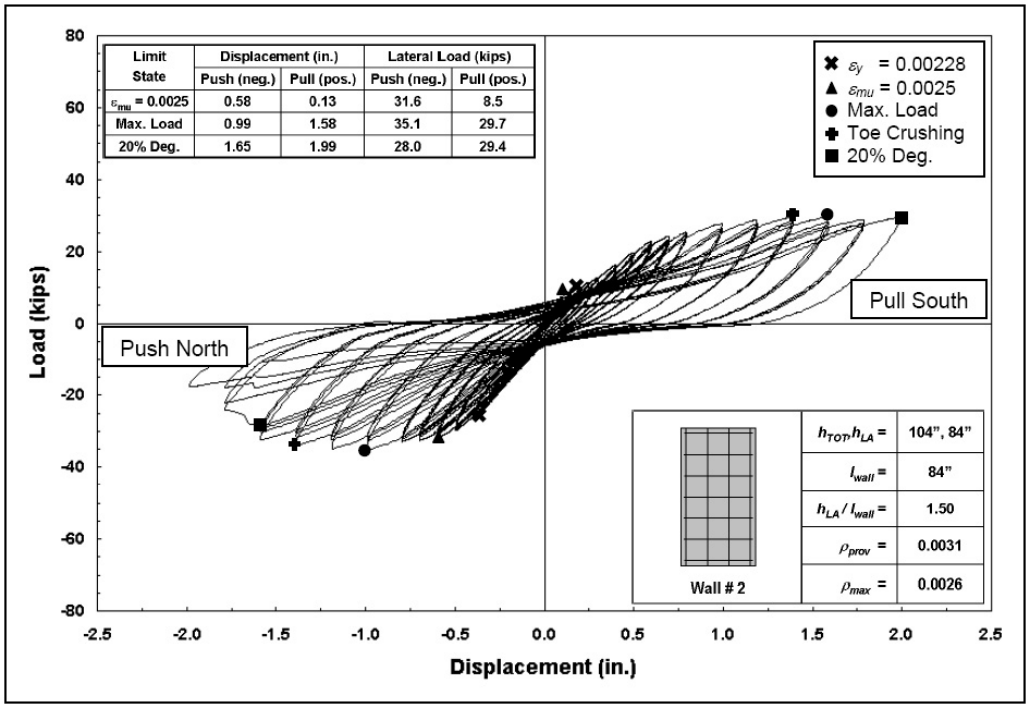

Figure 2.4 Eikanas – Load-Displacement Hysteresis Curves

Eikanas evaluated the effects of wall aspect ratio and flexural reinforcement ratio and checked the validity of the IBC provisions. One of the walls exhibited sliding deformation, which was reduced in the other walls with an increase in flexural reinforcement. Sliding in a squat wall, which the MSJC Code (2008) does not account for in flexural design, results in underestimation of total drift capacity. Eikanas observed that with decreasing aspect ratios, shear deformation increased and flexural deformations decreased. The 2000 IBC does not account for the effects of wall aspect ratios. At the critical masonry strain of 0.0025, drift capacity increased along with flexural reinforcement. The drift capacity decreased at the maximum load and 20% load degradation. However, all walls were able to obtain drift values higher than the allowable drift of 1.0% provided by the IBC. Eikanas concluded that the IBC provisions appeared overly

restrictive in their assumption that squat shear walls will behave primarily in flexural deformation.

2.4.4 Voon and Ingham

To examine the in-plane shear strength of masonry shear walls, Voon and Ingham (2006) tested ten single-story concrete masonry wall panels that were constructed in accordance with New Zealand techniques. The study examined the effect of the following variables: axial load levels, amount and distribution of shear reinforcement, grouting type, and aspect ratios. All except two walls had nominal dimensions of 1800 mm (72 in.) high by 1800 mm (72 in.) long. Eight of the walls were fully grouted while the other two were only grouted in the cells with flexural reinforcement (partially grouted); these two walls also had no shear reinforcement. All the walls were subjected to in-plane cyclic loading while two of them were additionally subjected to axial compressive loads. Each specified displacement (0.5, 1, 2, 4, 6, 8, 10, 12, and 14 mm) went through two cycles and then the test was stopped once failure occurred (i.e., a 20% drop in strength). One of the walls was expected to fail in flexure while the other 7 were expected to fail in shear. The typical instrumentation for each specimen is given in Figure 2.5.

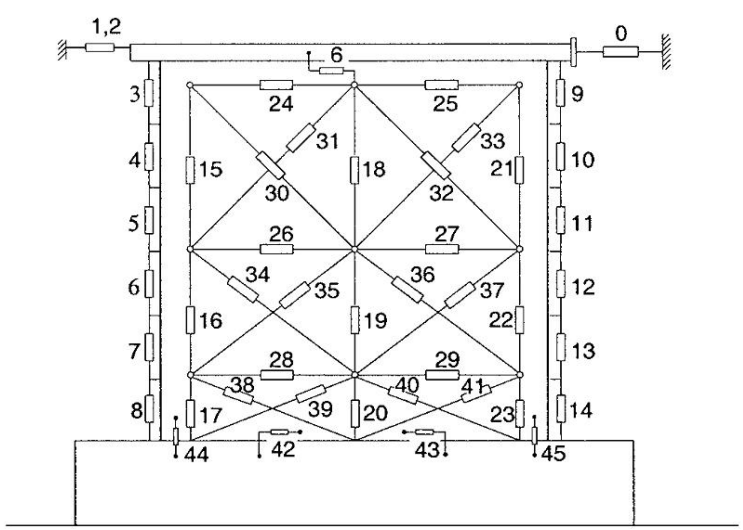

Figure 2.5 Voon and Ingham – Test Instrumentation

Two of the walls failed in a flexural or a flexural/shear behavior and the other walls exhibited shear failure. The flexural/shear failure was most likely caused by the lack of an axial load and the small shear reinforcement that was spaced closely together. The shear strength was influenced by the amount of shear reinforcement. The authors observed that the initial shear cracks did not widen with an increase in load, but the cracks instead developed at higher energy dissipation and ductility levels. The two partially grouted walls had significantly smaller shear strength than the fully grouted walls. The authors also observed a decrease in the shear strength of the walls with an increase in the slenderness.

2.4.5 Mjelde

Mjelde (2008) examined the effects of splicing flexural reinforcement in concrete masonry shear walls. This study investigated the following variables and their effects on the performance of the specimens: testing method, size of reinforcement, splice length, reduced cover, and layout of reinforcement. Lap splices were placed in the base of nine masonry shear walls and subjected to cyclic, in-plane loads. Nine masonry panels were also constructed with identical lap splices and subjected to direct tension; the results were used to compare between the two different testing methods. Mjelde investigated two different sizes of flexural reinforcement, No. 6 and No. 8 bars, and three different splice configurations illustrated in Figure 2.6 below. The top configuration shows a typical splice, the middle distributes the reinforcement to the adjacent cell, and the last configuration illustrates offsetting the reinforcement, resulting in reduced cover. Two design equations used to determine the required lap splice length were compared in this study, the Simplified Equation and the 2005 MSJC Lap Splice Equation. The Simplified Equation was specified in MSJC editions preceding 2005 and is equivalent to $48d_b$ for

Grade 60 steel, where d_b is the diameter of the spliced reinforcement. The 2005 MSJC Lap Splice Equation is equivalent to Equation 2.3 given previously.

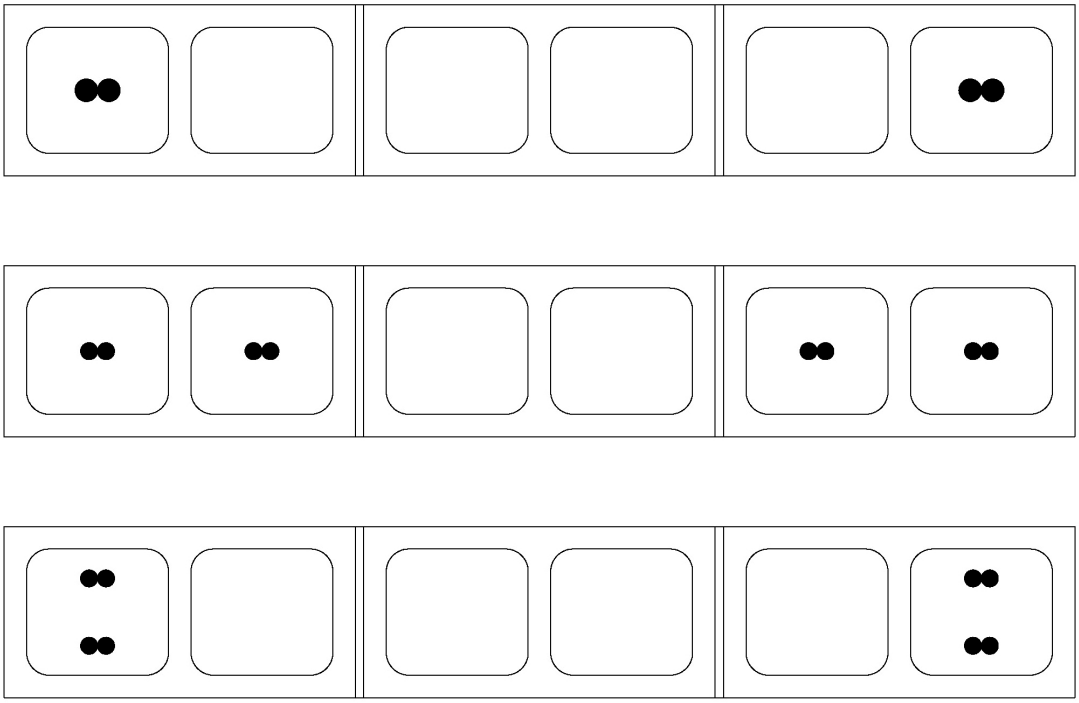

Figure 2.6 Mjelde – Splice Configurations

Mjelde summarized the effects of the design variables listed above from the test results. There were no notable differences when comparing the results from the direct tension tests to the cyclic, in-plane tests. A reduction in the clear cover (bottom configuration in Figure 2.6) caused a decreased in the ultimate load resistance and displacement capacity of the masonry shear walls compared to distributing the bars in adjacent cells (middle configuration). The Simplified Equation for lap splice length was adequate for all walls and panels except when there was reduced cover; these specimens exhibited a splice capacity much lower than expected. The 2005 MSJC Equation gave an accurate representation of the performance for the specimens with No. 6 reinforcement, including the specimens with reduced cover. However, the capacity of the specimens with No. 8 bars only reached 80% of the expected.

2.4.6 Shedid et al.

The objective of the study conducted by Shedid et al. (2008) was to evaluate the effects that different amounts of flexural reinforcement and axial load levels had on the inelastic behavior of masonry shear walls. All walls were subjected to in-plane cyclic loading until there was a 50% drop in strength. Two of the walls included axial compressive loads. The authors set all the wall dimensions to produce an aspect ratio of 2.0 (3.6 m high and 1.8 m long) to achieve a flexural failure. The flexural reinforcement in each wall was anchored into the foundation and extended to the full wall height without splicing. To resist any shear failures, the walls were designed in accordance with the reinforcement provisions of the 2005 MSJC Code. The wall types also varied between ordinary, intermediate, and special walls. String displacement potentiometers and strain gauges were placed on each specimen to measure displacements. The displacements from the strain gages were converted into strain measurements with a known gage length and were recorded on a computerized data acquisition system.

Each wall exhibited a flexure failure mechanism. An aspect ratio of 2.0 with symmetric distribution of reinforcement that did not exceed the permitted maximum limit was found to be an adequate assumption in producing flexural failure in the plastic hinge zones. The applied loads were increased until toe crushing was observed at one of the wall ends. The experimentally measured flexural capacities were compared to predictions made by the authors; one prediction neglected compression reinforcement, and the other included compression reinforcement. The MSJC Code recommends ignoring compression reinforcement in flexural design unless it is laterally tied. The authors noted that the addition of compression reinforcement was negligible. The flexural strengths of the walls were mostly dependent upon the amount of flexural reinforcement rather than the distribution of the reinforcement and increasing axial loads.

The displacement ductility was dependent upon the percentage of flexural reinforcement and slightly decreased with increasing axial loads. The authors proposed two alternatives to calculate the theoretical values of the displacement ductility. The first option suggests determining the displacement ductility at the structure's 1% drift, or by using the variables Δ_{ye2} and $\Delta_{1\%}$ from Figure 2.7 below. The second option recommends finding the displacement ductility at the structure's 80% load degradation, or by using variables Δ_{ye3} and $\Delta_{0.8u}$ from Figure 2.7. Both alternatives require finding equal energy under their specified curves. Displacement ductility indicates a potential in energy dissipation, which is associated with significant deformation and damage. The authors noted significant levels of energy dissipation at higher displacements up until failure occurred. The yield displacement, which is directly related to displacement ductility, increased with an increase in the amount of flexural reinforcement and axial loads.

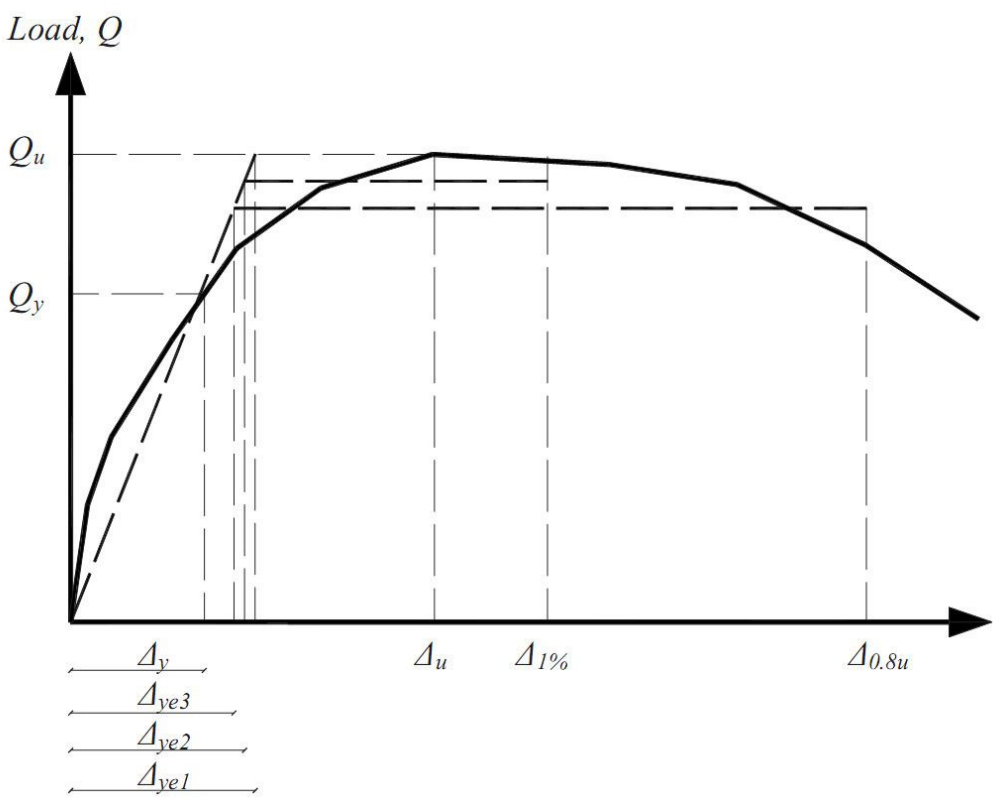

Figure 2.7 Shedid et al. – Displacement Ductility

2.4.7 Vaughan

Vaughan (2010) investigated the performance of 67 masonry shear walls that were tested in 6 previous studies. All 67 walls conformed to the current prescriptive requirements of the 2008 MSJC Code. Each wall was subjected to displacement-controlled, in-plane cyclic loading that was increased until failure. Three different walls types (ordinary, intermediate, and special) were categorized and in accordance with the MSJC Code, which provides minimum levels of ductility for each wall type. Vaughan collected the drift and ductility for each wall and then correlated them with a number of parameters including wall aspect ratios, vertical and horizontal reinforcement ratios, and levels of axial compressive stress. Theoretical values of ductility and displacement were also compared with the values obtained from the experiments for walls that failed in flexure. Theoretical values were not compared for the walls failing in shear. There were 29 walls that failed in flexure, and the other 38 failed in shear. All walls were fully grouted and composed of either concrete or clay masonry blocks. Most of the analyzed walls were cantilever walls, with a few walls tested in a fixed-fixed end condition.

The experimental results aligned with the performance and varying levels of ductility for each wall type intended by the MSJC Code. The ordinary walls had the lowest values of ductility, while the special walls produced the highest. Although the above trend corresponds with the MSJC Code, there was significant scatter of the data. This may have been caused by other failure modes such as sliding and shear influencing wall response. An example of the scatter is illustrated in Figure 2.8. This scatter indicates that a specific level of ductility for each wall could not be obtained, although the MSJC Code provides specific levels of ductility. Vaughan commented that the theoretical values of ductility were conservative compared to the experimental results.

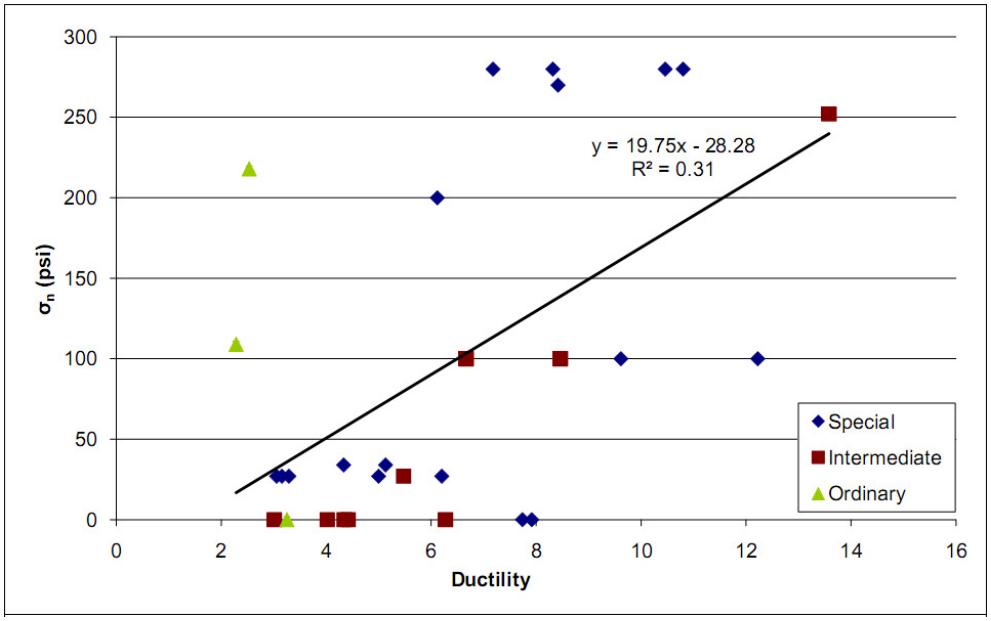

Figure 2.8 Vaughan – Comparison of Ductility to Compressive Stress

The results for drift also had scatter in the data, although it was not as significant. In this study, drift was defined as the ratio of the ultimate displacement to the overall wall height. Vaughan concluded that the walls that failed in flexure exhibited average drift capacities slightly higher than 1.0%, and for the walls that failed in shear the drift capacities were slightly lower than 1.0%; this reduction is one indication of the brittle behavior associated with shear failures. For the walls that failed in flexure, Vaughan also observed a higher level of drift for the ordinary walls than for the intermediate walls.

Vaughan examined the effects of various parameters on the performance of masonry shear walls including wall aspects ratios, reinforcement ratios, and levels of axial compressive stress. Increases in the aspect ratio revealed a decrease in ductility and an increase in drift. Ductility increased with respect to shear reinforcement, but decreased as the amount of flexural reinforcement increased. The amount of reinforcement did not generate an apparent effect on drift. Vaughan noted that although the effects of most parameters on these masonry shear walls coincided with previous studies, the effect of axial compression differed. It was concluded that

with an increase in the level of axial compressive stress, there was an increase in ductility and a decrease in drift. Vaughan concluded that many of the parameters had no statistical effect on the ductility and drift.

2.5 Summary

A review of four different failure modes including rocking, sliding, shear, and flexural that may occur when a masonry shear wall is subjected to cyclic, in-plane lateral loads was provided in this chapter. The seismic design provisions, which include prescriptive minimum requirements for the reinforcement, shear capacity, and maximum permitted reinforcement of the 2008 MSJC *Building Code Requirements for Masonry Structures* (MSJC, 2008), were also presented. Additionally, a review of previous experimental studies that investigated the performance of masonry shear walls under cyclic, in-plane loads was provided in this chapter.

CHAPTER 3

EXPERIMENTAL PROGRAM

3.1 Introduction

Eight cantilever masonry shear walls were constructed and tested to analyze the effects of key design and wall parameters on wall performance. This chapter provides detailed descriptions of each specimen as well as the instrumentation and procedures used during testing.

3.2 Footing Description

The wall specimens were built on heavily-reinforced concrete footings that were anchored to the laboratory floor using threaded rods to ensure that the footings would not rock or slide during testing. The rods were placed inside PVC piping (bolt tubes) cast inside the concrete footings. Specimens 1A, 1B, 2A, and 2B had 68-in. long footings with nine No. 5 longitudinal bars. The remaining four walls had 104-in. long footings with nine No.7 longitudinal bars. All of the footings were 24-in. wide, 18-in. high and included No. 4 stirrups spaced every 8-in. on center. Four lifting hooks, fabricated from No. 3 bars, were placed inside the footings to allow for mobility of the wall specimens within the laboratory using an overhead crane. The flexural reinforcement from the walls was anchored into the footings with 90° hooks. General details of the specimen footings are given in Figure 3.1.

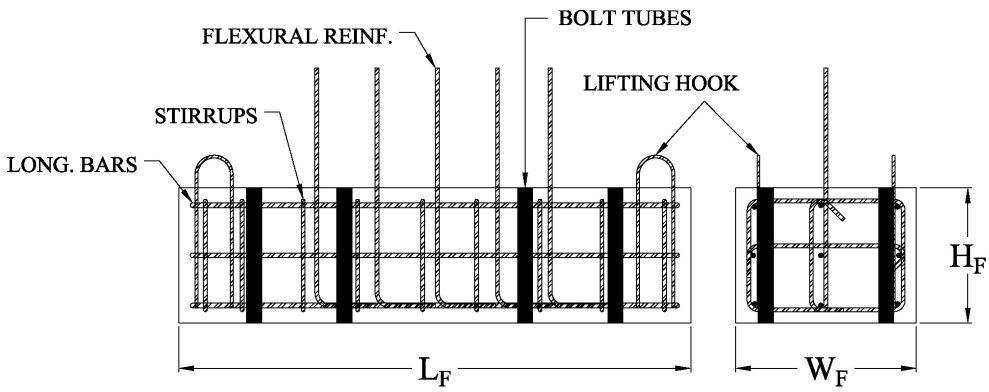

Figure 3.1 Footing Details

3.3 Loading Beam Description

A reinforced concrete beam was constructed on top of each wall for use in applying the lateral load. Each loading beam was reinforced with six No. 5 longitudinal bars and No. 4 stirrups spaced every 8 in. on center. The length of the beams for Specimens 1A, 1B, 2A, and 2B were 44 in. while the other four specimens had a loading beam length of 76 in. The width and height of all the loading beams were 12 in. and 16 in., respectively.

3.4 Specimen Description

The eight, fully grouted, masonry shear walls were composed of 7.625-in. (nominally 8-in.) thick concrete masonry units (CMU) placed in running bond. Three different aspect ratios (height-to-length) were considered in this study and are illustrated in Table 3.1; notation is provided in Figure 3.2. Two of the walls contained No. 6 vertical (flexural) reinforcement while the other six specimens had No. 4 bars placed every 8 in. on center. Flexural reinforcement in six of the walls was spliced at the wall base according to 2008 MSJC Code requirements while the flexural reinforcement for Specimens 1A and 2A extended the full height of the walls. Horizontal (shear) reinforcement was provided to ensure that the nominal shear strength

exceeded the shear to produce the calculated flexural capacity or to meet the prescriptive requirements of Section 1.17.3.2.6 of the 2008 MSJC Code, whichever was greater. The shear reinforcement included 180° hooks at each end that were placed around the extreme flexural reinforcement in accordance with Section 3.3.3.3.2.1 of the MSJC Code. Details for the flexural reinforcement including the lap splice length, and shear reinforcement are given in Table 3.1.

In order to analyze the effects of lap splices, Specimens 1A and 1B and Specimens 2A and 2B were designed with identical parameters except that the B specimens included a lap splice. Specimens 1A, 1B, 2A, and 2B contained flexural reinforcement ratios that were approximately equal to the maximum reinforcement limits prescribed by Section 3.3.3.4 of the MSJC Code for special reinforced masonry shear walls. The flexural reinforcement ratio was defined as the total cross-sectional area of reinforcement divided by the gross cross-sectional area of the wall. Specimens 3, 4, 5, and 6 were designed in accordance with Section 3.3 of the MSJC Code with varying levels of aspect ratio. The level of the axial compressive stress applied on top of each wall during testing was also varied in this study. Details of the test specimens are given in Table 3.1.

Table 3.1 Specimen Properties

Specimen	H_{LA} (in.)	H_W (in.)	L_W (in.)	H_{LA}/L_W	$P/(f'_m A_g)$	Flexural Reinf.	Shear Reinf.	Splice Length (in.)
1A	79 ¼	72	39 ⅝	2.0	0.0625	#6 @ 8 in.	#4 @ 8 in.	N/A
1B	79 ¼	72	39 ⅝	2.0	0.0625	#6 @ 8 in.	#4 @ 8 in.	33
2A	79 ¼	72	39 ⅝	2.0	0.125	#4 @ 8 in.	#4 @ 8 in.	N/A
2B	79 ¼	72	39 ⅝	2.0	0.125	#4 @ 8 in.	#4 @ 8 in.	16
3	71 ⅝	64	71 ⅝	1.0	0	#4 @ 8 in.	#4 @ 24 in.	16
4	71 ⅝	64	71 ⅝	1.0	0.0625	#4 @ 8 in.	#4 @ 8 in.	16
5	55 ⅝	48	71 ⅝	0.78	0	#4 @ 8 in.	#4 @ 8 in.	16
6	55 ⅝	48	71 ⅝	0.78	0.0625	#4 @ 8 in.	(2) #4 @ 8 in.	16

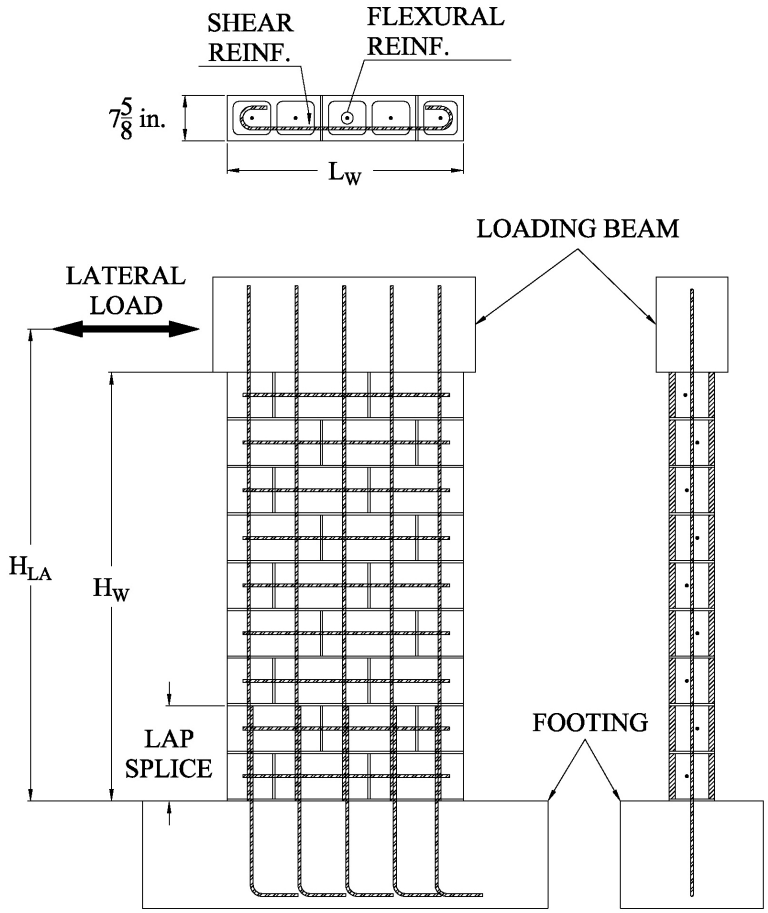

Figure 3.2 Specimen Details

3.5 Material Properties

The concrete masonry blocks used in this study were nominally 8x8x16-in. hollow concrete masonry units. Bond-beam units were placed in the courses that contained horizontal reinforcement (reference Table 3.1 for spacing), starting with the first course. The outside webs of standard and half units were cut to accommodate the courses with horizontal reinforcement. The walls were constructed in two separate sets; the first set contained Specimens 1A and 2A, and the other six walls were constructed later. Material properties for each construction set are presented in Table 3.2. Type S mortar that conformed to ASTM C270-10 was used in both construction sets. Mortar test cylinders with a 2-in. diameter and 4-in. height were built and

tested in accordance with ASTM C780-10. Fine aggregate grout was used in the first and second construction sets, respectively, and conformed to ASTM C476-10. Grout test prisms 3-½-in. square by 7-in. high were built and tested in accordance with ASTM C1019-11. Full 2-block masonry prisms were also built and tested in accordance with ASTM C1314-11 for the two construction sets. The average 28-day compressive strengths for the mortar cylinders, grout prisms, and masonry prisms are listed in Table 3.2 for both construction sets. All vertical reinforcement was Grade 60 steel and was obtained in three lots, resulting in different yield strengths as presented in Table 3.3.

Table 3.2 Average Compressive Strengths of Masonry Materials, in psi

Construction Set	Masonry Units	Mortar	Grout	Masonry Prisms
1	3470	2,970	6,490	2,770
2		3,220	5,530	3,040

Table 3.3 Average Yield Strengths of Vertical Reinforcement, in ksi

Order Set	Specimens	#4 Bars	#6 Bars
1	1A & 2A	66.2	65.4
2	2B, 3, 4, 5, & 6	65.3	--
3	1B	--	64.7

3.6 Specimen Construction

The eight walls were constructed at the Composite Materials and Engineering Center at Washington State University. The walls were constructed in two separate sets: the first set contained Specimens 1A and 2A, and the other six walls were constructed later. Steps taken to construct each wall were identical for both sets. The footings were constructed first, which included assembling the reinforcement cages and lifting hooks and securing them inside the wooden forms. PVC pipes were also placed inside the forms prior to the concrete pour so that threaded rods could secure the footing to the floor during testing to prevent rocking or sliding. Strain gages were attached to the flexural reinforcement, which was then secured into the

reinforcement cages. Before the masonry walls were constructed, the lap splices on six of the walls were tied to the dowels that extended from the footing. Figure 3.3 illustrates the footing construction just before pouring the concrete. Once the concrete was poured and consolidated with a vibrator, the wall footprint was slightly roughened with a trowel to reduce the potential for sliding.

Figure 3.3 Footing Construction

Professional masons constructed the eight walls in two phases spread over two days. The first phase consisted of laying the block for the entire wall height of 72 in., 64 in., or 48 in. Standard and half units were cut and placed along with the bond beam units in courses that required horizontal reinforcement. The blocks were placed in running bond with face shell mortar bedding. Figure 3.4 illustrates phase one of construction. Grouting and consolidating the walls with a vibrator took place during the second phase of construction. The last step in constructing the specimens was adding the concrete loading beams on top of the walls.

Reinforcement cages were assembled and placed into wooden forms, then secured to the flexural reinforcement from the walls. Finally the concrete was poured, consolidated with a vibrator, and smoothed with a trowel.

Figure 3.4 Wall Construction: Phase 1

3.7 Test Setup

The specimens were designed as cantilever walls with a fixed base and the top free to translate and rotate. The specimens were anchored to the floor using 1¼-in.-diameter threaded rods. Eight rods were used for Specimens 1A, 1B, 2A, and 2B, while the other six specimens used 12 rods. The footings were laterally braced using steel fixtures to prevent sliding on the laboratory floor during testing. Three identical hydraulic jacks were placed on top of six of the walls to provide a constant axial stress, representing a roof or floor load from above. Specimens 3 and 5 had no axial stress, Specimens 1A, 1B, 4, and 6 had a constant axial stress of 156 psi,

and Specimens 2A and 2B had an axial stress of 313 psi. All three jacks were attached to a pump that kept the system pressure constant as the jacks were extending and retracting to accommodate vertical deflection of the wall. The jacks were symmetrically spaced on a steel HSS shaped beam. The load from the jacks transferred through the beam and into a trolley that ran on low-friction rollers on a smooth stainless steel plate attached to the frame crossbeam. This setup allowed the wall to act as a cantilever wall (free moving top) because the jacks were able to move in-plane with the wall while maintaining a constant axial stress. A 220-kip actuator, which was operated under displacement control, was used to apply the lateral load through a load cell and into the top of the wall. Two steel plates were placed on the ends of the concrete loading beam and then secured using four 1-in. diameter rods. The actuator was then secured to one of the steel plates that had four tapped holes. Figure 3.5 illustrates the test frame setup for the specimens during testing.

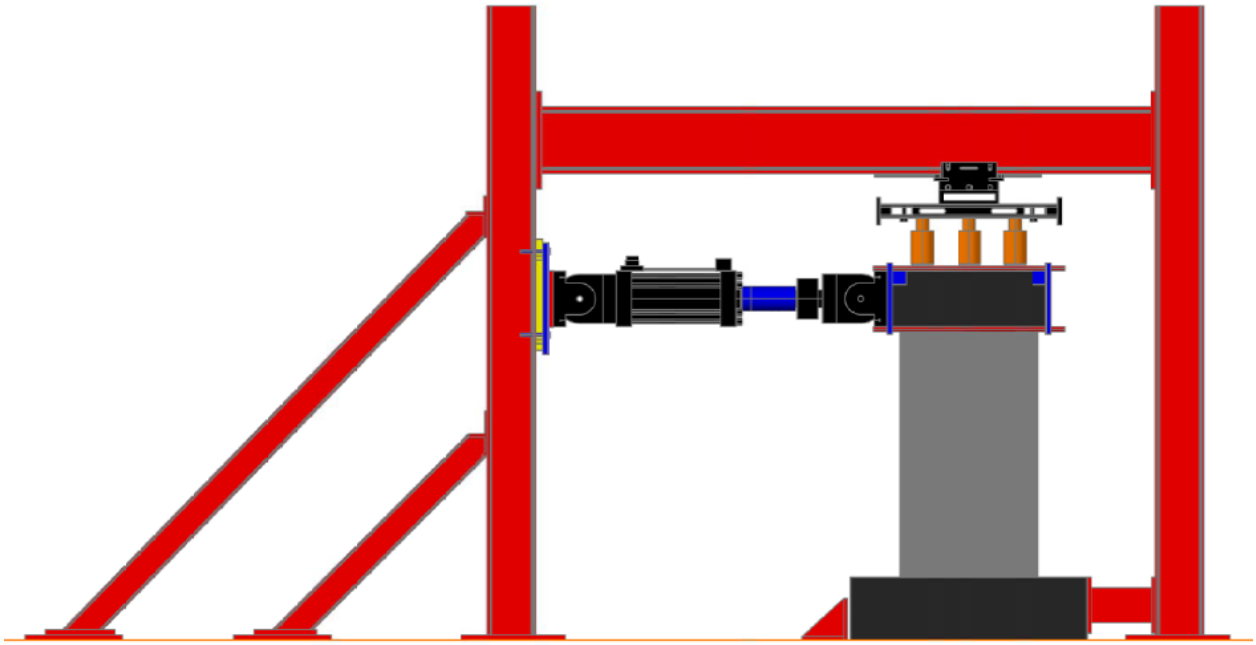

Figure 3.5 Test Setup

3.8 Instrumentation

String potentiometers, strain gages, and a load cell attached to the actuator were used to measure and monitor the walls during testing. String potentiometers (labeled P1-P18 in Figure 3.6) were used to measure the total lateral, vertical, sliding, and shear displacements. Black dots in the figure indicate the actual attachment location of the potentiometers. Since the wall heights varied, note that P10, P11, and P12 were attached to the second course below the loading beams. The measurements from P1-P8, which ran along the north and south ends of the walls, were used to calculate flexural curvatures over the wall height. P9-P14 measured displacements that were used to determine the drift contribution from shear. Any sliding that occurred between the base of the wall and the footings was measured at P15 and P16. Similar sliding between the loading beams and the top of the walls were measured by P17. P18, which was attached to an external support, provided the lateral, in-plane displacement of the wall during testing. Linear pattern strain gages (labeled S1-S22 in Figure 3.7) were attached at various locations along the flexural and shear reinforcement. A single strain gage, or SSG, was located on one side of the reinforcement. Double strain gages, which consisted of two independent gages, were mirrored on two sides of the reinforcement and were oriented in the same direction. The layout of gages for Specimen 1B are shown in Figure 3.7. The only discrepancies with the other specimens were the number of SSGs at spliced vertical bars and at the base of the wall. The vertical bars on Specimens 1A and 2A were not spliced, and they therefore did not have SSGs at spliced vertical bars. Due to the shorter splice length, Specimens 2B through 6 only contained SSGs at two locations (one on each end) on the spliced vertical bars. Since Specimens 3-6 had longer wall lengths than Specimen 1B, there were four additional SSGs located just above the footing-to-wall interface. The load cell that was attached to the actuator piston measured the lateral loads.

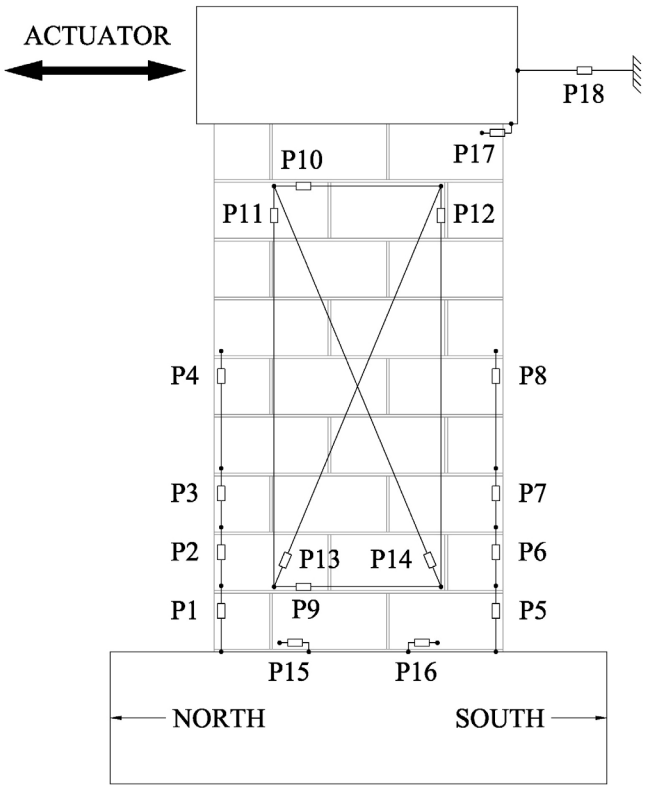

Figure 3.6 String Potentiometer Locations

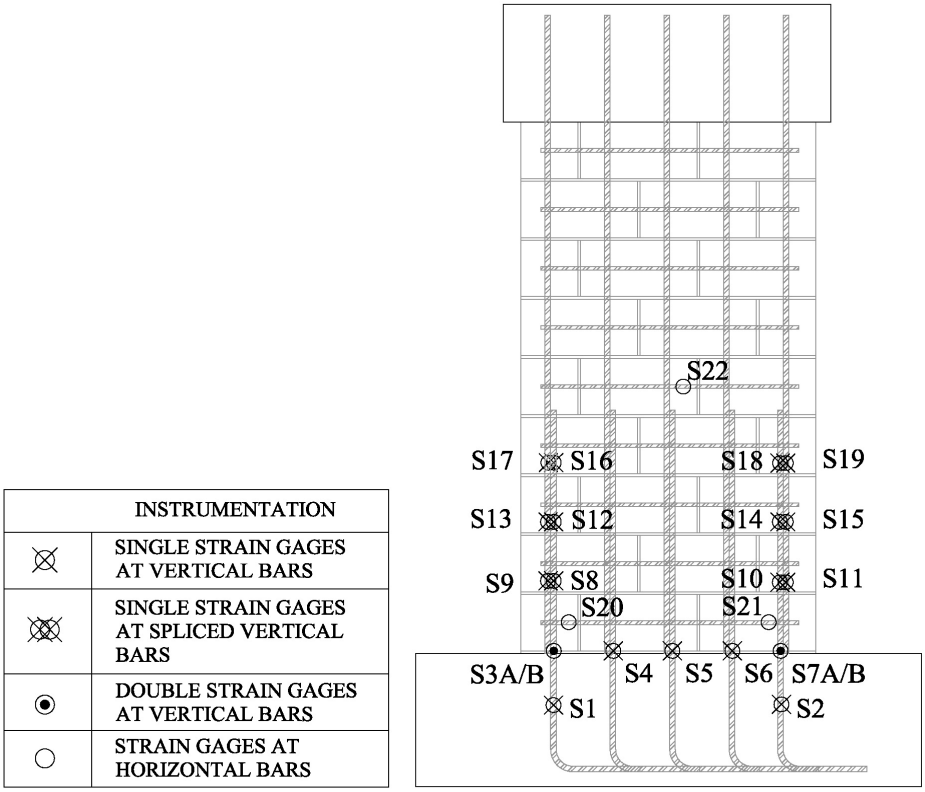

Figure 3.7 Strain Gage Locations

3.9 System Control and Data Acquisition

Two separate computer systems controlled the lateral load application and data acquisition, as shown in Figure 3.8. Commercial software was utilized in one of the computers to send a signal containing a loading rate and target end displacement to a servocontroller that provided hydraulic pressure to a 220-kip actuator. Data from string potentiometers and strain gages attached to the wall and a load cell attached to the actuator were recorded in commercial software at a rate of 1 scan/sec and displayed in real-time.

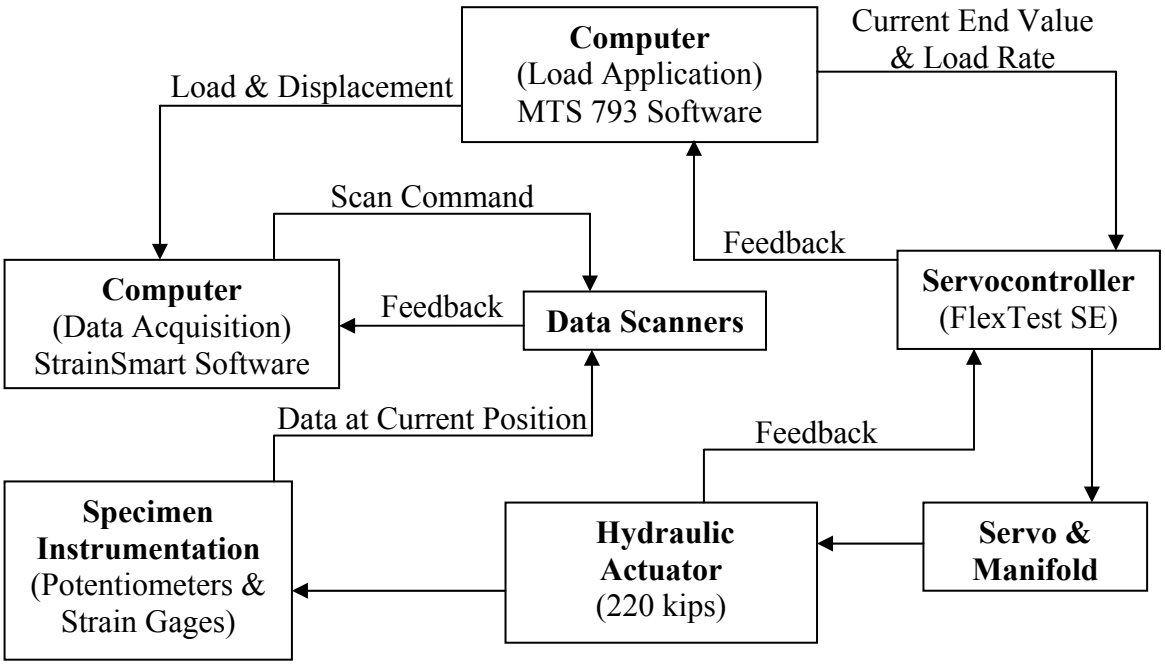

Figure 3.8 System Control Flow Chart

3.10 Test Procedures

The walls were tested under displacement control and were subjected to fully reversed, cyclic, quasi-static, sequential-phased displacements. Amplitudes of displacement were based on standard multiples of a specimen-specific critical displacement, referred to as the first major event (FME) displacement. For this study, the FME was defined as the displacement associated

with first yield of the extreme vertical reinforcement (Δ_y). Yielding was attained once the strain in the reinforcement exceeded the yielding strain value, which was specified at a strength of 65 ksi. FME displacements were calculated in a preliminary test that was based on a theoretical peak horizontal load capacity. XTRACT, a cross-sectional analysis program, produces moment-curvature results for a monotonic push test of a user-defined cross-section. Moment-curvature results were obtained for each specimen, from which the maximum moment capacities were calculated and then converted into peak horizontal loads. Each specimen was then subjected to two fully reversed cycles of loads ±25%, ±50%, and ±75% of the theoretical peak horizontal load. The average displacement at 75% of the peak horizontal load was then used to establish the probable Δ_y by extrapolating the displacement at 75% of the peak load to the displacement at 100% of the peak load ($\Delta_{y@100\%} = 4/3\Delta_{y@75\%}$). Each specimen was then loaded at a rate of 0.3 in./min. to reverse-cyclic displacements shown in Figure 3.9. Testing was stopped once there was 50% load degradation from the measured peak horizontal load.

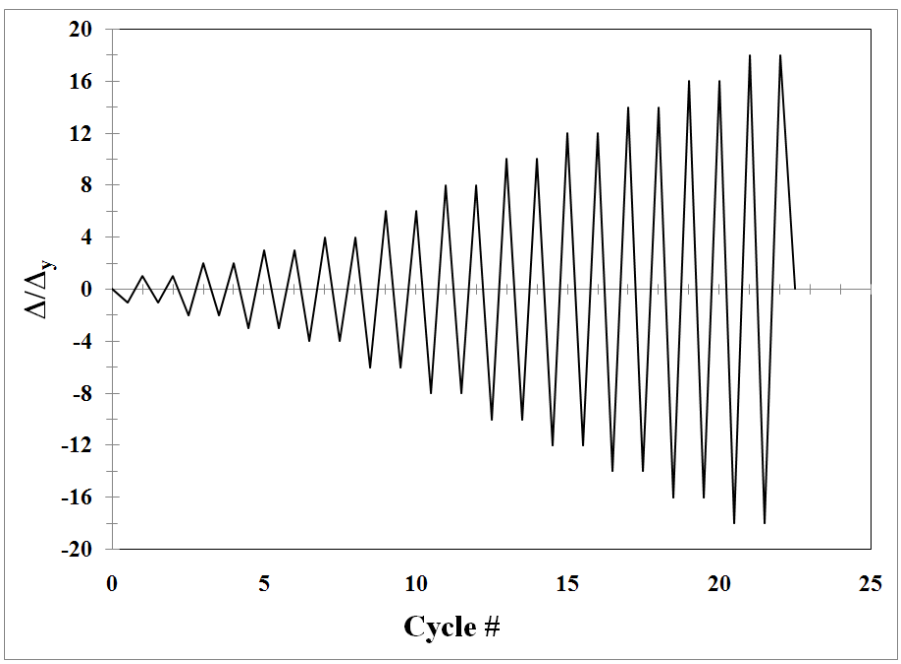

Figure 3.9 Standard Loading Protocol: Sequential-Phased Displacements

CHAPTER 4

RESULTS OF WALL TESTS

4.1 Introduction

In this chapter, results for the eight masonry shear walls are presented including test observations, load-displacement measurements, components of displacements and drifts, curvature measurements, displacement and curvature ductility, height of plasticity, equivalent plastic hinge length, and energy dissipation.

4.2 Specimen 1A

Specimen 1A had an aspect ratio of 2.0, No. 6 flexural reinforcement spaced 8-in. on center with no splice at the wall base, No. 4 shear reinforcement spaced 8-in. on center, and an axial load of 48 kips. Predicted capacities for the maximum lateral load were calculated using two methods: the first was based on Section 3.3 of the 2008 MSJC Code, and the second method was based on XTRACT analysis. All material and strength reduction factors were neglected for the predicted capacities from the MSJC Code. The influence of compression reinforcement was considered in the predicted capacities from the MSJC Code, although the code recommends neglecting compression reinforcement unless it is adequately tied (Section 3.1.8.3, MSJC 2008). Specimen 1A had a predicted capacity of 34 kips using the 2008 MSJC Code and 38.1 kips from the XTRACT analysis. Strains were measured on the horizontal reinforcement located at the first and fifth courses to determine if these bars yielded. Neither of these locations experienced yielding of the horizontal reinforcement. Strains were also measured on the extreme vertical reinforcement at mid-height of the footing. Specimen 1A experienced yielding of the extreme vertical reinforcement in the footing.

Test Observations:

A yield displacement (Δ_y) of 0.44 in. was obtained from the preliminary test. The specimen was then loaded to displacements of ±1, 2, 3, 4, and 6 times the yield displacement for the primary test. The entire specimen and the north and south toe regions of the wall at test completion are presented in Figure 4.1 and 4.2. Test observations along with corresponding lateral displacements and loads follow. Wall behavior was dominated by flexure during testing with minimal shear cracking. Flexural cracks developed at $1\Delta_y$ in the primary test, and moderate crushing and spalling of both toes up to the second course occurred near failure. Vertical splitting was observed on the end faces of the walls at $3\Delta_y$. Separation at the mortar joints occurred at the wall base and gradually decreased along the height of the wall. Figure 4.2 illustrates buckling of the extreme reinforcement that occurred near the end of testing at higher displacement levels.

Figure 4.1 End-of-Test Picture of Entire Specimen 1A

Figure 4.2 End-of-Test Pictures for Specimen 1A: South Toe (left) and North Toe (right)

Table 4.1 Specimen 1A Test Observations

Load (kips)	Disp. (in.)	Test Observation
27.3	0.28	1st Yield of extreme vertical reinforcement bar in north toe (pull)
-27.6	-0.31	1st Yield of extreme vertical reinforcement bar in south toe (push)
29.9	0.35	Critical masonry strain in north toe (pull)
-32.2	-0.43	Critical masonry strain in south toe (push)
-32.5	-0.44	*Flexural cracking in north toe (push)
34.2	0.46	*Flexural cracking in south toe (pull)
-39.9	-0.76	1% Drift in push to south
39.6	0.76	1% Drift in pull to north
-40.7	-0.88	Maximum load resistance in push to south
-40.7	-0.88	*Onset of toe crushing in south toe (push)
41.4	0.89	Maximum load resistance in pull to north
37.5	1.33	*Onset of toe crushing in north toe (pull)
34.5	1.77	20% load degradation from maximum load resistance in pull to north
-33.6	-2.64	20% load degradation from maximum load resistance in push to south

* visual observation

Load-Displacement:

The load-displacement hysteresis curves for the preliminary and primary tests for Specimen 1A are given in Figure 4.3. The upper left hand corner contains a key referencing six major events that represent limit states in both the push (negative load and displacement) and pull (positive load and displacement) directions. The major events include initial yielding of the extreme tensile reinforcement (ε_y = 0.00226 in./in.), reaching the critical masonry strain (ε_{mu} = 0.0025 in./in.), attaining maximum load resisted, reaching 1% drift, onset of toe crushing, and failure which was defined at 20% load degradation of the maximum load resisted. The initial yielding of the extreme tensile reinforcement was measured from strain gages attached to the flexural reinforcement. Critical masonry strain was measured from string potentiometers located in the first eight in. of the wall height. The data recorded from the potentiometers were converted into an average strain over a given gage length and was assigned at mid-height of the gage length. The maximum load resisted was recorded from the load cell measurements. The point of reaching 1% drift was determined by dividing the recorded lateral displacements by the height to

the point of load application. The onset of toe crushing was established based on visual observations during testing. The 20% load degradation was defined as the cycle in a specific displacement level following the peak lateral load that the wall failed to reach within 20% of the maximum load resistance. All major events were marked on the load-displacement curve and are presented in Table 4.1 with their corresponding lateral displacement and load values at a specific point during the scan.

For Specimen 1A, the initial yielding of the extreme tensile reinforcement occurred near the end of the preliminary test. Critical masonry strain occurred in $1\Delta_y$ of the primary test and was located at the cycle peak in the push direction. The specimen reached 1% drift preceding the peak lateral load resisted at $2\Delta_y$ in both loading directions. The wall reached the peak load and onset of toe crushing at the same point in the push direction, while toe crushing did not develop until $3\Delta_y$ in the pull direction. Figure 4.4 illustrates the onset of toe crushing in both toe regions. The specimen exhibited nearly symmetrical responses between the two loading directions for the entire test.

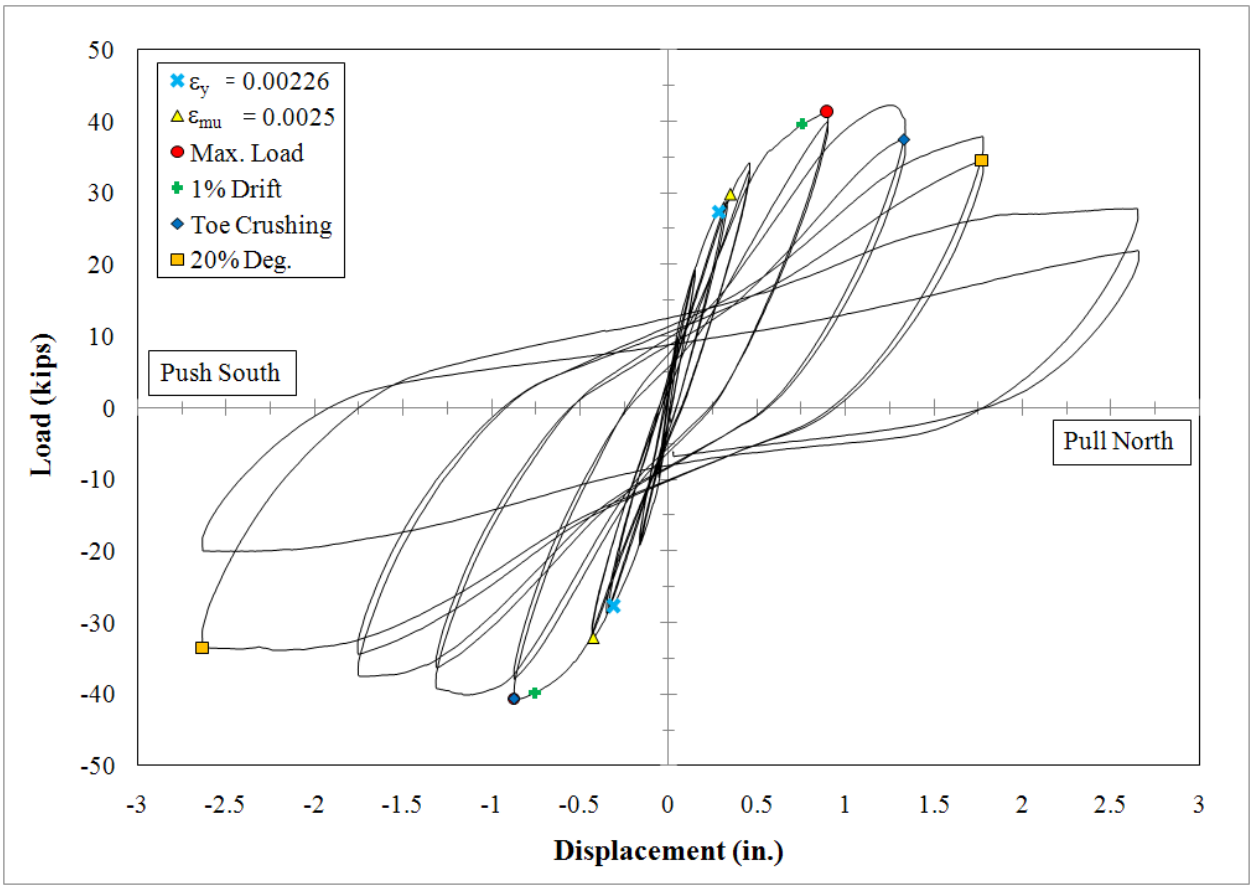

Figure 4.3 Specimen 1A: Load-Displacement Hysteresis Curve

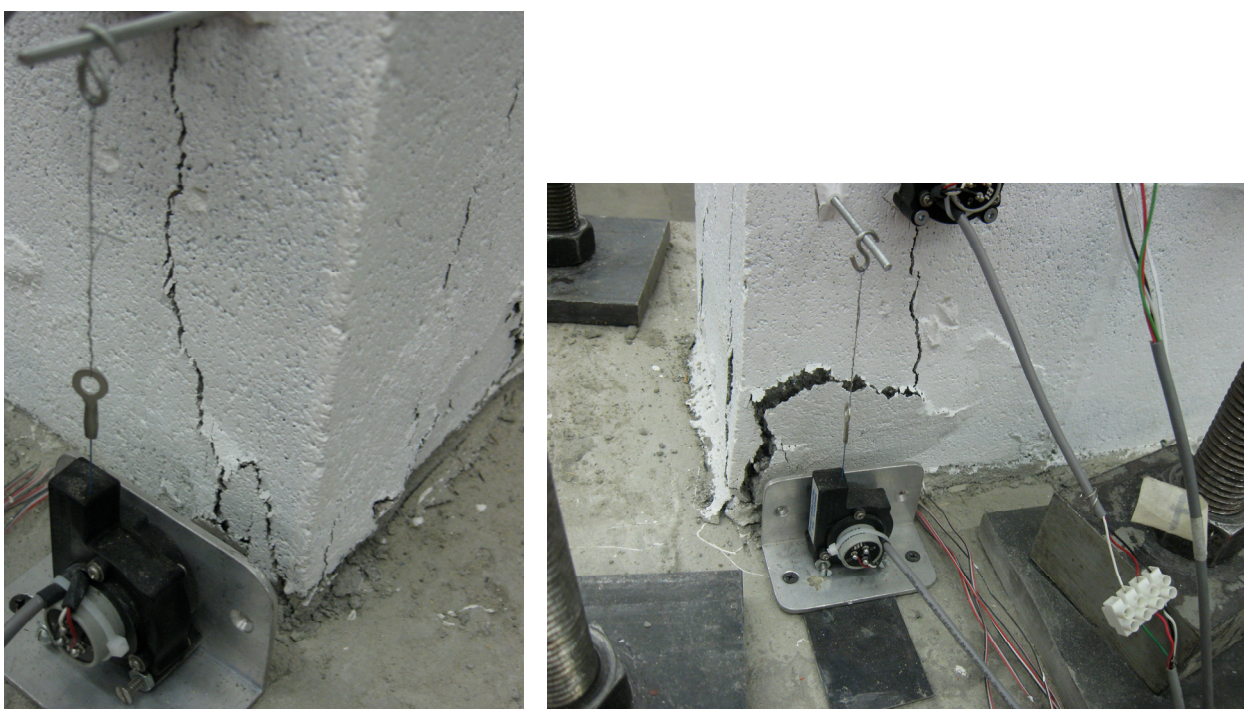

Figure 4.4 Onset of Toe Crushing for Specimen 1A: South Toe (left) and North Toe (right)

Components of Displacements and Drifts:

The lateral displacements of the wall were determined as total, flexural, sliding, and shear displacements. The total in-plane lateral displacement was measured with a string potentiometer attached to an external reference frame at the height of load application. Flexural displacements were determined by subtracting the sliding and shear displacements from the total displacements. Two string potentiometers recorded the average sliding displacements between the wall base and the footing. Sliding was also measured between the top of the wall and the top concrete beam, but the readings were very small and deemed negligible for all specimens. Shear displacements were measured with two diagonally- and two vertically-oriented string potentiometers and were calculated based on a previous study by Massone and Wallace (2004). The authors in this previous study determined the shear displacement of a wall with contributions from both shear and flexural deformations by the geometry given in Figure 4.5. The broken lines represent the original, undeformed wall; the shaded rhomboid represents the shear deformation; and the combined shear and flexural deformations are shown in solid lines.

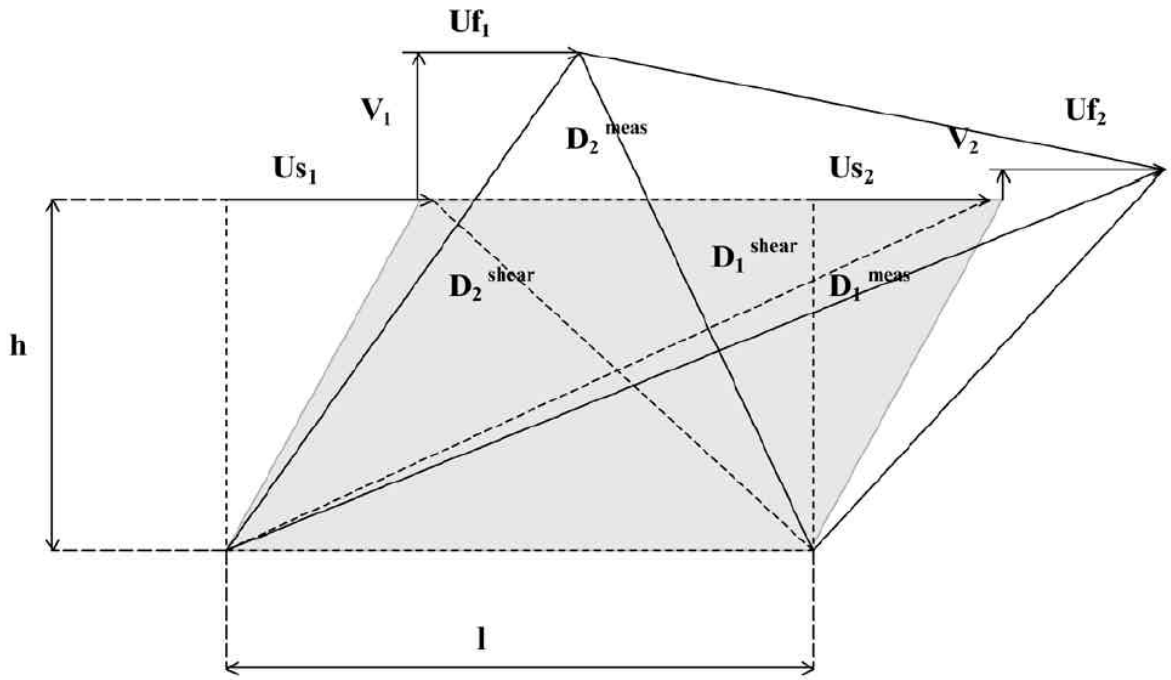

Figure 4.5 Massone & Wallace – Flexural & Shear Deformations

The average shear displacements based on contributions from shear and flexural deformations were derived from Figure 4.5 as:

$$\Delta_{SH} = \frac{\sqrt{\left(D_1^{meas}\right)^2 - h^2} - \sqrt{\left(D_2^{meas}\right)^2 - h^2}}{2} + \left(\frac{1}{2} - \alpha\right)\left(\frac{V_1 - V_2}{l}\right)(h) \quad \text{(Eqn. 4.1)}$$

Where:

Δ_{SH} = average shear displacement (in.);

$D_{1,2}^{meas}$ = diagonal lengths for the deformed X configuration (in.);

h = height of diagonal pattern (in.);

α = distance from the top of wall to the center of rotation;

$V_{1,2}$ = measured displacements from vertical potentiometers (in.); and

l = width of diagonal pattern (in.).

The authors in the previous study used an α value of 0.67 based on assuming the center of rotation occurred at 1/3 of the wall height; this value was also used in this study. The first term in Equation 4.1 represents the shear displacements from shear deformation, and the second term represents the shear displacements from flexural deformations. Load-displacement curves for each component of displacement and the total displacement are given in Figure 4.6.

Drift was defined as the total in-plane lateral displacement divided by the height to the application of load, given as a percentage. Average drift contributions from sliding, shear, and flexural deformations and total drift at the three limit states of critical masonry strain, peak lateral load, and failure are given in Table 4.2. Specimen 1A was dominated by flexural deformations, with small levels of shear and sliding deformations occurring near failure.

Table 4.2 Specimen 1A: Component Percentages of Total Drift

Limit State	Total Drift (%)	Sliding (% Total)	Shear (% Total)	Flexural (% Total)
ε_{mu}	0.5	0.6	3.9	97.8
Peak Load	1.1	0.5	5.4	94.1
Failure	2.8	5.3	7.4	87.3

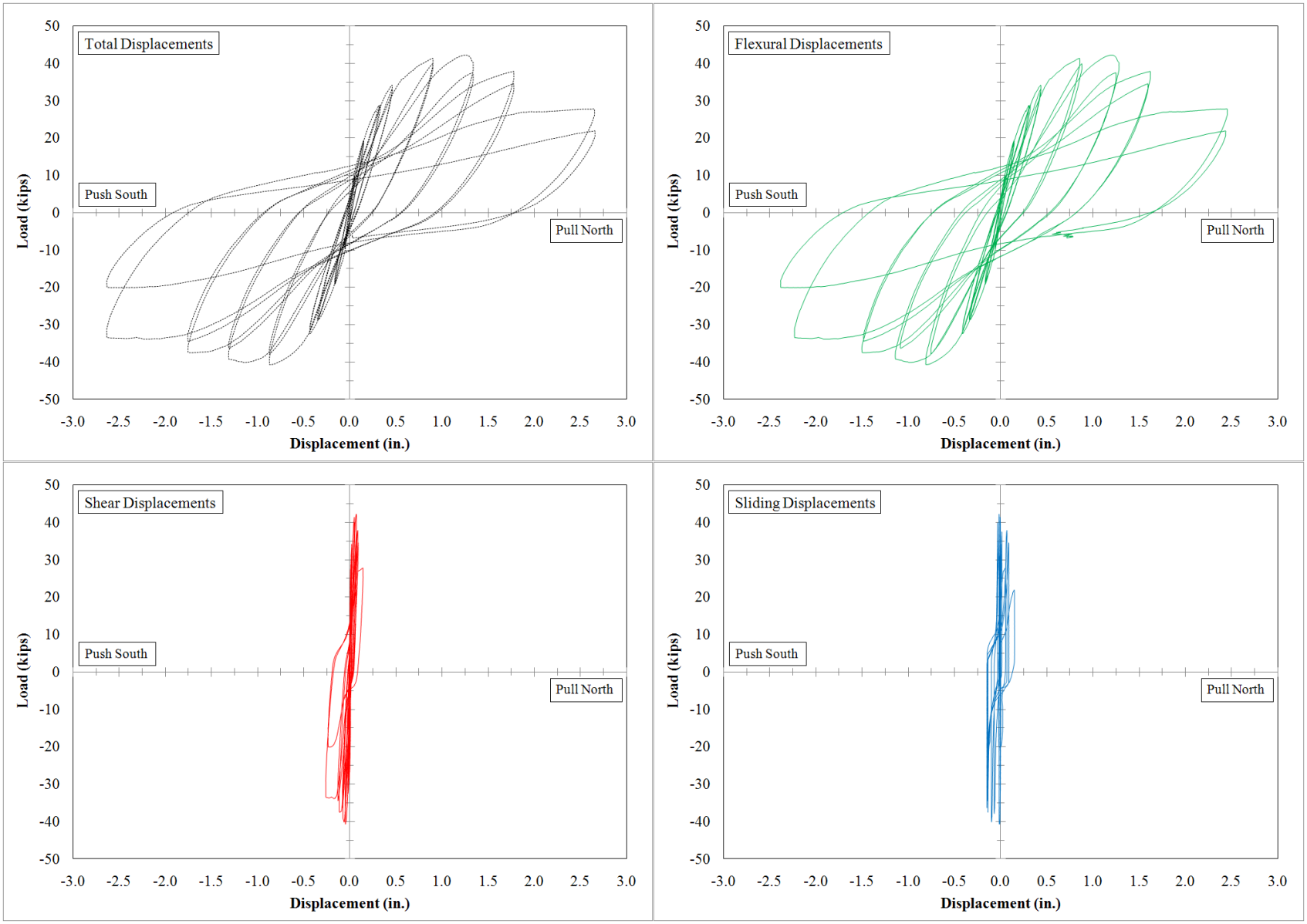

Figure 4.6 Specimen 1A: Displacements from Associated Components

Wall Curvatures:

The curvatures over the wall height were determined based on the strain profiles calculated using four potentiometers along the inside edge of the wall (mirrored on both sides). The curvatures were determined for the first cycle at each displacement level in the primary test only. Strain calculations from the potentiometers were converted into an average strain over a given gage length and were assigned at mid-height of the gage length. Strains and curvatures were unavailable at larger displacement levels due to spalling of the face shells. Figure 4.7 depicts a strain profile at a typical cross section, which assumes plane sections remain plane. Strains of the vertical reinforcement at the wall base were measured and compared with a typical strain profile provided by the string potentiometers at a specific point during the test. The strains of the vertical reinforcement generally followed the linear relationship shown in Figure 4.7 and thereby justified the assumption that plane sections remain plane.

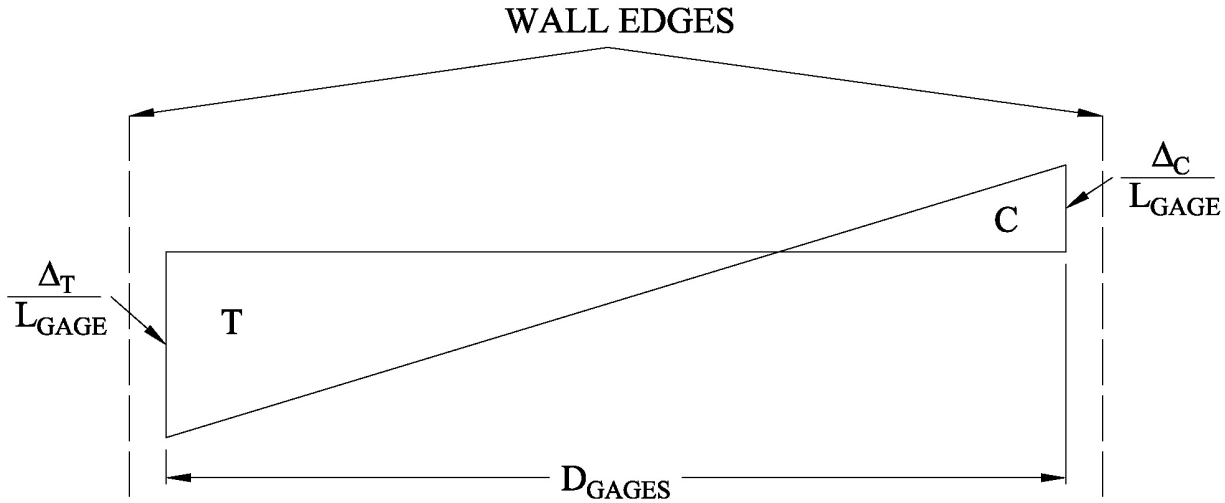

Figure 4.7 Typical Strain Profile

Average curvature for a given cross-section was derived from Figure 4.7 as:

$$\phi = \frac{\left|\frac{\Delta_T}{L_{GAGE}}\right| + \left|\frac{\Delta_C}{L_{GAGE}}\right|}{D_{GAGES}} \qquad \text{(Eqn. 4.2)}$$

Where:

ϕ = curvature at a given cross-section (in.$^{-1}$);

$\Delta_{T,C}$ = measured tensile and compressive displacements (in.);

L_{GAGE} = applicable gage length (in.); and

D_{GAGES} = in-plane distance between gages (in.).

A plot of curvature along the wall height of Specimen 1A is shown in Figure 4.8. Curvatures along the wall height of Specimen 1A were symmetric about the wall center line (mid-length of wall) up to $4\Delta_y$. The ultimate curvature was defined at the first cycle of $4\Delta_y$ for both loading directions instead of the 20% load degradation of the peak. This was due to invalid measurements from the potentiometers beyond $4\Delta_y$. The curvatures for Specimen 1A gradually decreased over wall weight. This was expected since the separation of the mortar joints gradually decreased over the wall height and thereby gradually decreased the wall rotation over wall height.

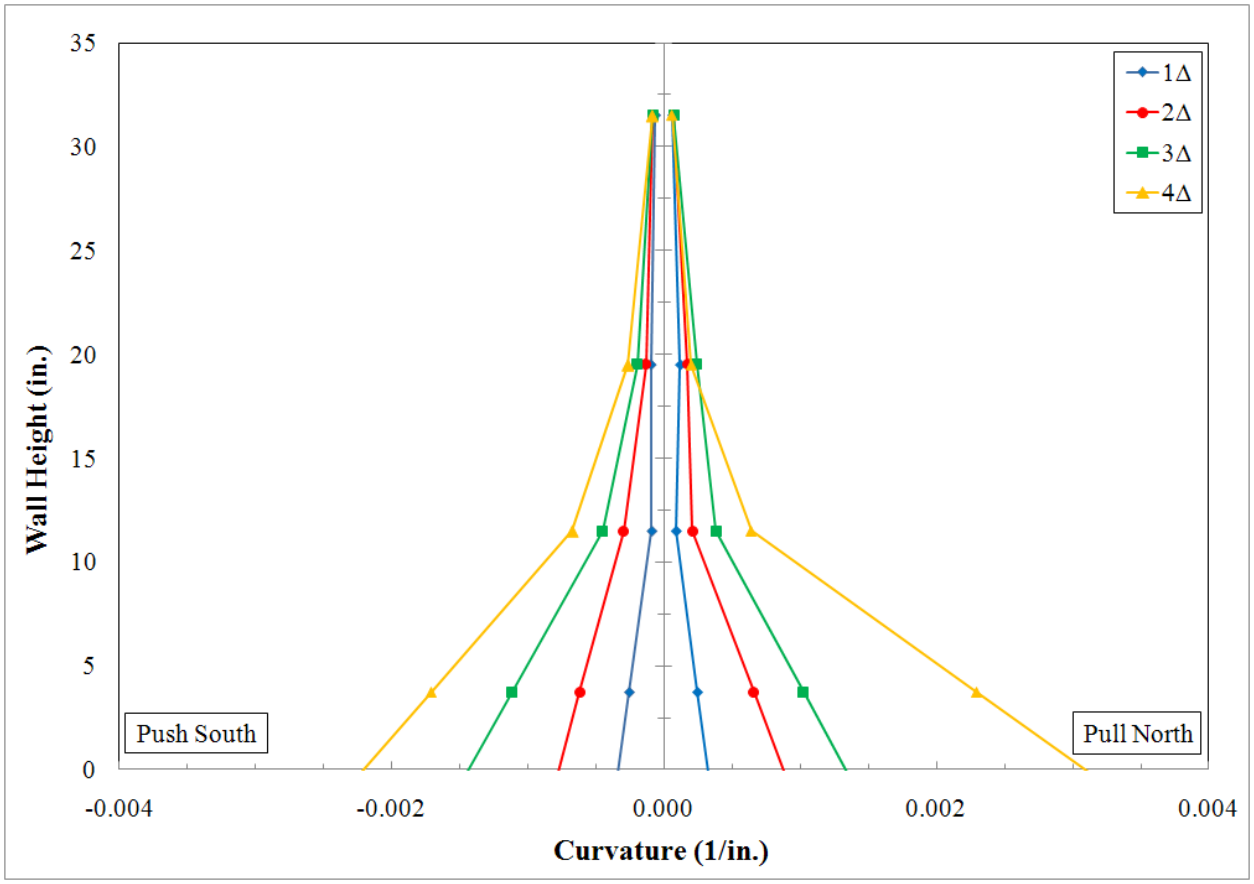

Figure 4.8 Specimen 1A: Wall Curvature

Ductility:

The displacement ductility was based on equal areas under the elastoplastic approximation and the load-displacement envelope shown in Figure 4.9. The load-displacement envelope was comprised of the peak loads from the first cycle at each load/displacement level in both the preliminary and primary tests. The load-displacement envelope ended at the 20% load degradation of the maximum load. The displacement ductility is defined as:

$$\mu_{\Delta} = \frac{\Delta_u}{\Delta_y} \qquad \text{(Eqn. 4.3)}$$

Where:

μ_{Δ} = displacement ductility;

Δ_u = ultimate displacement at 20% load degradation (in.); and

Δ_y = yield displacement of elastoplastic approximation (in.).

The ultimate displacement was defined as the point at which 20% load degradation of the maximum load resistance occurred. The yield displacement was defined as the intersection of the secant stiffness through the initial measured yielding of the extreme tensile reinforcement to the yield force of the elastoplastic approximation. The yield force of the elastoplastic approximation was defined as:

$$P_y = \left(\frac{P'_y}{\Delta'_y} \right) \Delta_y \qquad \text{(Eqn. 4.4)}$$

Where:

P_y = yield force of elastoplastic approximation (kips);

P'_y = yield force at first yield of tensile reinforcement (kips);

Δ'_y = yield displacement at first yield of tensile reinforcement (in.); and

Δ_y = yield displacement of elastoplastic approximation (in.).

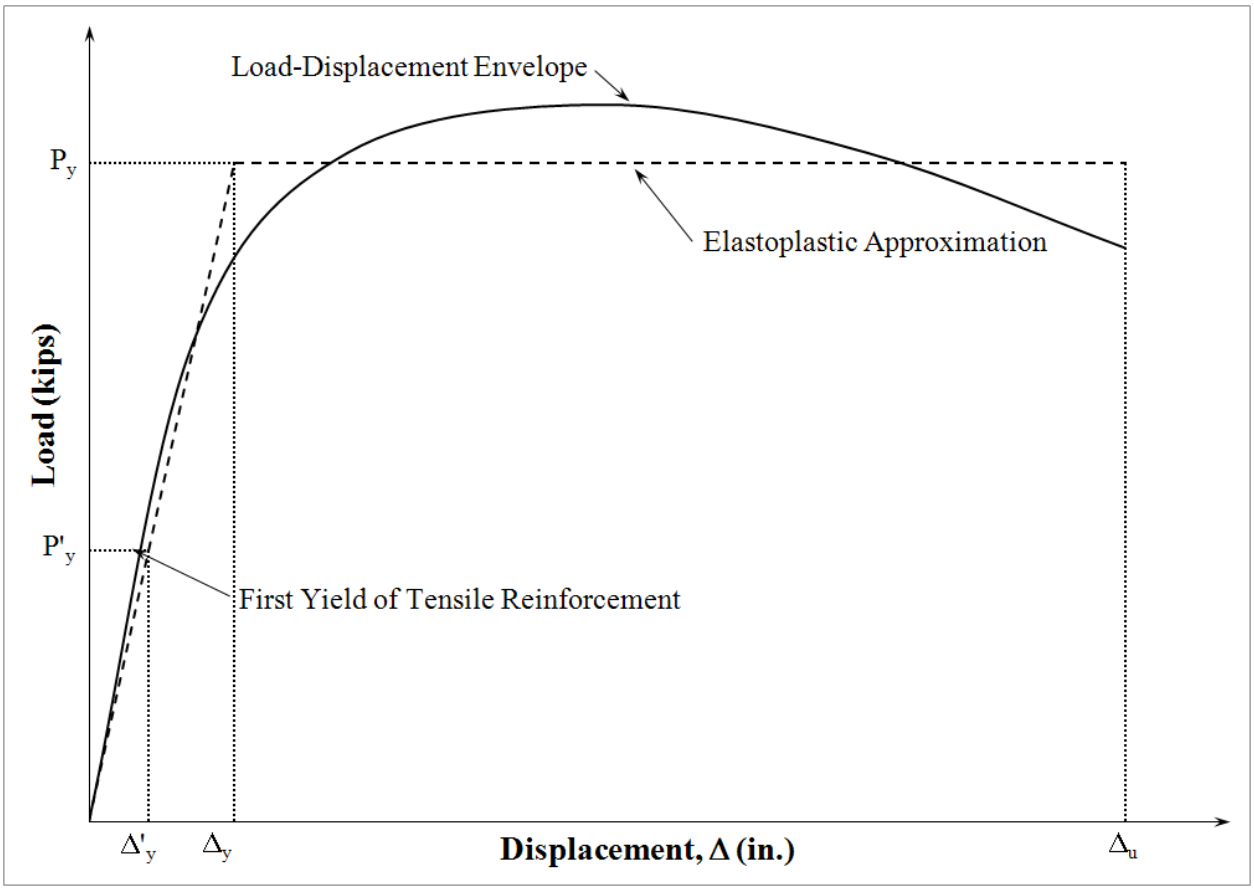

Figure 4.9 Elastoplastic Approximation

The displacement ductility for Specimen 1A is presented in Table 4.3 for both loading directions along with the average value. The total drift obtained at 20% load degradation (with Δ_u = 2.20 in.) was 2.8%.

Table 4.3 Specimen 1A: Displacement Ductility

Direction of Load	Displacement					
	P'_y (kips)	Δ'_y (in.)	Δ_u (in.)	P_y (kips)	Δ_y (in.)	μ_Δ
Push South	-27.6	-0.31	-2.64	-37.5	-0.42	6.2
Pull North	27.3	0.28	1.77	38.9	0.40	4.4
Average	27.5	0.30	2.20	38.2	0.41	5.3

The curvature ductility was also determined using a similar process as the displacement ductility and was defined as:

$$\mu_\phi = \frac{\phi_u}{\phi_y} \qquad \text{(Eqn. 4.5)}$$

Where:

μ_ϕ = curvature ductility;

ϕ_u = ultimate curvature at 20% load degradation (in.$^{-1}$); and

ϕ_y = yield curvature of elastoplastic approximation (in.$^{-1}$).

The ultimate curvature was defined as 20% load degradation or the last valid reading from the potentiometers. The elastoplastic approximations for the curvature ductility was based on the area under the moment-curvature envelope obtained using the Trapezoidal Rule. The curvature ductility for Specimen 1A is presented in Table 4.4 for both loading directions along with the average value.

Table 4.4 Specimen 1A: Curvature Ductility

Direction of Load	Curvature					
	M'_y (kip-in.)	ϕ'_y (in.$^{-1}$)	ϕ_u (in.$^{-1}$)	M_y (kip-in.)	ϕ_y (in.$^{-1}$)	μ_ϕ
Push South	-2190	-0.00017	-0.0017	-3063	-0.00023	7.3
Pull North	2165	0.00013	0.0023	3092	0.00019	12.3
Average	2178	0.00015	0.0020	3077	0.00021	9.5

Height of Plasticity and Equivalent Plastic Hinge Length:

The height of the plasticity zone (L_p) was defined as the height above the base of the wall where the average curvatures at failure were higher than the average curvature at the initial yield of the extreme tensile reinforcement. Failure was defined as 20% load degradation or the last valid reading from the potentiometers. The height of plasticity for Specimen 1A is presented in Table 4.5 for both loading directions along with the average value. The ratio of the average plasticity zone height to the wall length is also tabulated.

Table 4.5 Specimen 1A: Height of Plasticity

Direction of Load	Height of Plasticity Zone (in.)
Push South	26.1
Pull North	25.4
Average	25.7
L_p/L_w	65.0%

The equivalent plastic hinge length (l_p) was determined by rearranging Equation 4.6, presented by Paulay and Priestley (1992), which represents the ultimate displacement of the wall at 20% load degradation. The first term is the yield displacement, and the second term was defined as the plastic displacement for the idealized curvature profile over the wall height. By use of an elastoplastic approximation, the equivalent plastic hinge length for both loading directions and their average are given in Table 4.6. The ratio of the average equivalent plastic hinge length to the wall length is also tabulated.

$$\Delta_u = \frac{\phi_y h_w^2}{3} + (\phi_u - \phi_y)(l_p)\left(h_w - \frac{l_p}{2}\right) \qquad \text{(Eqn. 4.6)}$$

Table 4.6 Specimen 1A: Equivalent Plastic Hinge Length

Direction of Load	Plastic Hinge Length (in.)
Push South	22.1
Pull North	9.2
Average	15.7
l_p/L_w	39.5%

Energy Dissipation:

The total energy dissipated by a wall was determined at the end of the displacement level in which failure occurred for both loading directions. The area (energy) under the hysteresis loops was obtained by using the Trapezoidal Rule shown in Equation 4.7, the basis of which is illustrated in Figure 4.10. The equation calculates the energy under the curve to the axis between

the data points. The equation assumes a straight line between the two points and calculates the total area contained within the loops by adding area for the data points (Δ_1, L_1) and (Δ_2, L_2) and then subtracting the area for data points (Δ_3, L_3) and (Δ_4, L_4). The equation applies in all four load-displacement quadrants.

$$E = \frac{1}{2}(\Delta_2 - \Delta_1)(L_2 + L_1) \qquad \text{(Eqn. 4.7)}$$

Where:

E = energy between data points (kip-in.);

$\Delta_{1,2}$ = displacement at data points (in.); and

$L_{1,2}$ = load at data points (kip);

The total energy dissipated by Specimen 1A through the displacement level at which failure occurred in both loading directions was 529 kip-in.

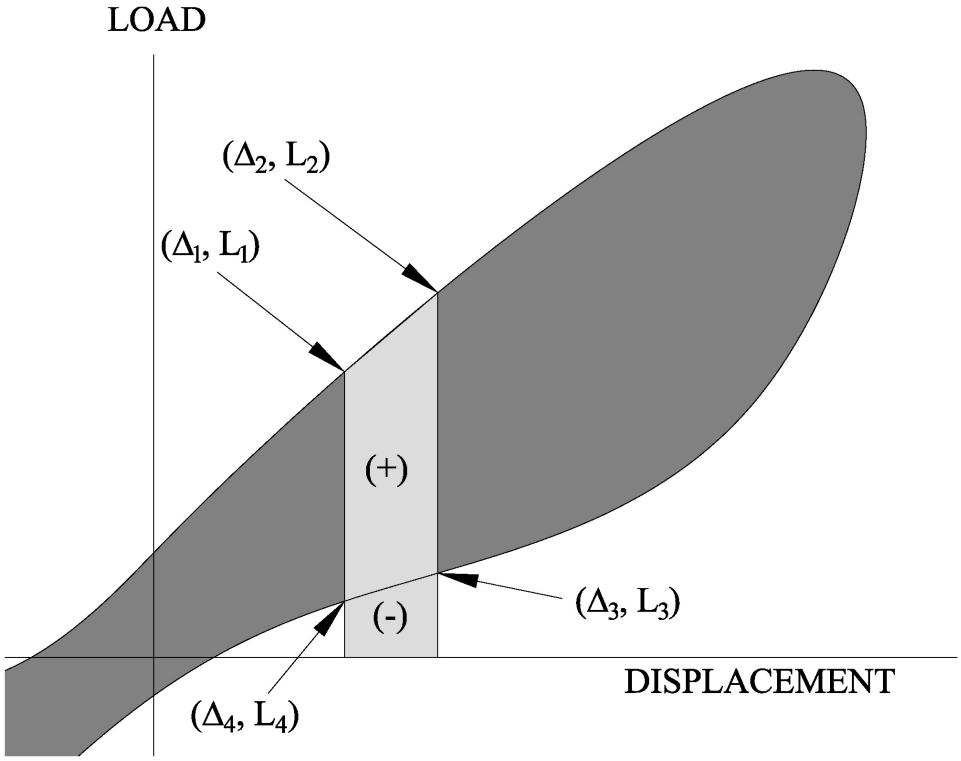

Figure 4.10 Total Energy Equation Illustration (adapted from Snook, 2005)

4.3 Specimen 1B

Specimen 1B had an aspect ratio of 2.0, No. 6 flexural reinforcement spaced 8 in. on center with a 33-in. long splice at the wall base, No. 4 shear reinforcement spaced 8 in. on center, and an axial load of 48 kips. Specimen 1B had a predicted capacity of 34 kips from the 2008 MSJC Code and 38.1 kips from the XTRACT analysis. The horizontal reinforcement yielded in both the first and fifth courses. Specimen 1B experienced yielding of the extreme vertical reinforcement in the footing.

Test Observations:

A yield displacement (Δ_y) of 0.33 in. was obtained from the preliminary test. The specimen was then loaded to displacements of ±1, 2, 3, 4, 6, and 8 times the yield displacement for the primary test. The entire specimen and north and south toe regions of the wall at test completion are presented in Figures 4.11 and 4.12. Test observations along with corresponding lateral displacements and loads follow. Wall behavior was dominated by flexure during testing with minimal shear cracking. Flexural cracks developed at $1\Delta_y$, and moderate crushing and spalling of both toes in the first and second courses occurred near failure. Vertical splitting was observed on the end faces of the wall at $3\Delta_y$. All of the separation at the mortar joints occurred at the wall base.

Figure 4.11 End-of-Test Picture of Entire Specimen 1B

Figure 4.12 End-of-Test Pictures for Specimen 1B: South Toe (left) and North Toe (right)

Table 4.7 Specimen 1B Test Observations

Load (kips)	Disp. (in.)	Test Observation
-27.0	-0.24	1st Yield of extreme vertical reinforcement bar in south toe (push)
30.2	0.24	1st Yield of extreme vertical reinforcement bar in north toe (pull)
-30.8	-0.33	*Flexural cracking in north toe (push)
-30.8	-0.33	Critical masonry strain in south toe (push)
35.6	0.34	*Flexural cracking in south toe (pull)
34.1	0.34	Critical masonry strain in north toe (pull)
-39.5	-0.75	1% Drift in push to south
43.2	0.75	1% Drift in pull to north
-38.9	-0.99	*Onset of toe crushing in south toe (push)
47.3	1.01	Maximum load resistance in pull to north
-42.9	-1.34	Maximum load resistance in push to south
44.3	1.35	*Onset of toe crushing in north toe (pull)
41.7	1.35	20% load degradation from maximum load resistance in pull to north
-33.4	-2.00	20% load degradation from maximum load resistance in push to south

* visual observation

Load-Displacement:

The load-displacement hysteresis curves for the preliminary and primary tests for Specimen 1B are given in Figure 4.13. All major events were marked on the load-displacement curve and are presented in Table 4.7 with their corresponding lateral displacement and load values at a specific point during the scan. The initial yielding of the extreme tensile reinforcement (ε_y = 0.00223 in./in.) occurred near the end of the preliminary test in the push direction and at $1\Delta_y$ in the pull direction. Critical masonry strain occurred at the cycle peaks of $1\Delta_y$ of the primary test in both loading directions. The specimen reached 1% drift at $3\Delta_y$ of the primary test. Toe crushing occurred at the second cycle of $3\Delta_y$, preceding the peak load in the push direction and at $4\Delta_y$ following peak load in the pull direction. The onset of toe crushing in both toe regions is presented in Figure 4.14. The wall experienced a rapid drop in strength at $6\Delta_y$ in the pull direction, with a gradual decrease in strength in the push direction following the peak load. The wall exhibited more yielding in the south toe region (push direction) than in the north toe.

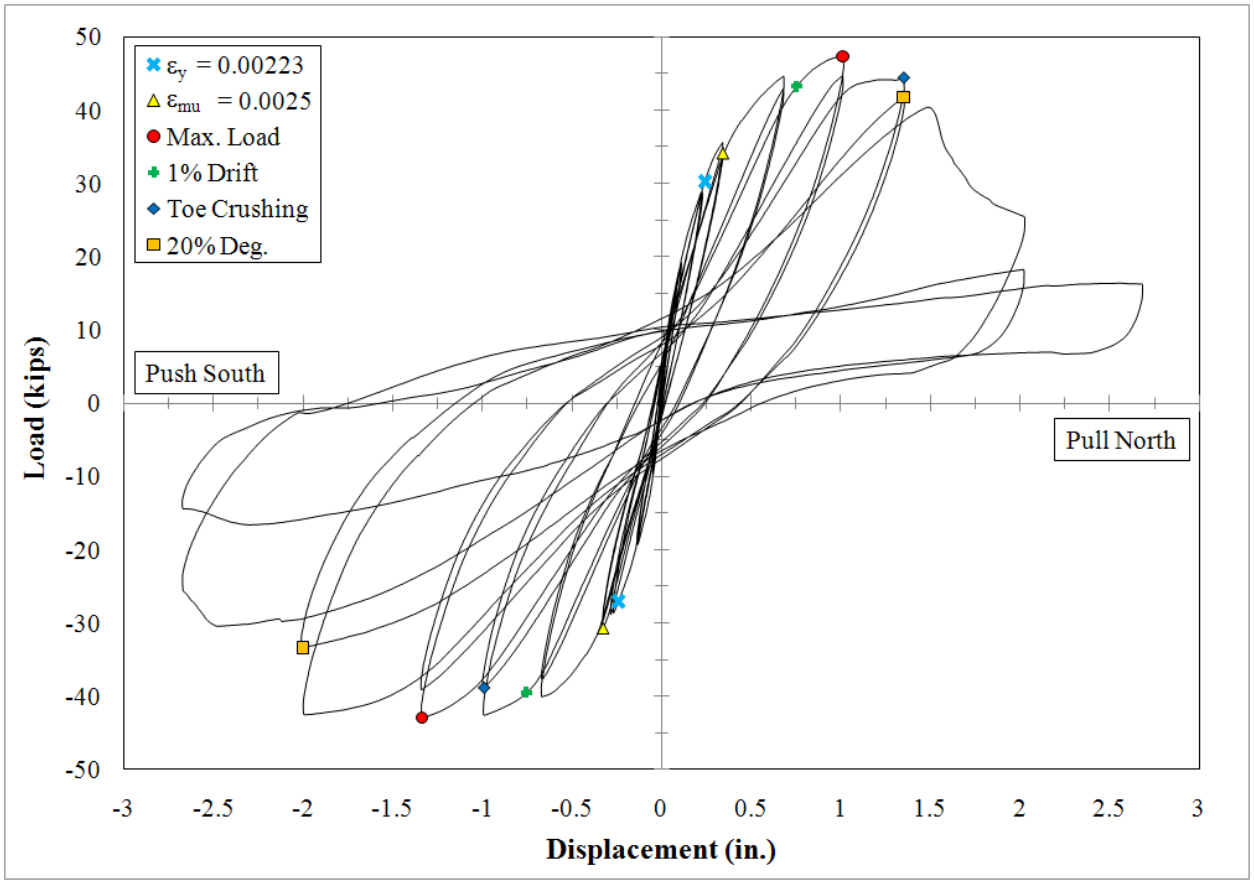

Figure 4.13 Specimen 1B: Load-Displacement Hysteresis Curve

Figure 4.14 Onset of Toe Crushing for Specimen 1B: South Toe (left) and North Toe (right)

Components of Displacements and Drifts:

Load-displacement curves for each component of displacement and the total displacement are given in Figure 4.15. Average drift contributions from sliding, shear, and flexural deformations and total drift at the three limit states of critical masonry strain, peak lateral load, and failure are given in Table 4.8. Specimen 1B was dominated by flexural deformations, with small levels of shear and sliding deformations occurring near failure.

Table 4.8 Specimen 1B: Component Percentages of Total Drift

Limit State	Total Drift (%)	Sliding (% Total)	Shear (% Total)	Flexural (% Total)
ε_{mu}	0.4	0.4	3.1	96.6
Peak Load	1.5	1.6	5.5	92.9
Failure	2.1	1.6	5.3	93.1

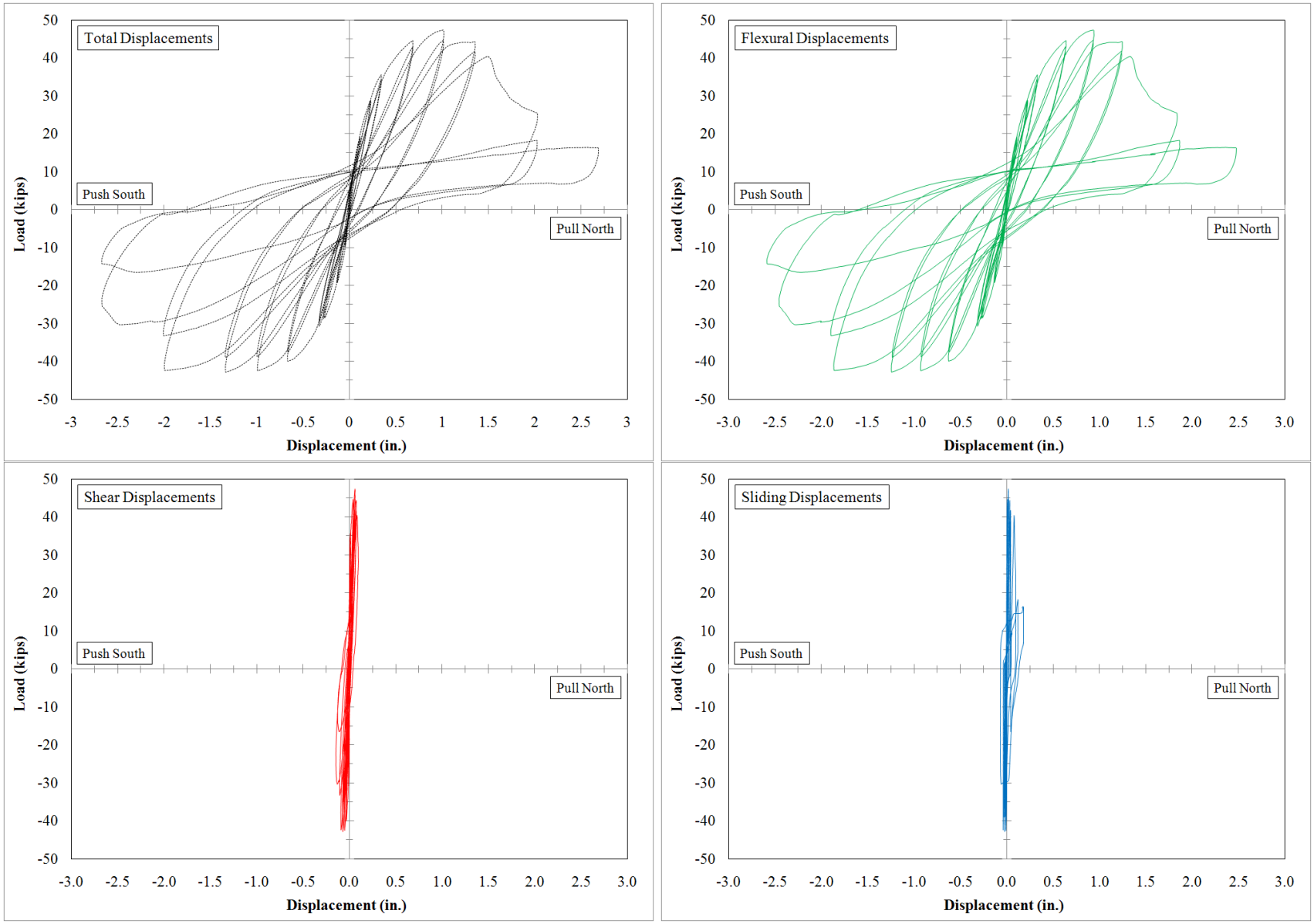

Figure 4.15 Specimen 1B: Displacements from Associated Components

Wall Curvatures:

A plot of curvature over the wall height of Specimen 1B is shown in Figure 4.16. Curvatures along the wall height of Specimen 1B were symmetric about its center line (mid-length of wall) up to $6\Delta_y$ in both directions. The ultimate curvature was defined at the 20% load degradation of the peak load for both directions. The curvature was approximately zero at the second height level (~12 in. above the footing) with a significant increase at the first height level (~4 in. above the footing).

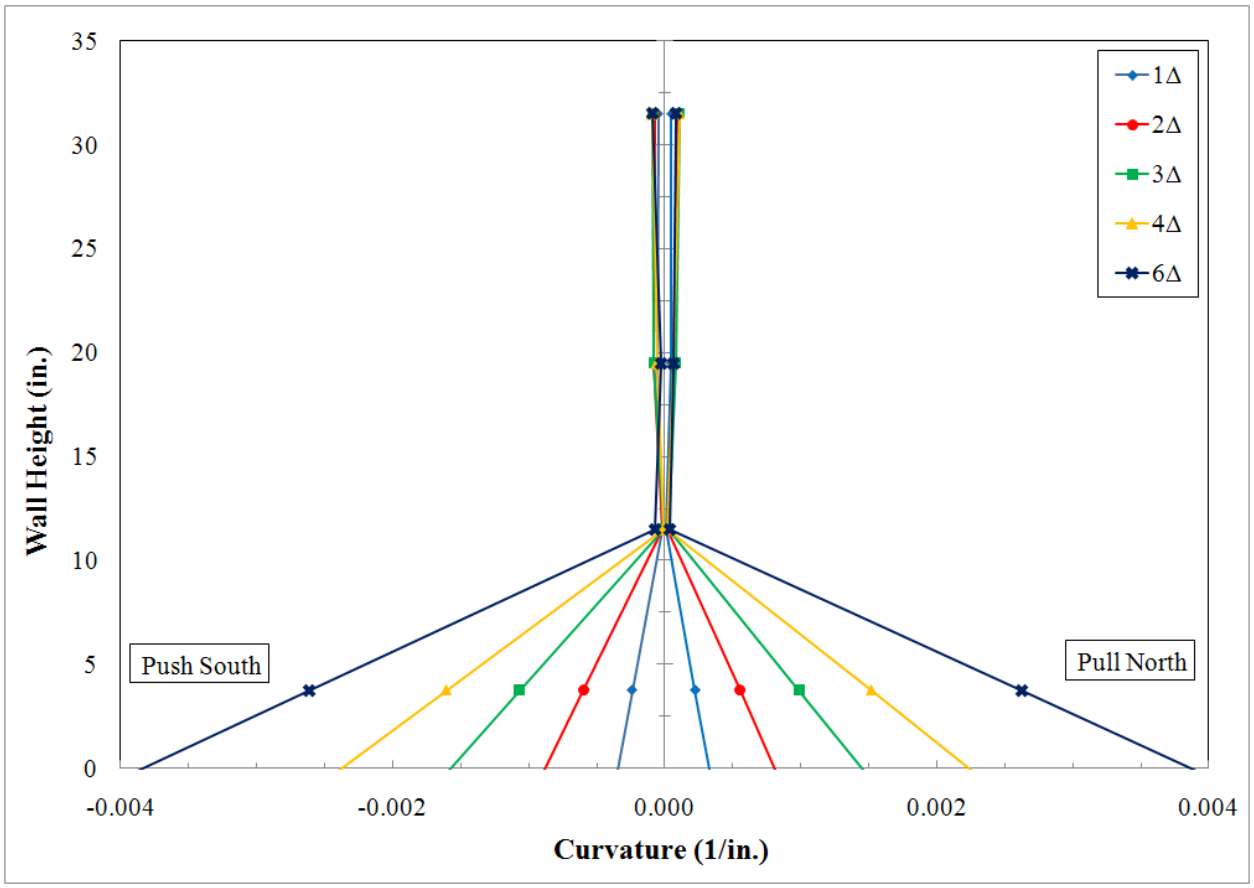

Figure 4.16 Specimen 1B: Wall Curvature

Ductility:

The displacement ductility for Specimen 1B is presented in Table 4.9 for both loading directions along with the average value. The total drift obtained at 20% load degradation (with Δ_u = 1.68 in.) was 2.1%.

Table 4.9 Specimen 1B: Displacement Ductility

Direction of Load	Displacement					
	P'_y (kips)	Δ'_y (in.)	Δ_u (in.)	P_y (kips)	Δ_y (in.)	μ_Δ
Push South	-27.0	-0.24	-2.00	-39.4	-0.35	5.7
Pull North	30.2	0.24	1.35	43.9	0.35	3.8
Average	28.6	0.24	1.68	41.7	0.35	4.8

The curvature ductility for Specimen 1B is presented in Table 4.10 for both loading directions along with the average value.

Table 4.10 Specimen 1B: Curvature Ductility

Direction of Load	Curvature					
	M'_y (kip-in.)	ϕ'_y (in.$^{-1}$)	ϕ_u (in.$^{-1}$)	M_y (kip-in.)	ϕ_y (in.$^{-1}$)	μ_ϕ
Push South	-2142	-0.00017	-0.0023	-3153	-0.00025	9.2
Pull North	2396	0.00015	0.0016	3488	0.00022	7.0
Average	2269	0.00016	0.0019	3321	0.00023	8.1

Height of Plasticity and Equivalent Plastic Hinge Length:

The height of plasticity and equivalent plastic hinge length for both loading directions and their averages are given in Table 4.11. The ratio of the average plasticity zone height to the wall length and the equivalent plastic hinge length to the wall length are also tabulated.

Table 4.11 Specimen 1B: Height of Plasticity & Equivalent Plastic Hinge Length

Direction of Load	Height of Plasticity Zone (in.)	Plastic Hinge Length (in.)
Push South	11.0	11.4
Pull North	11.0	10.7
Average	11.0	11.1
(L_p or l_p)/L_w	27.7%	27.9%

Energy Dissipation:

The total energy dissipated by Specimen 1B through the displacement level at which failure occurred in both loading directions was 356 kip-in.

4.4 Specimen 2A

Specimen 2A had an aspect ratio of 2.0, No. 4 flexural reinforcement spaced 8 in. on center with no splice at the wall base, No. 4 shear reinforcement spaced 8 in. on center, and an axial load of 95 kips. Specimen 2A had a predicted capacity of 30 kips from the 2008 MSJC Code and 31.6 kips from the XTRACT analysis. The horizontal reinforcement yielded in the first course, but not in the fifth course. Specimen 2A experienced yielding of the extreme vertical reinforcement in the footing.

Test Observations:

A yield displacement (Δ_y) of 0.18 in. was obtained from the preliminary test. The specimen was then loaded to displacements of ±1, 2, 3, 4, 6, 8, 10, and 12 times the yield displacement for the primary test. The entire specimen and north and south toe regions of the wall at test completion at presented in Figures 4.17 and 4.18. Test observations along with corresponding lateral displacements and loads follow.

Wall behavior was dominated by flexure during testing with minimal shear cracking. Flexural cracks developed at $2\Delta_y$, and moderate crushing and spalling of both toes in the second and third courses occurred near failure. Vertical splitting was observed on the end faces of the wall at $4\Delta_y$. Most of the separation at the mortar joints occurred at the wall base and gradually decreased along the height of the wall. Buckling of the extreme reinforcement that occurred near the end of testing at higher displacement levels is shown in Figure 4.18.

Figure 4.17 End-of-Test Picture of Entire Specimen 2A

Figure 4.18 End-of-Test Pictures for Specimen 2A: South Toe (left) and North Toe (right)

Table 4.12 Specimen 2A Test Observations

Load (kips)	Disp. (in.)	Test Observation
-27.1	-0.21	1st Yield of extreme vertical reinforcement bar in south toe (push)
28.7	0.21	1st Yield of extreme vertical reinforcement bar in north toe (pull)
-32.9	-0.36	*Flexural cracking in north toe (push)
34.9	0.37	*Flexural cracking in south toe (pull)
-34.3	-0.43	Critical masonry strain in south toe (push)
36.2	0.46	Critical masonry strain in north toe (pull)
37.2	0.55	Maximum load resistance in pull to north
-37.4	-0.71	Maximum load resistance in push to south
-32.2	-0.76	1% Drift in push to south
34.6	0.76	1% Drift in pull to north
-33.3	-1.08	*Onset of toe crushing in south toe (push)
36.2	1.09	*Onset of toe crushing in north toe (pull)
-31.8	-1.79	20% load degradation from maximum load resistance in push to south
21.0	1.82	20% load degradation from maximum load resistance in pull to north

* visual observation

Load-Displacement:

The load-displacement hysteresis curves for the preliminary and primary tests for Specimen 2A are given in Figure 4.19. All major events were marked on the load-displacement curve and are presented in Table 4.12 with their corresponding lateral displacement and load values at a specific point during the scan. The initial yielding of the extreme tensile reinforcement (ε_y = 0.00228 in./in.) occurred just beyond the peak of $1\Delta_y$ in both directions. Critical masonry strain occurred near the cycle peaks of $3\Delta_y$ of the primary test in both loading directions. The specimen reached peak load at the first cycle of $3\Delta_y$ in the pull direction and at the first cycle of $4\Delta_y$ in the push direction. The 1% drift was reached at $4\Delta_y$, which preceded the onset of toe crushing (illustrated in Figure 4.20) that occurred in the first cycle of $4\Delta_y$. The 20% load degradation was defined at the first cycle of $10\Delta_y$ in both loading directions. The specimen exhibited nearly symmetrical responses between the two loaded directions for the entire test.

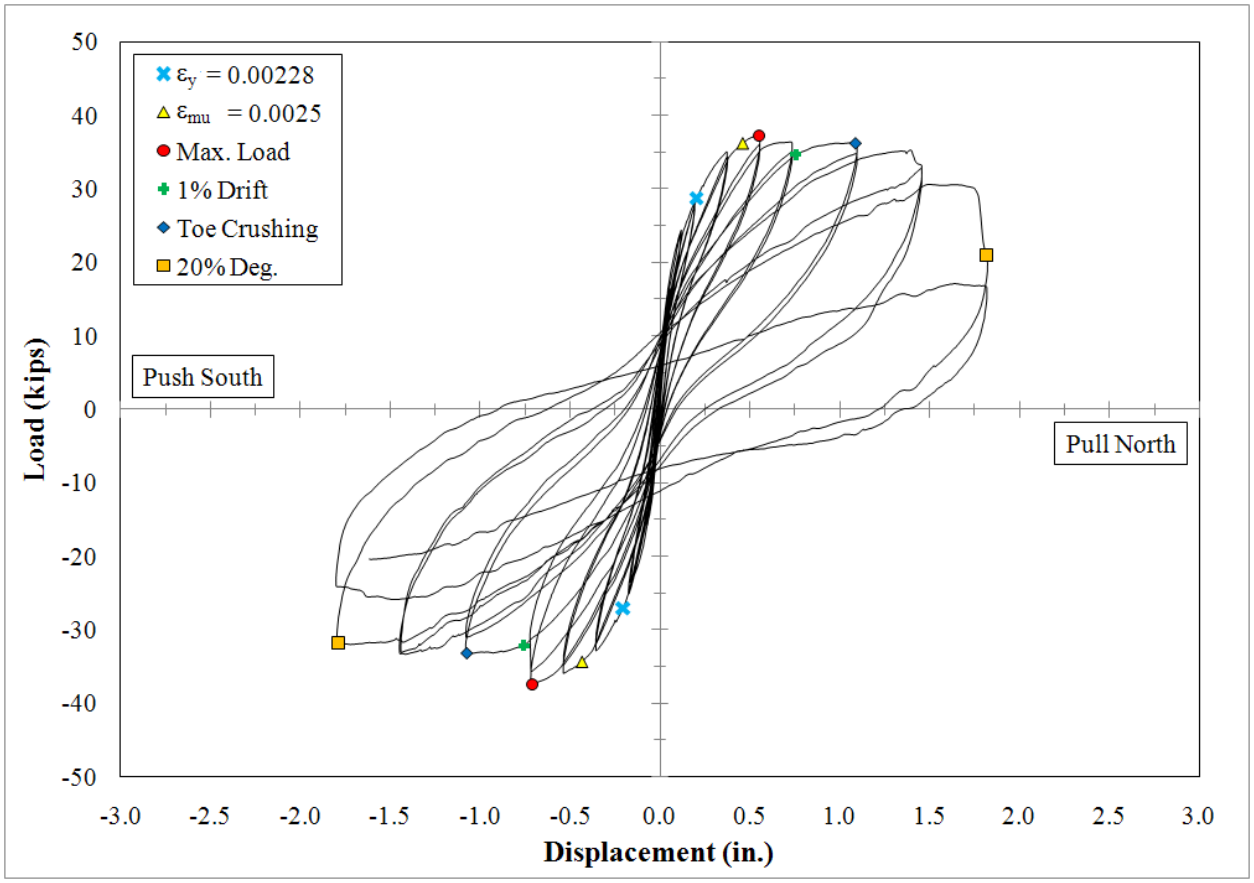

Figure 4.19 Specimen 2A: Load-Displacement Hysteresis Curve

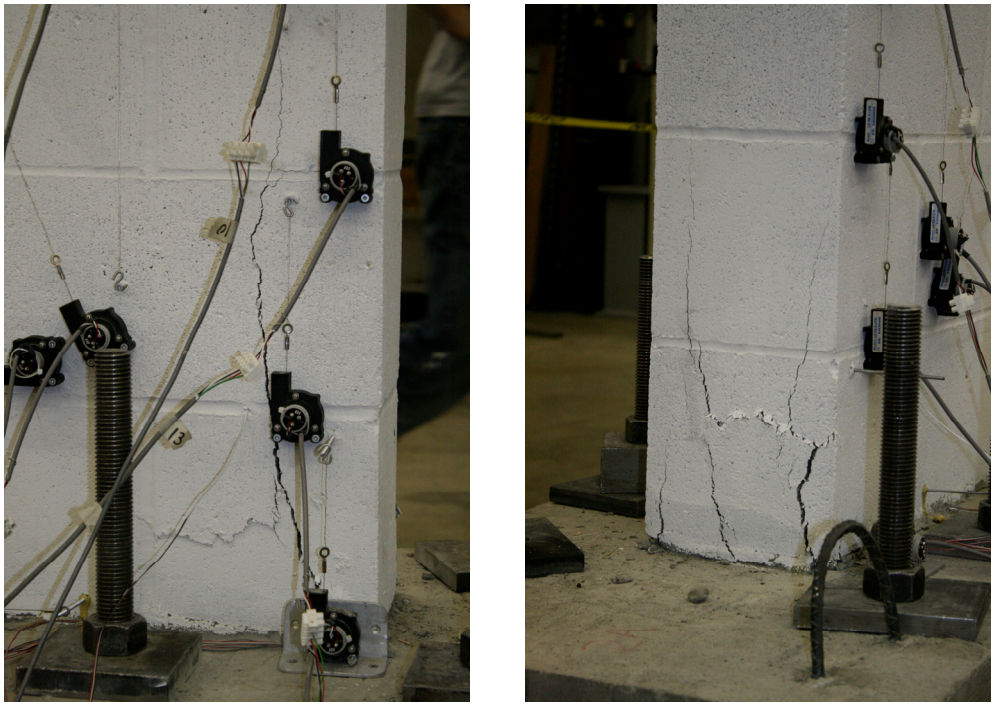

Figure 4.20 Onset of Toe Crushing for Specimen 2A: South Toe (left) and North Toe (right)

Components of Displacements and Drifts:

Load-displacement curves for each component of displacement and the total displacement are presented in Figure 4.21. Average drift contributions from sliding, shear, and flexural deformations and total drift at the three limit states of critical masonry strain, peak lateral load, and failure are given in Table 4.13. Specimen 2A was dominated by flexural deformations, with small levels of shear and sliding deformations occurring near failure.

Table 4.13 Specimen 2A: Component Percentages of Total Drift

Limit State	Total Drift (%)	Sliding (% Total)	Shear (% Total)	Flexural (% Total)
ε_{mu}	0.6	0.6	5.2	94.7
Peak Load	0.8	0.5	5.4	94.3
Failure	2.3	0.0	4.9	95.3

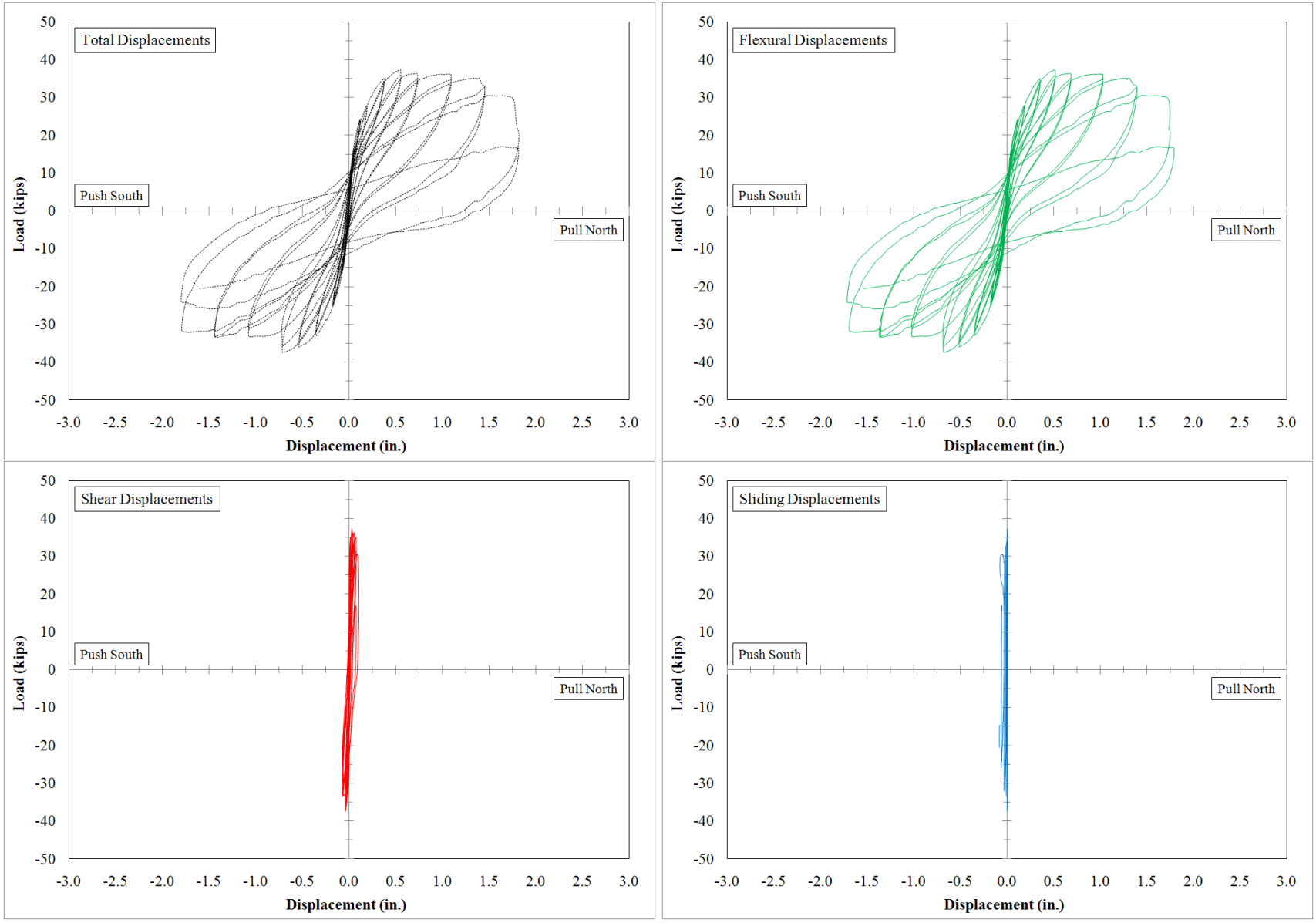

Figure 4.21 Specimen 2A: Displacements from Associated Components

Wall Curvatures:

A plot of curvature along the wall height of Specimen 2A is shown in Figure 4.22. Curvatures were symmetric about its center line (mid-length of wall) up to $4\Delta_y$ in both loading directions. The ultimate curvature was defined at the second cycle of $6\Delta_y$ for both loading directions instead of the 20% load degradation of the peak load. This was due to invalid measurements from the potentiometers that began in the pull direction of $6\Delta_y$.

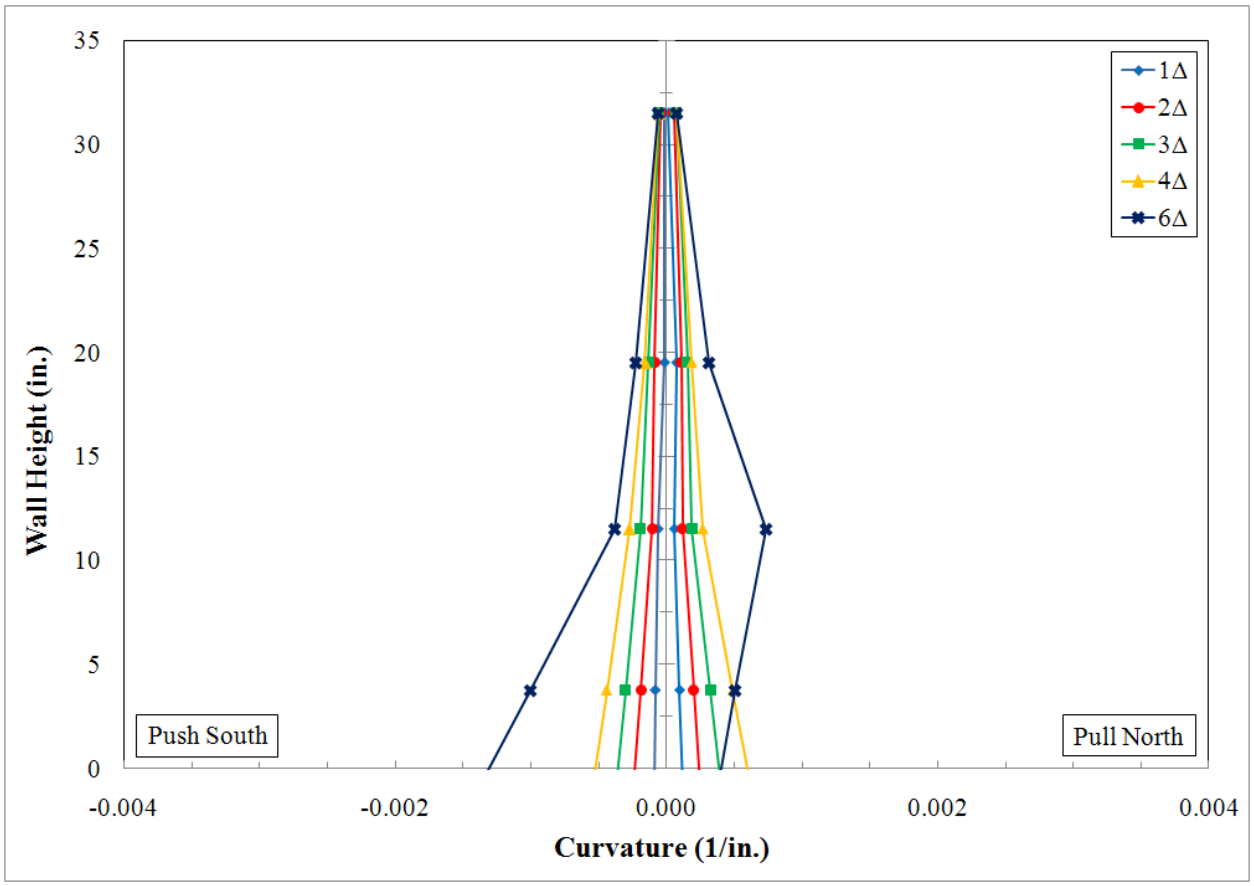

Figure 4.22 Specimen 2A: Wall Curvature

Ductility:

The displacement ductility for Specimen 2A is presented in Table 4.14 for both loading directions along with the average value. The total drift obtained at 20% load degradation (with Δ_u = 1.80 in.) was 2.3%.

Table 4.14 Specimen 2A: Displacement Ductility

Direction of Load	Displacement					
	P'_y (kips)	Δ'_y (in.)	Δ_u (in.)	P_y (kips)	Δ_y (in.)	μ_Δ
Push South	-27.1	-0.21	-1.79	-34.4	-0.26	6.8
Pull North	28.6	0.21	1.82	34.1	0.24	7.4
Average	27.9	0.21	1.80	34.2	0.25	7.1

The curvature ductility for Specimen 2A is presented in Table 4.15 for both loading directions along with the average value.

Table 4.15 Specimen 2A: Curvature Ductility

Direction of Load	Curvature					
	M'_y (kip-in.)	ϕ'_y (in.$^{-1}$)	ϕ_u (in.$^{-1}$)	M_y (kip-in.)	ϕ_y (in.$^{-1}$)	μ_ϕ
Push South	-2149	-0.00009	-0.0012	-2756	-0.00012	9.8
Pull North	2270	0.00010	0.0009	2861	0.00012	7.6
Average	2209	0.00010	0.0011	2808	0.00012	8.7

Height of Plasticity and Equivalent Plastic Hinge Length:

The height of plasticity and equivalent plastic hinge length for both loading directions and their averages are given in Table 4.16. The ratio of the average plasticity zone height to the wall length and the equivalent plastic hinge length to the wall length are also tabulated.

Table 4.16 Specimen 2A: Height of Plasticity & Equivalent Plastic Hinge Length

Direction of Load	Height of Plasticity Zone (in.)	Plastic Hinge Length (in.)
Push South	29.0	20.9
Pull North	30.4	29.8
Average	29.7	25.4
(L_p or l_p)/L_w	74.9%	64.0%

Energy Dissipation:

The total energy dissipated by Specimen 2A through the displacement level at which failure occurred in both loading directions was 363 kip-in.

4.5 Specimen 2B

Specimen 2B had an aspect ratio of 2.0, No. 4 flexural reinforcement spaced 8 in. on center with a 16-in. long splice at the wall base, No. 4 shear reinforcement spaced 8 in. on center, and an axial load of 95 kips. Specimen 2B had a predicted capacity of 30 kips from the 2008 MSJC Code and 31.6 kips from the XTRACT analysis. The horizontal reinforcement in the first and fifth courses did not yield during testing. The extreme vertical reinforcement did not yield in the footing for Specimen 2B.

Test Observations:

A yield displacement (Δ_y) of 0.21 in. was obtained from the preliminary test. The specimen was then loaded to displacements of ±1, 2, 3, 4, 6, 8, and 10 times the yield displacement for the primary test. The entire specimen and north and south toe regions of the wall at test completion are presented in Figures 4.23 and 4.24. Test observations along with corresponding lateral displacements and loads follow. Wall behavior was dominated by flexure during testing with minimal shear cracking. Flexural cracks developed at $2\Delta_y$, and moderate crushing and spalling of both toes up to the third course occurred later in testing. Vertical splitting was observed on the end faces of the wall at $3\Delta_y$. Larger separation cracks at the joint between the second and third courses rather than at the joint between the first and second courses were observed during testing. Slight buckling of the extreme reinforcement occurred near the end of testing at higher displacement levels.

Figure 4.23 End-of-Test Picture of Entire Specimen 2B

Figure 4.24 End-of-Test Pictures for Specimen 2B: South Toe (left) and North Toe (right)

Table 4.17 Specimen 2B Test Observations

Load (kips)	Disp. (in.)	Test Observation
26.5	0.16	1st Yield of extreme vertical reinforcement bar in north toe (pull)
-25.9	-0.21	1st Yield of extreme vertical reinforcement bar in south toe (push)
-32.3	-0.36	Critical masonry strain in south toe (push)
-33.7	-0.41	*Flexural cracking in north toe (push)
34.8	0.42	Critical masonry strain in north toe (pull)
35.6	0.42	*Flexural cracking in south toe (pull)
37.2	0.63	*Onset of toe crushing in north toe (pull)
38.4	0.63	Maximum load resistance in pull to north
-37.5	-0.75	1% Drift in push to south
38.2	0.75	1% Drift in pull to north
-37.1	-0.82	*Onset of toe crushing in south toe (push)
-37.1	-0.82	Maximum load resistance in push to south
-29.1	-1.23	20% load degradation from maximum load resistance in push to south
29.7	1.24	20% load degradation from maximum load resistance in pull to north

* visual observation

Load-Displacement:

The load-displacement hysteresis curves for the preliminary and primary tests for Specimen 2B are given in Figure 4.25. All major events were marked on the load-displacement curve and are presented in Table 4.17 with their corresponding lateral displacement and load values at a specific point during the scan. The initial yielding of the extreme tensile reinforcement (ε_y = 0.00225 in./in.) occurred near the cycle peak of $1\Delta_y$ in both loading directions. Critical masonry strain occurred near the cycle peaks of $2\Delta_y$ in the primary test in both loading directions. The wall reached the peak load and onset of toe crushing at $3\Delta_y$ in the pull direction and $4\Delta_y$ in the push direction. The onset of toe crushing in both toe regions is presented in Figure 4.26. The 1% drift was attained at $4\Delta_y$ of the primary test. The 20% load degradation was defined at the second cycle of $6\Delta_y$ in both loading directions. The specimen exhibited nearly symmetrical responses in the two loading directions for the entire test.

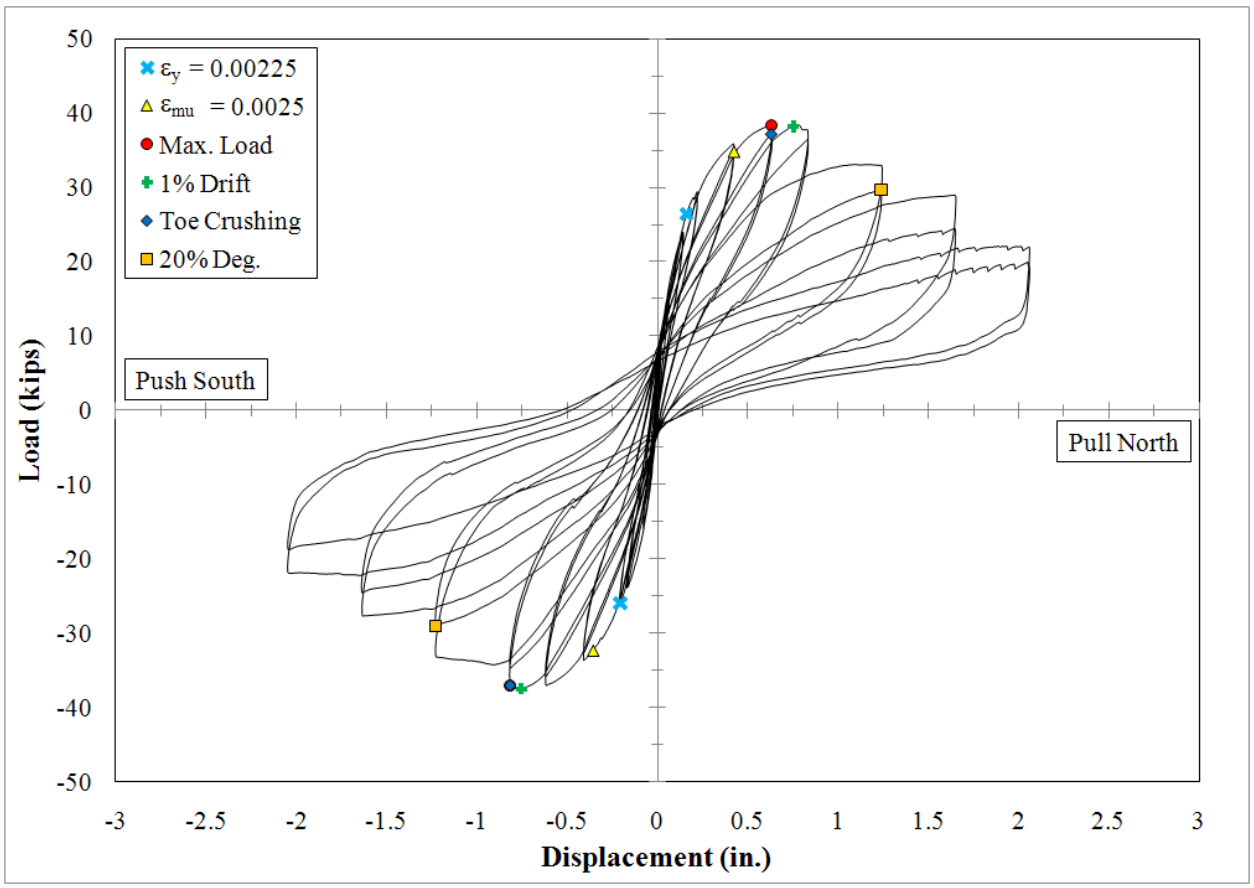

Figure 4.25 Specimen 2B: Load-Displacement Hysteresis Curve

Figure 4.26 Onset of Toe Crushing for Specimen 2B: South Toe (left) and North Toe (right)

Components of Displacements and Drifts:

Load-displacement curves for each component of displacement and the total displacement are given in Figure 4.27. Average drift contributions from sliding, shear, and flexural deformations and total drift at the three limit states of critical masonry strain, peak lateral load, and failure are given in Table 4.18. Specimen 2B was dominated by flexural deformations, with small levels of shear and sliding deformations occurring near failure in the pull direction.

Table 4.18 Specimen 2B: Component Percentages of Total Drift

Limit State	Total Drift (%)	Sliding (% Total)	Shear (% Total)	Flexural (% Total)
ε_{mu}	0.5	1.1	5.2	94.1
Peak Load	0.9	1.6	5.9	93.4
Failure	1.5	1.3	4.4	95.5

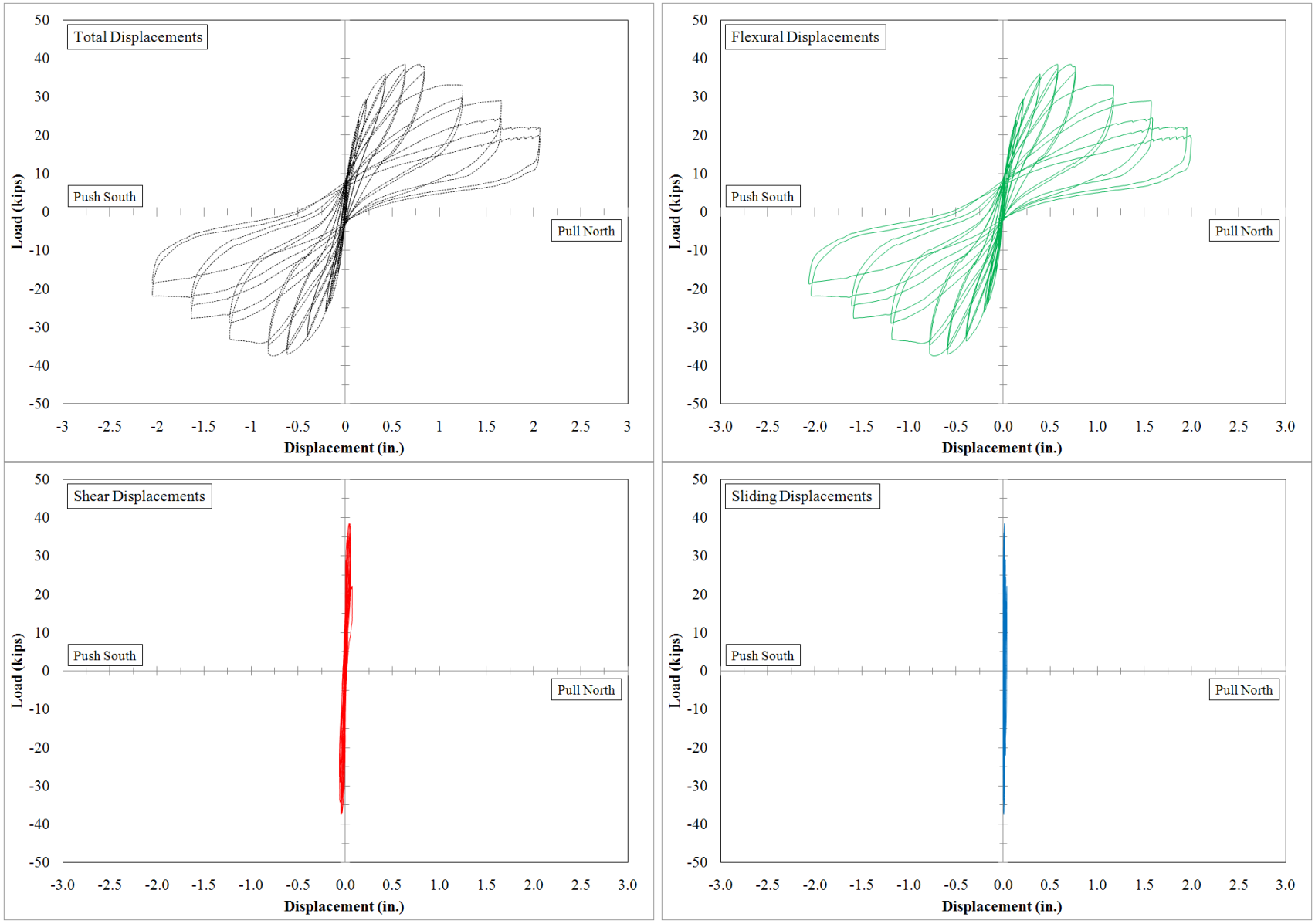

Figure 4.27 Specimen 2B: Displacements from Associated Components

Wall Curvatures:

A plot of curvature along the wall height of Specimen 2B is shown in Figure 4.28. Curvatures along the wall height of Specimen 2B were symmetric about its center line (mid-length of wall) up to $6\Delta_y$ in both directions. The ultimate curvature was defined at the 20% load degradation of the peak load for both directions. The curvature at the third height level (~20 in. above the footing) was higher than at the second height level (~12 in. above the footing). The potentiometer at the third height level was disconnected prior to pulling in the north direction at $8\Delta_y$.

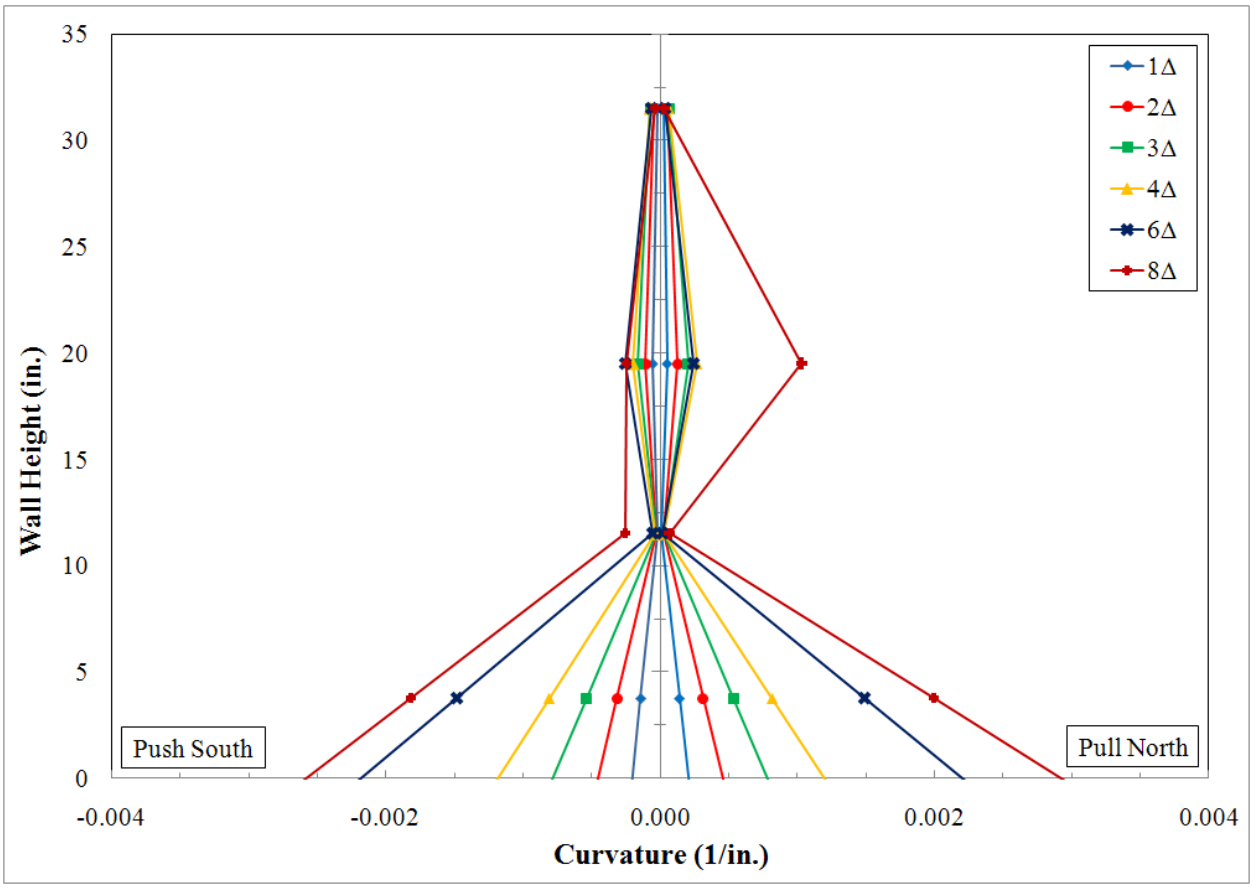

Figure 4.28 Specimen 2B: Wall Curvature

Ductility:

The displacement ductility for Specimen 2B is presented in Table 4.19 for both loading directions along with the average value. The total drift obtained at 20% load degradation (with Δ_u = 1.23 in.) was 1.6%.

Table 4.19 Specimen 2B: Displacement Ductility

Direction of Load	Displacement					
	P'_y (kips)	Δ'_y (in.)	Δ_u (in.)	P_y (kips)	Δ_y (in.)	μ_Δ
Push South	-25.9	-0.21	-1.23	-34.7	-0.27	4.5
Pull North	26.5	0.16	1.24	35.4	0.22	5.7
Average	26.2	0.18	1.23	35.0	0.25	5.0

The curvature ductility for Specimen 2B is presented in Table 4.20 for both loading directions along with the average value.

Table 4.20 Specimen 2B: Curvature Ductility

Direction of Load	Curvature					
	M'_y (kip-in.)	ϕ'_y (in.$^{-1}$)	ϕ_u (in.$^{-1}$)	M_y (kip-in.)	ϕ_y (in.$^{-1}$)	μ_ϕ
Push South	-2056	-0.00014	-0.0015	-2742	-0.00019	8.1
Pull North	2097	0.00011	0.0015	2792	0.00015	10.2
Average	2076	0.00013	0.0015	2767	0.00017	9.0

Height of Plasticity and Equivalent Plastic Hinge Length:

The height of plasticity and equivalent plastic hinge length for both loading directions and their averages are given in Table 4.21. The ratio of the average plasticity zone height to the wall length and the equivalent plastic hinge length to the wall length are also tabulated.

Table 4.21 Specimen 2B: Height of Plasticity & Equivalent Plastic Hinge Length

Direction of Load	Height of Plasticity Zone (in.)	Plastic Hinge Length (in.)
Push South	24.6	9.9
Pull North	27.2	10.6
Average	25.9	10.2
(L_p or l_p)/L_w	65.4%	25.8%

Energy Dissipation:

The total energy dissipated by Specimen 2B through the displacement level at which failure occurred in both loading directions was 155 kip-in.

4.6 Specimen 3

Specimen 3 had an aspect ratio of 1.0, No. 4 flexural reinforcement spaced 8 in. on center with a 16-in. long splice at the wall base, No. 4 shear reinforcement spaced 24 in. on center, and zero axial load. Specimen 3 had a predicted capacity of 49 kips from the 2008 MSJC Code and 59.7 kips from the XTRACT analysis. The horizontal reinforcement in the first and fourth courses did not yield during testing. The extreme vertical reinforcement did not yield in the footing for Specimen 3.

Test Observations:

A yield displacement (Δ_y) of 0.25 in. was obtained from the preliminary test. The specimen was then loaded to displacements of ±1, 2, 3, and 4 times the yield displacement for the primary test. The entire specimen and north and south toe regions of the wall at test completion are presented in Figures 4.29 and 4.30. Test observations along with corresponding lateral displacements and loads follow. Wall behavior was dominated by flexure, but diagonal shear cracks were evident in every course. Toe crushing and spalling of the toe regions did not occur in this wall. Vertical splitting was observed on the end faces of the wall at $3\Delta_y$.

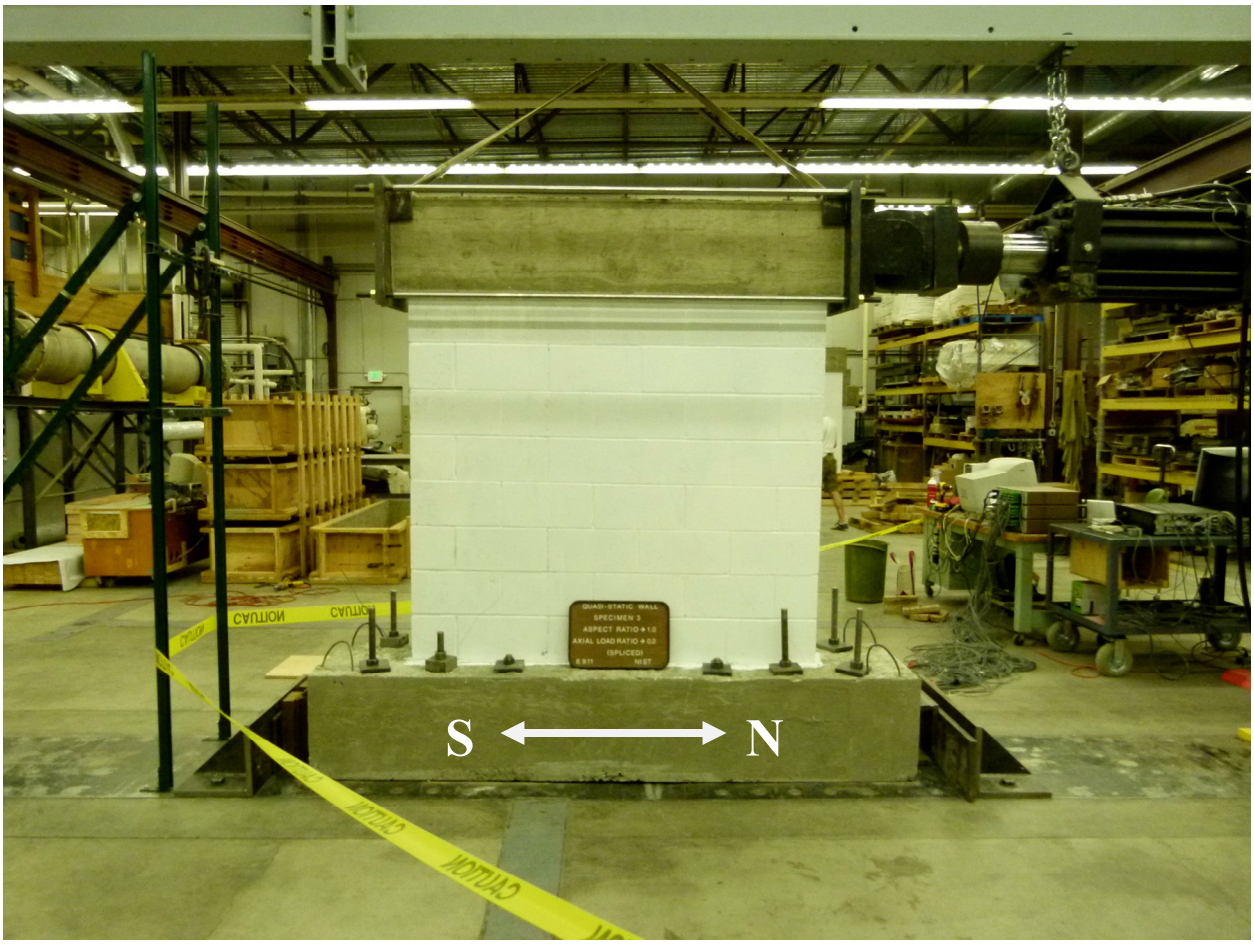

Figure 4.29 End-of-Test Picture of Entire Specimen 3

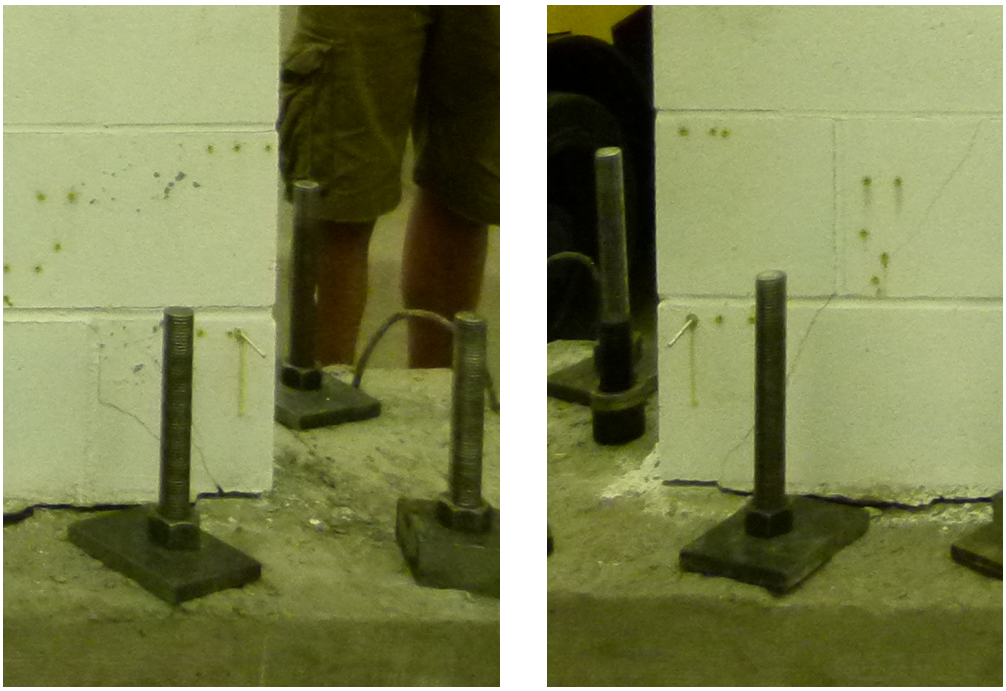

Figure 4.30 End-of-Test Pictures for Specimen 3: South Toe (left) and North Toe (right)

Table 4.22 Specimen 3 Test Observations

Load (kips)	Disp. (in.)	Test Observation
32.6	0.09	1st Yield of extreme vertical reinforcement bar in north toe (pull)
-33.8	-0.11	1st Yield of extreme vertical reinforcement bar in south toe (push)
-21.0	-0.12	Critical masonry strain in south toe (push)
36.2	0.15	Critical masonry strain in north toe (pull)
-48.0	-0.25	*Flexural cracking in north toe (push)
49.9	0.26	*Flexural cracking in south toe (pull)
-61.3	-0.48	Maximum load resistance in push to south
57.4	0.50	Maximum load resistance in pull to north
-49.3	-0.68	1% Drift in push to south
36.3	0.68	1% Drift in pull to north
-45.0	-0.74	20% load degradation from maximum load resistance in push to south
36.8	0.75	20% load degradation from maximum load resistance in pull to north

* visual observation

Load-Displacement:

The load-displacement hysteresis curves for the preliminary and primary tests for Specimen 3 are shown in Figure 4.31. All major events were marked on the load-displacement curve and are presented in Table 4.22 with their corresponding lateral displacement and load values at a specific point during the scan. The initial yielding of the extreme tensile reinforcement (ε_y = 0.00225 in./in.) occurred near the end of the preliminary test in both loading directions. Critical masonry strain was attained early at $1\Delta_y$ in the push direction and near the end of the same displacement level in the pull direction. The wall reached the peak load at the first cycle of $3\Delta_y$ in both loading directions. The 1% drift and 20% load degradation were attained at the first cycle of $4\Delta_y$. The wall strength degraded more rapidly in the pull direction following attainment of the peak lateral load.

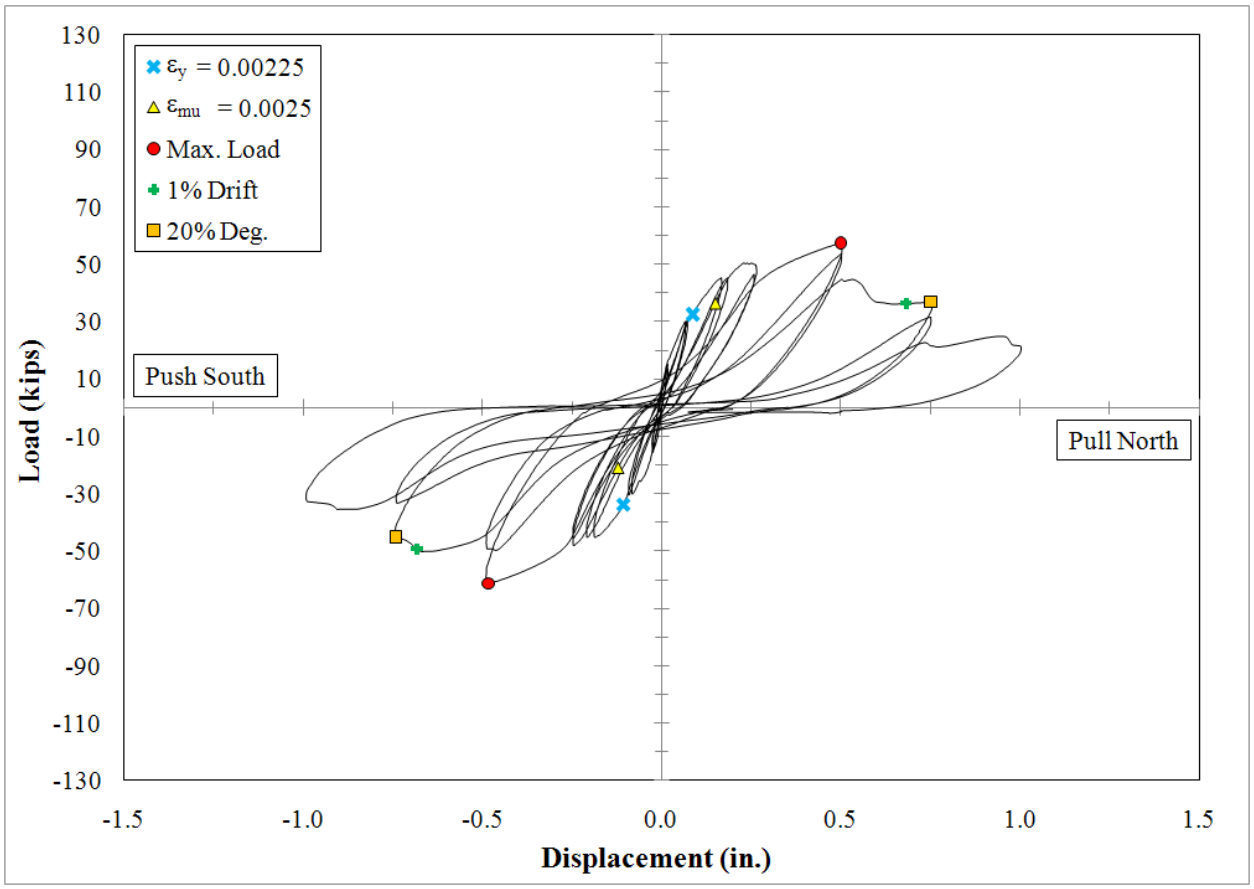

Figure 4.31 Specimen 3: Load-Displacement Hysteresis Curve

Components of Displacements and Drifts:

Load-displacement curves for each component of displacement and the total displacement are presented in Figure 4.32. Average drift contributions from sliding, shear, and flexural deformations and total drift at the three limit states of critical masonry strain, peak lateral load, and failure are given in Table 4.23. Specimen 3 was dominated by flexural deformations, with significant (~15% of total displacement) shear deformations and small levels of sliding deformations occurring near failure.

Table 4.23 Specimen 3: Component Percentages of Total Drift

Limit State	Total Drift (%)	Sliding (% Total)	Shear (% Total)	Flexural (% Total)
ε_{mu}	0.2	2.2	11.9	85.9
Peak Load	0.7	6.1	18.1	75.8
Failure	1.0	7.2	15.5	77.2

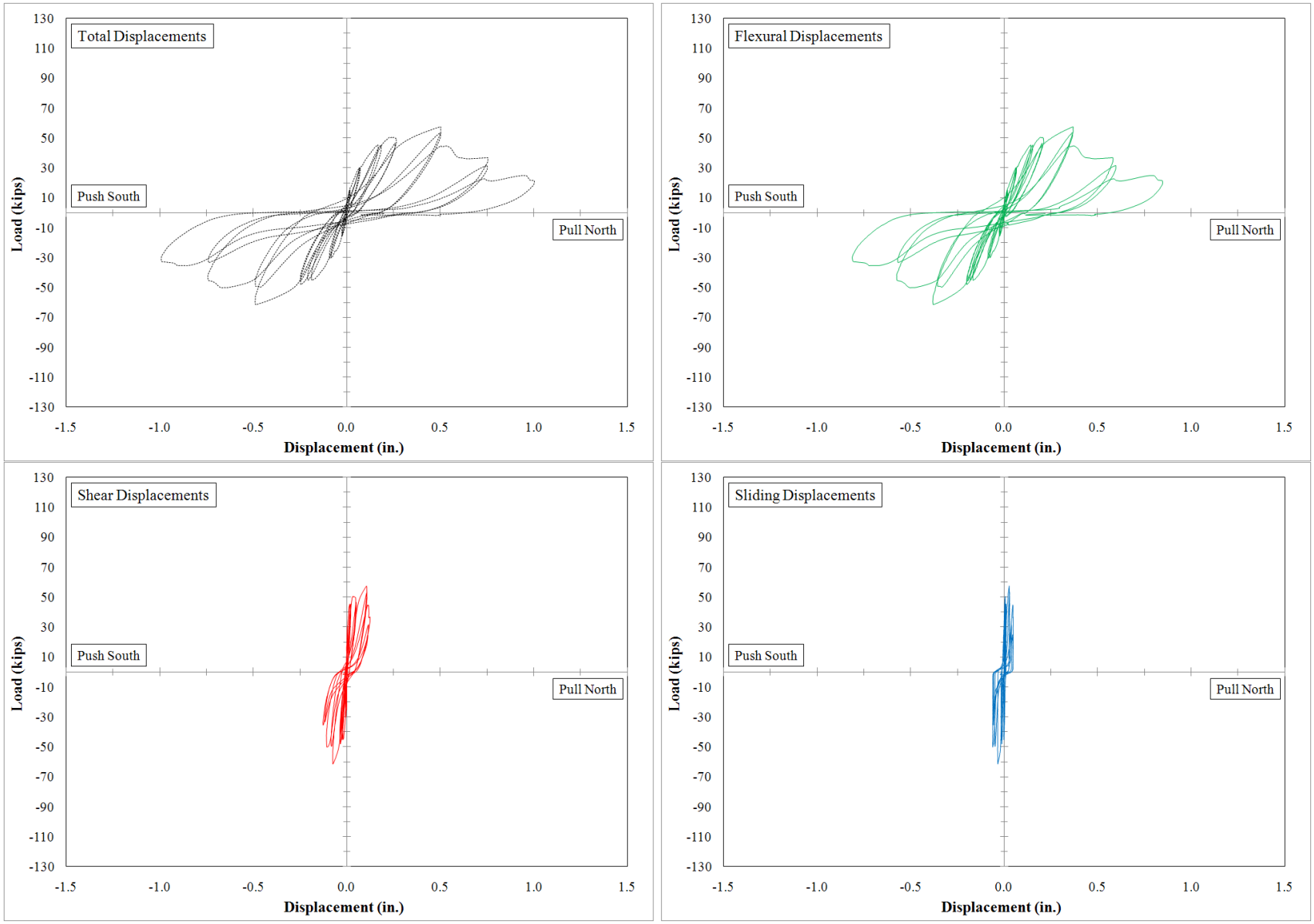

Figure 4.32 Specimen 3: Displacements from Associated Components

Wall Curvatures:

A plot of curvature along the wall height of Specimen 3 is shown in Figure 4.33. Curvatures along the wall height of Specimen 3 were symmetric about its center line (mid-length of wall) up to the end of the test in both directions. The ultimate curvature was defined at the 20% load degradation of the peak load for both directions. The curvatures at the second level height (~12 in. above the footing) were approximately zero.

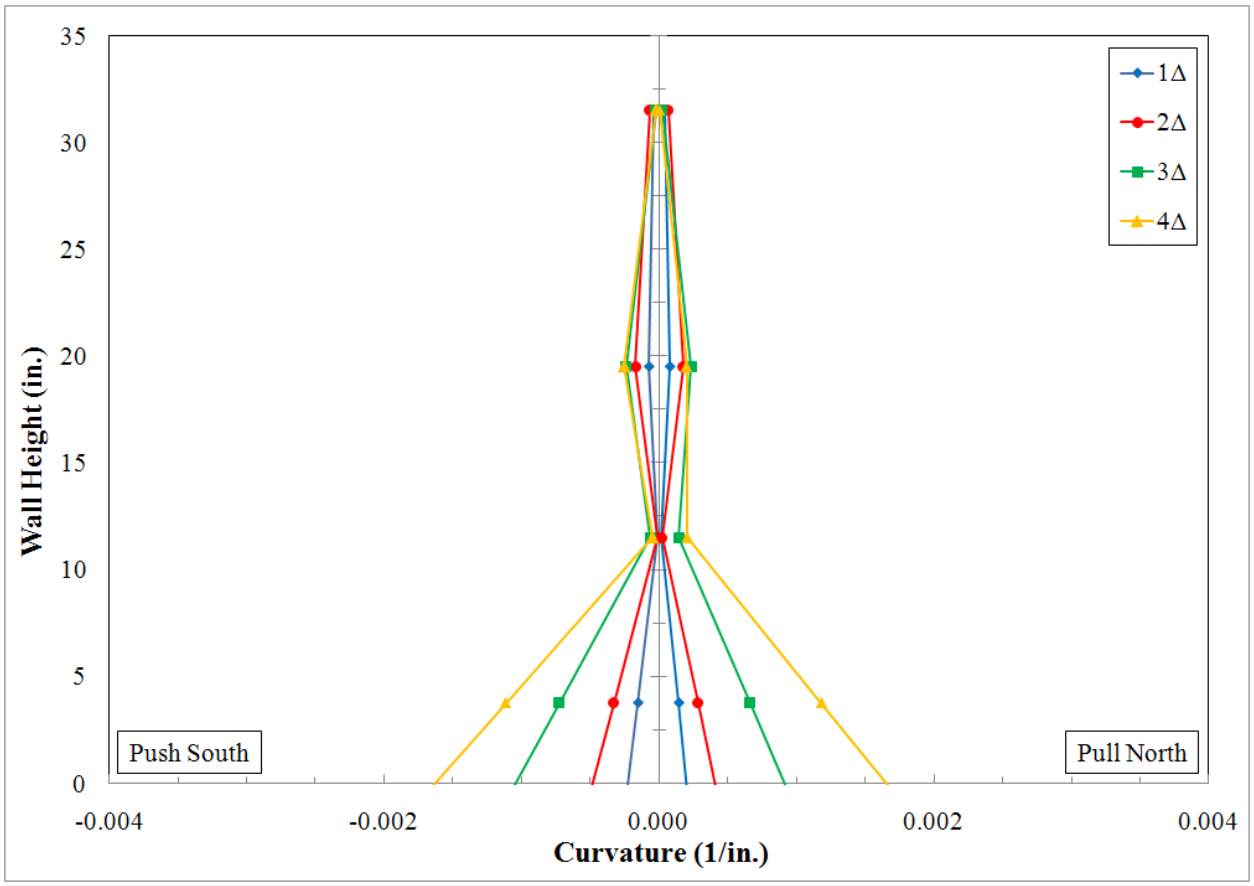

Figure 4.33 Specimen 3: Wall Curvature

Ductility:

The displacement ductility for Specimen 3 is presented in Table 4.24 for both loading directions along with the average value. The total drift obtained at 20% load degradation (with Δ_u = 0.75 in.) was 1.0%.

Table 4.24 Specimen 3: Displacement Ductility

Direction of Load	Displacement					
	P'_y (kips)	Δ'_y (in.)	Δ_u (in.)	P_y (kips)	Δ_y (in.)	μ_Δ
Push South	-33.8	-0.11	-0.74	-53.2	-0.17	4.4
Pull North	32.6	0.09	0.75	49.9	0.13	5.6
Average	33.2	0.10	0.75	51.6	0.15	4.9

The curvature ductility for Specimen 3 is presented in Table 4.25 for both loading directions along with the average value.

Table 4.25 Specimen 3: Curvature Ductility

Direction of Load	Curvature					
	M'_y (kip-in.)	ϕ'_y (in.$^{-1}$)	ϕ_u (in.$^{-1}$)	M_y (kip-in.)	ϕ_y (in.$^{-1}$)	μ_ϕ
Push South	-2421	-0.00007	-0.0007	-3807	-0.00010	7.0
Pull North	2336	0.00006	0.0007	3523	0.00009	7.0
Average	2379	0.00006	0.0007	3665	0.00010	7.0

Height of Plasticity and Equivalent Plastic Hinge Length:

The height of plasticity and equivalent plastic hinge length for both loading directions and their averages are given in Table 4.26. The ratio of the average plasticity zone height to the wall length and the equivalent plastic hinge length to the wall length are also tabulated.

Table 4.26 Specimen 3: Height of Plasticity & Equivalent Plastic Hinge Length

Direction of Load	Height of Plasticity Zone (in.)	Plastic Hinge Length (in.)
Push South	29.1	15.0
Pull North	29.2	17.6
Average	29.1	16.3
(L_p or l_p)/L_w	40.6%	22.8%

Energy Dissipation:

The total energy dissipated by Specimen 3 through the displacement level at which failure occurred in both loading directions was 110 kip-in.

4.7 Specimen 4

Specimen 4 had an aspect ratio of 1.0, No. 4 flexural reinforcement spaced 8 in. on center with a 16-in. long splice at the wall base, No. 4 shear reinforcement spaced 8 in. on center, and an axial load of 86 kips. Specimen 4 had a predicted capacity of 81 kips from the 2008 MSJC Code and 88.2 kips from the XTRACT analysis. The horizontal reinforcement in the first and fourth courses did not yield during testing. The extreme vertical reinforcement did not yield in the footing for Specimen 4.

Test Observations:

A yield displacement (Δ_y) of 0.16 in. was obtained from the preliminary test. The specimen was then loaded to displacements of ±1, 2, 3, 4, 6, and 8 times the yield displacement for the primary test. The entire specimen and north and south toe regions of the wall at test completion are presented in Figures 4.34 and 4.35. Test observations along with corresponding lateral displacements and loads follow. Wall behavior was dominated by flexure during testing with small levels of shear cracking in the bottom three courses. Flexural cracks developed at $1\Delta_y$, and moderate crushing and spalling of both toes occurred in the first and second courses near failure.

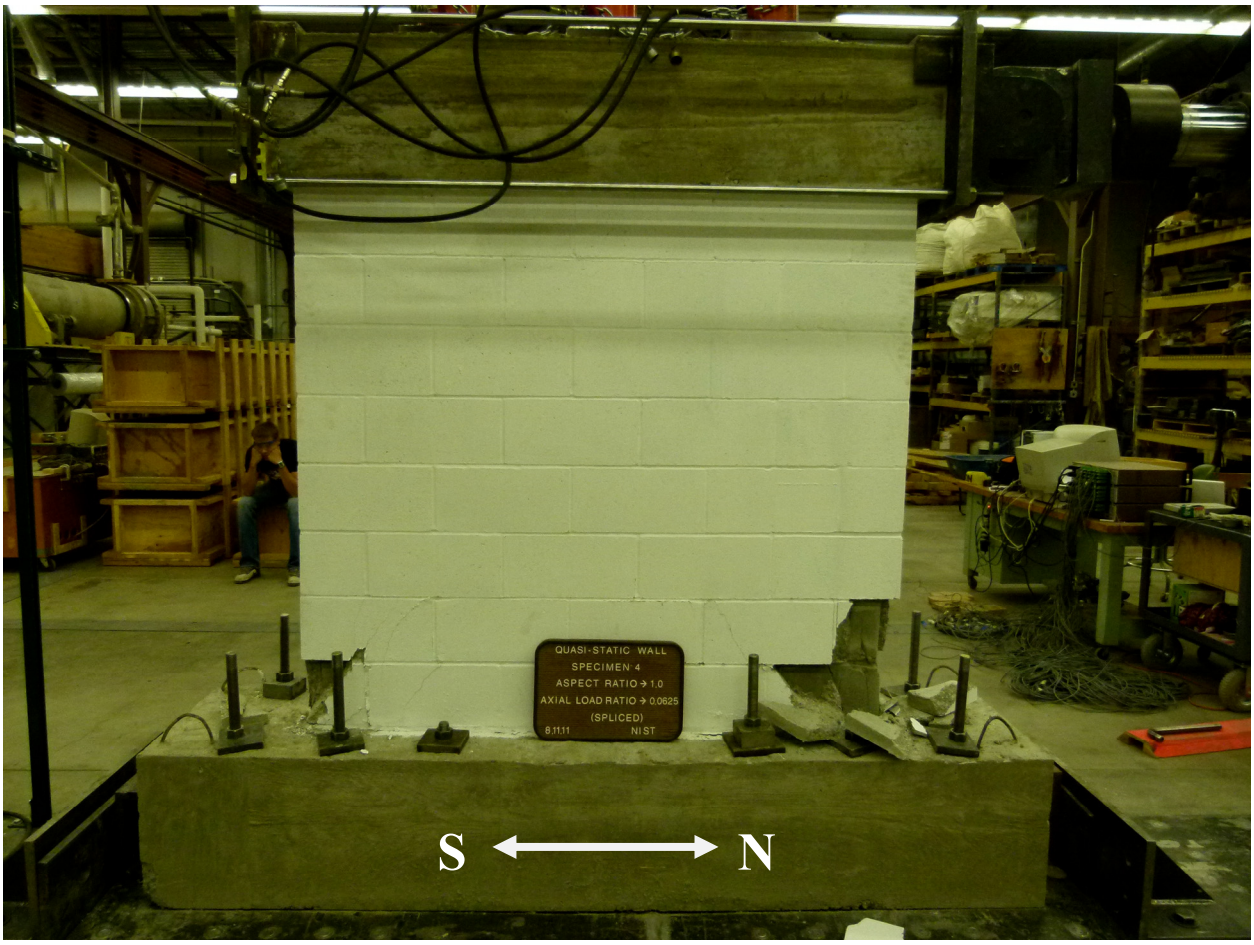

Figure 4.34 End-of-Test Picture of Entire Specimen 4

Figure 4.35 End-of-Test Pictures for Specimen 4: South Toe (left) and North Toe (right)

Table 4.27 Specimen 4 Test Observations

Load (kips)	Disp. (in.)	Test Observation
60.4	0.09	1st Yield of extreme vertical reinforcement bar in north toe (pull)
-62.8	-0.10	1st Yield of extreme vertical reinforcement bar in south toe (push)
-75.7	-0.16	*Flexural cracking in north toe (push)
72.1	0.17	*Flexural cracking in south toe (pull)
75.1	0.19	Critical masonry strain in north toe (pull)
-90.1	-0.33	Critical masonry strain in south toe (push)
-101.6	-0.47	Maximum load resistance in push to south
95.7	0.49	Maximum load resistance in pull to north
-80.9	-0.64	20% load degradation from maximum load resistance in push to south
75.5	0.65	20% load degradation from maximum load resistance in pull to north
89.7	0.66	*Onset of toe crushing in north toe (pull)
66.7	0.68	1% Drift in pull to north
-72.7	-0.69	1% Drift in push to south
-71.4	-0.96	*Onset of toe crushing in south toe (push)

* visual observation

Load-Displacement:

The load-displacement hysteresis curves for the preliminary and primary tests for Specimen 4 are given in Figure 4.36. All major events were marked on the load-displacement curve and are presented in Table 4.27 with their corresponding lateral displacement and load values at a specific point during the scan. The initial yielding of the extreme tensile reinforcement (ε_y = 0.00225 in./in.) occurred near the end of the preliminary test in both loading directions. Critical masonry strain was attained just beyond the cycle peak of $1\Delta_y$ in the pull direction and at the cycle peak of $2\Delta_y$ in the push direction. The wall reached the peak load at $3\Delta_y$ of the primary tests in both loading directions. Toe crushing (shown in Figure 4.37) occurred at the first cycle of $4\Delta_y$ and $6\Delta_y$ in the pull and push directions, respectively. The 20% load degradation was defined at the second cycle of $6\Delta_y$ in both loading directions, and the 1% drift was reached at $8\Delta_y$. The wall strength degraded more rapidly in the pull direction following the attainment of the peak lateral load.

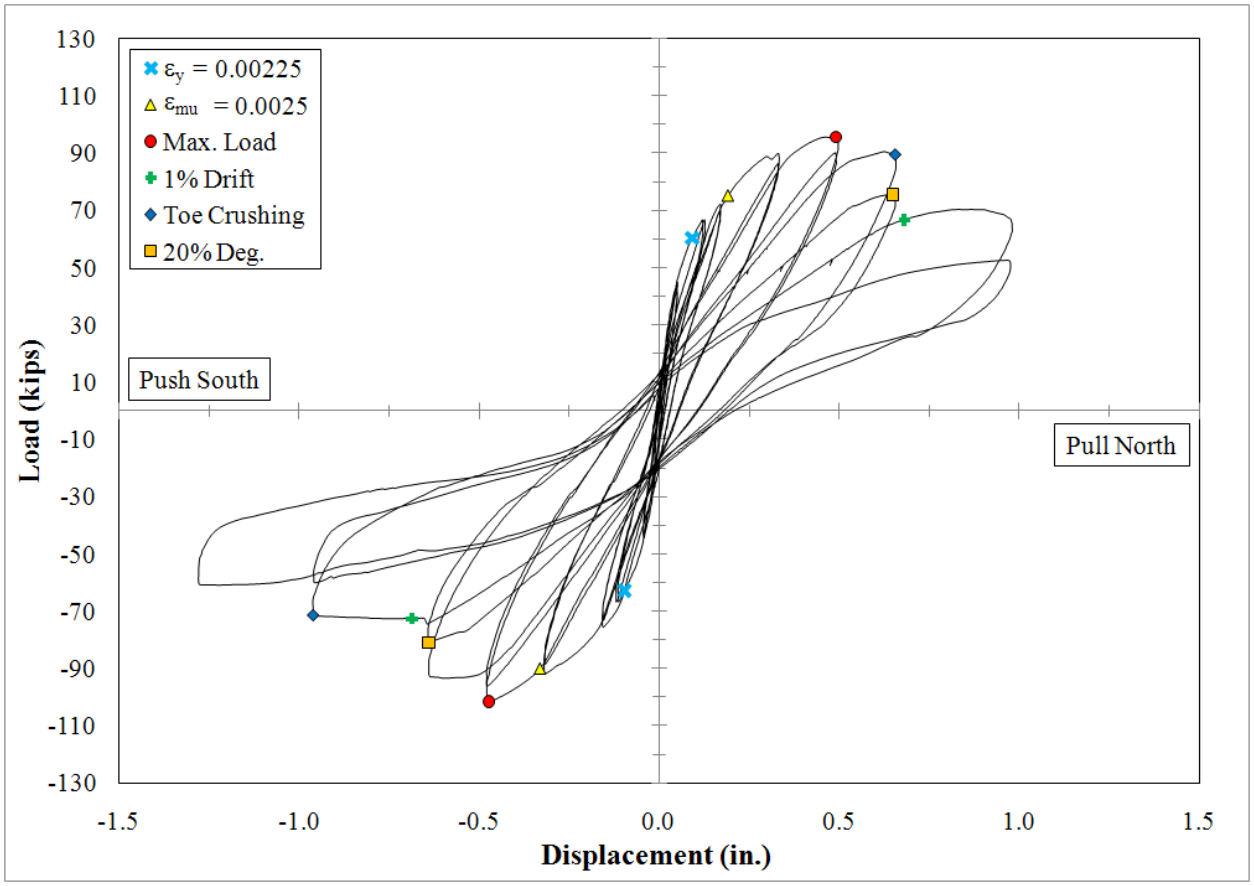

Figure 4.36 Specimen 4: Load-Displacement Hysteresis Curve

Figure 4.37 Onset of Toe Crushing for Specimen 4: South Toe (left) and North Toe (right)

Components of Displacements and Drifts:

Load-displacement curves for each component of displacement and the total displacement are shown in Figure 4.38. Average drift contributions from sliding, shear, and flexural deformations and total drift at the three limit states of critical masonry strain, peak lateral load, and failure are given in Table 4.28. Specimen 4 was dominated by flexural deformations, with small levels of shear and some sliding deformations occurring near failure.

Table 4.28 Specimen 4: Component Percentages of Total Drift

Limit State	Total Drift (%)	Sliding (% Total)	Shear (% Total)	Flexural (% Total)
ε_{mu}	0.4	1.2	11.1	87.7
Peak Load	0.7	2.2	13.3	84.5
Failure	0.9	2.1	11.9	86.0

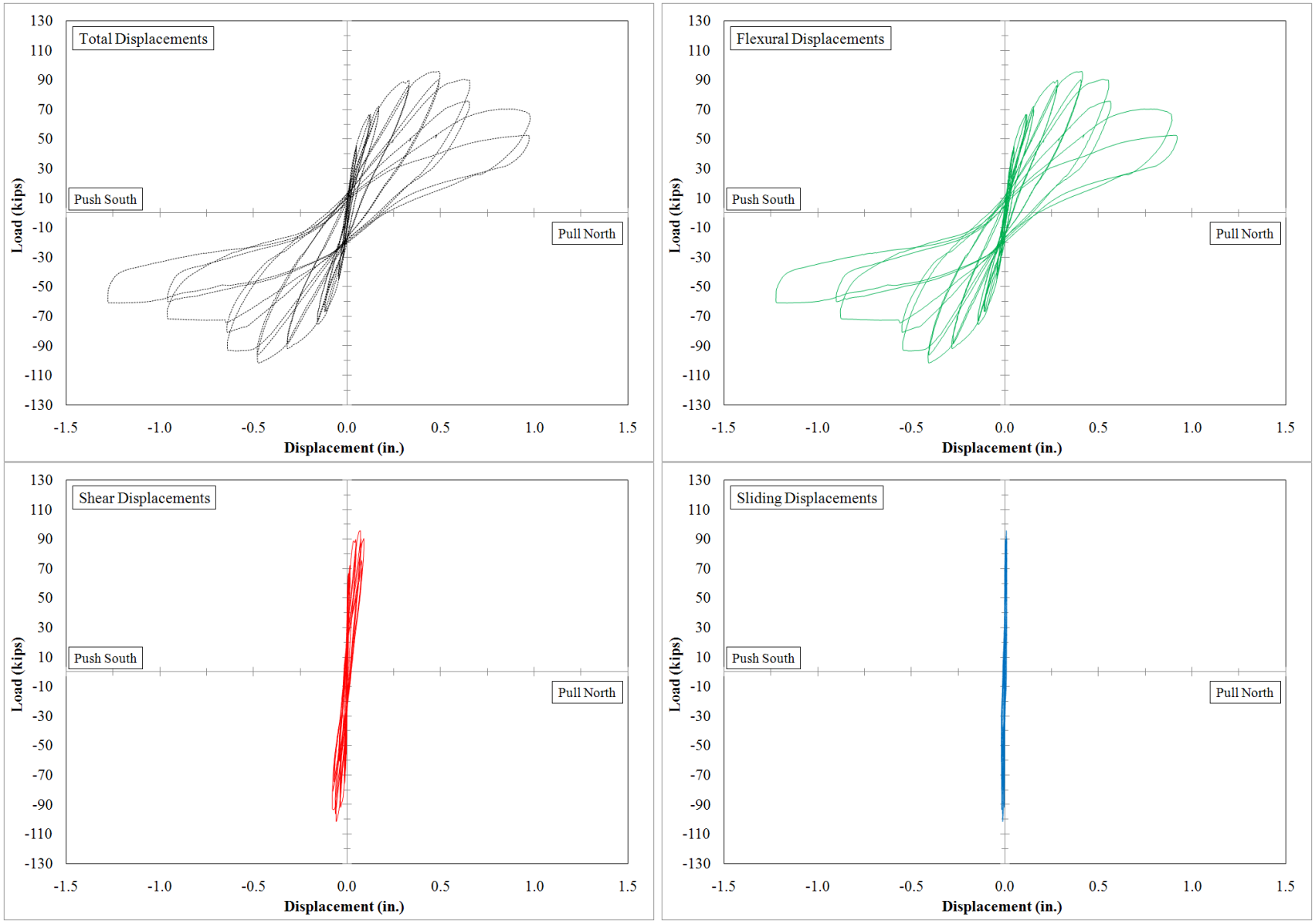

Figure 4.38 Specimen 4: Displacements from Associated Components

Wall Curvatures:

A plot of curvature along the wall height of Specimen 4 is shown in Figure 4.39. Curvatures along the wall height of Specimen 4 were symmetric about its center line (mid-length of wall) up to $6\Delta_y$ in both directions. The ultimate curvature was defined at the second cycle of $4\Delta_y$ for both loading directions instead of the 20% load degradation of the peak load. This was due to invalid measurements from the potentiometers beyond $6\Delta_y$. The curvatures at the second level height (~12 in. above the footing) were approximately zero.

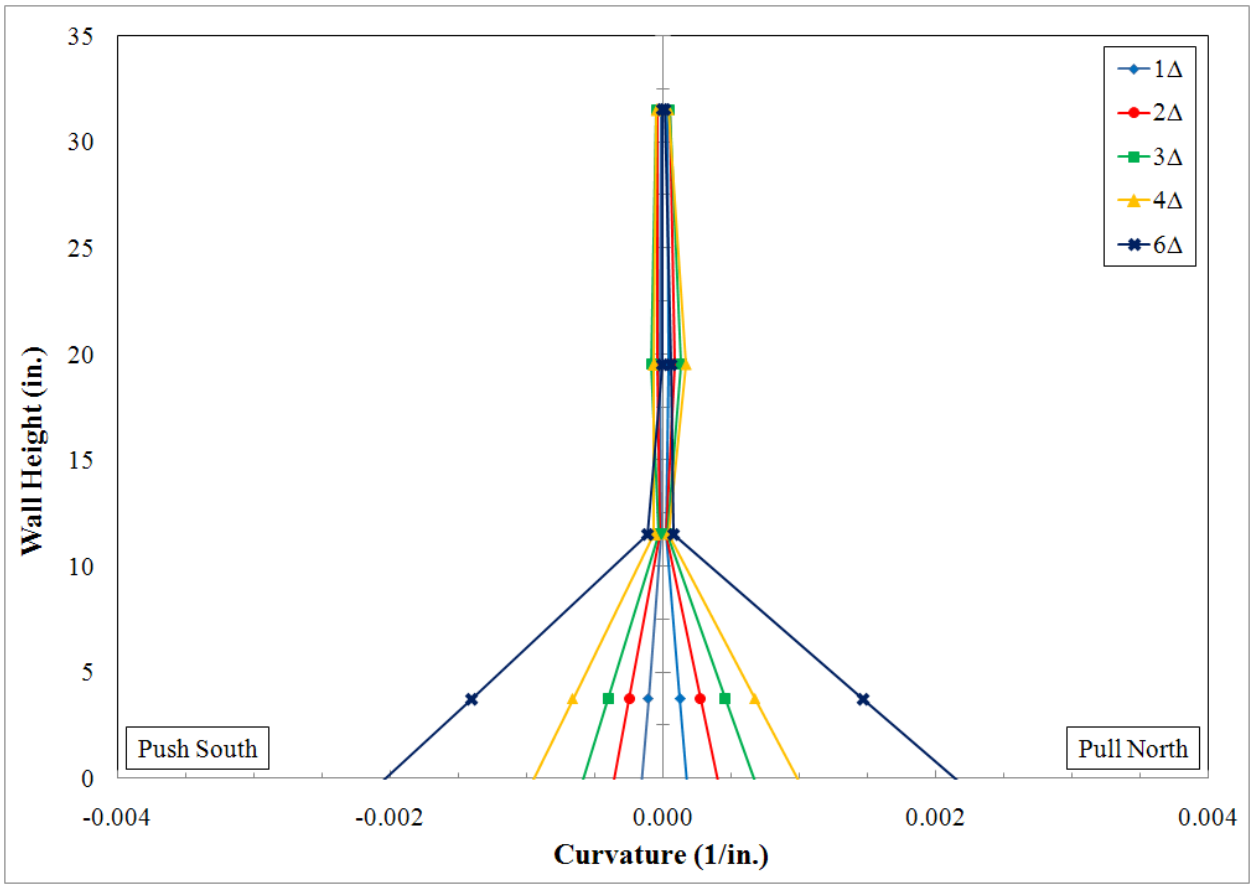

Figure 4.39 Specimen 4: Wall Curvature

Ductility:

The displacement ductility for Specimen 4 is presented in Table 4.29 for both loading directions along with the average value. The total drift obtained at 20% load degradation (with Δ_u = 0.64 in.) was 0.9%.

Table 4.29 Specimen 4: Displacement Ductility

Direction of Load	Displacement					
	P'_y (kips)	Δ'_y (in.)	Δ_u (in.)	P_y (kips)	Δ_y (in.)	μ_Δ
Push South	-62.8	-0.10	-0.64	-90.9	-0.14	4.7
Pull North	60.4	0.09	0.65	85.7	0.13	5.0
Average	61.6	0.09	0.64	88.3	0.13	4.8

The curvature ductility for Specimen 4 is presented in Table 4.30 for both loading directions along with the average value.

Table 4.30 Specimen 4: Curvature Ductility

Direction of Load	Curvature					
	M'_y (kip-in.)	ϕ'_y (in.$^{-1}$)	ϕ_u (in.$^{-1}$)	M_y (kip-in.)	ϕ_y (in.$^{-1}$)	μ_ϕ
Push South	-4498	-0.00006	-0.0008	-6510	-0.00008	9.3
Pull North	4324	0.00008	0.0007	6231	0.00011	6.4
Average	4411	0.00007	0.0007	6371	0.00010	7.6

Height of Plasticity and Equivalent Plastic Hinge Length:

The height of plasticity and equivalent plastic hinge length for both loading directions and their averages are given in Table 4.31. The ratio of the average plasticity zone height to the wall length and the equivalent plastic hinge length to the wall length are also tabulated.

Table 4.31 Specimen 4: Height of Plasticity & Equivalent Plastic Hinge Length

Direction of Load	Height of Plasticity Zone (in.)	Plastic Hinge Length (in.)
Push South	15.9	11.9
Pull North	13.9	13.0
Average	14.9	12.4
(L_p or l_p)/L_w	20.8%	17.3%

Energy Dissipation:

The total energy dissipated by Specimen 4 through the displacement level at which failure occurred in both loading directions was 195 kip-in.

4.8 Specimen 5

Specimen 5 had an aspect ratio of 0.78, No. 4 flexural reinforcement spaced 8 in. on center with a 16-in. long splice at the wall base, No. 4 shear reinforcement spaced 8 in. on center, and zero axial load. Specimen 5 had a predicted capacity of 63 kips from the 2008 MSJC Code and 76.7 kips from the XTRACT analysis. The horizontal reinforcement yielded in the first and fourth courses during testing.

Test Observations:

A yield displacement (Δ_y) of 0.21 in. was obtained from the preliminary test. The specimen was then loaded to displacements of ±1, 2, 3, 4, and 6 times the yield displacement for the primary test. The entire specimen and north and south toe regions of the wall at test completion are presented in Figures 4.40 and 4.41. Test observations along with corresponding lateral displacements and loads follow. Wall behavior was dominated by flexure, but diagonal shear cracks were evident in every course. Sliding between the wall base and footing was also evident during testing, and toe crushing and spalling of the toe regions did not occur in this wall.

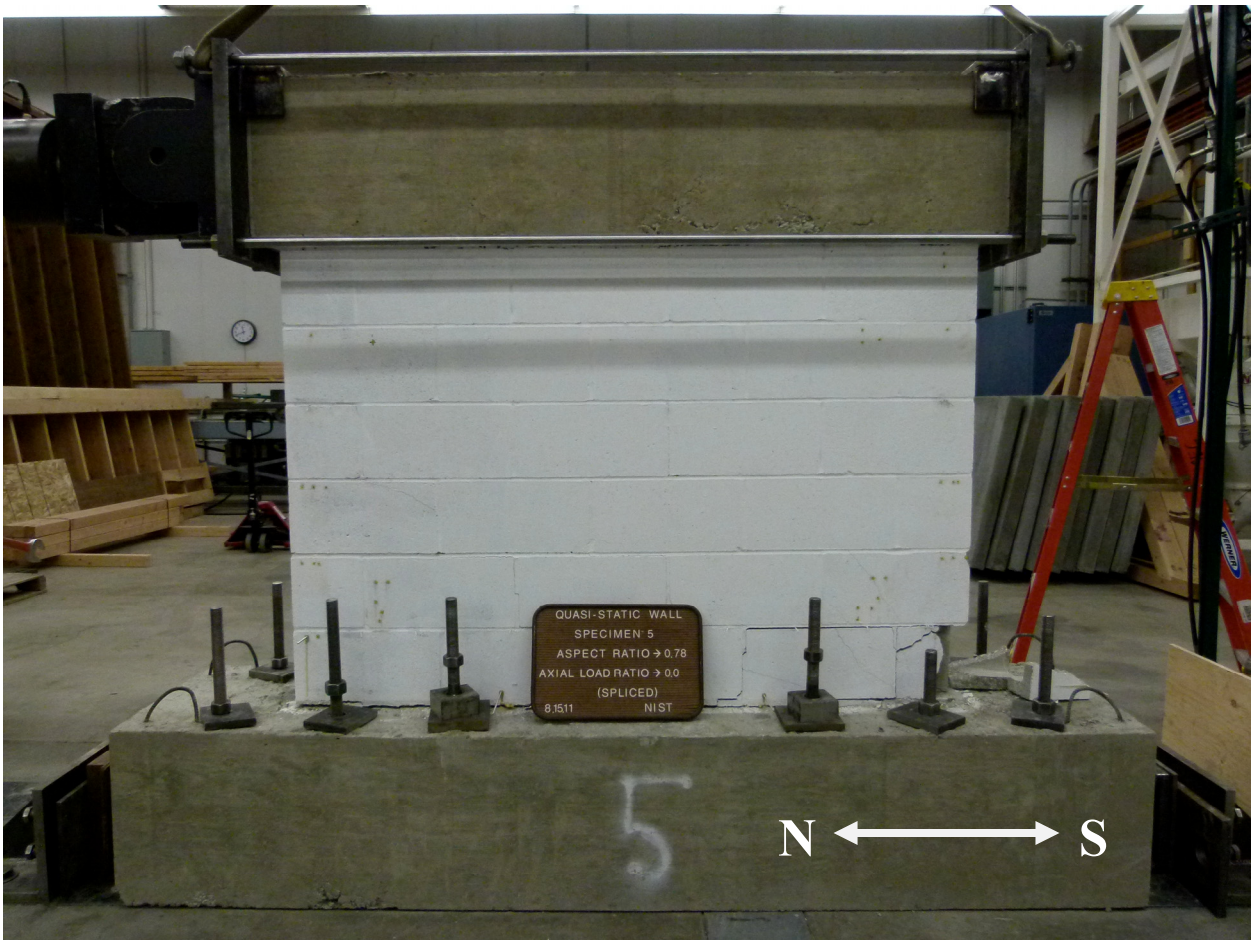

Figure 4.40 End-of-Test Picture of Entire Specimen 5

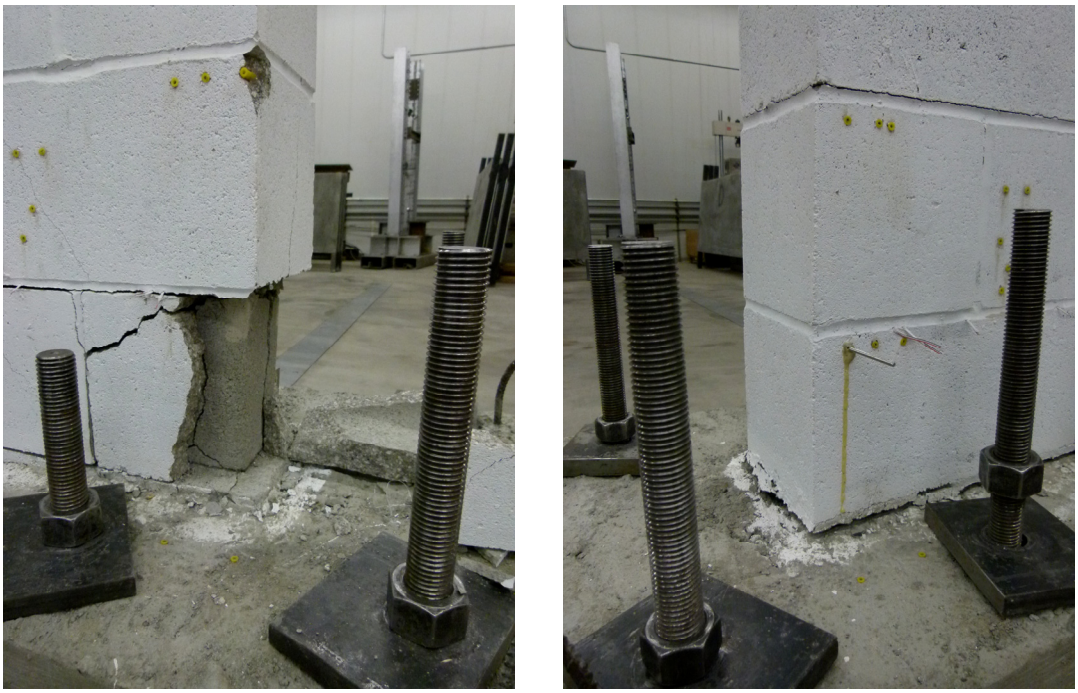

Figure 4.41 End-of-Test Pictures for Specimen 5: South Toe (left) and North Toe (right)

Table 4.32 Specimen 5 Test Observations

Load (kips)	Disp. (in.)	Test Observation
10.0	0.05	Critical masonry strain in north toe (pull)
32.7	0.06	1st Yield of extreme vertical reinforcement bar in north toe (pull)
-38.1	-0.06	1st Yield of extreme vertical reinforcement bar in south toe (push)
-64.1	-0.20	*Flexural cracking in north toe (push)
59.9	0.22	*Flexural cracking in south toe (pull)
-69.7	-0.29	Critical masonry strain in south toe (push)
71.3	0.43	Maximum load resistance in pull to north
59.5	0.53	1% Drift in pull to north
-72.8	-0.53	1% Drift in push to south
-77.4	-0.62	Maximum load resistance in push to south
40.7	0.65	20% load degradation from maximum load resistance in pull to north
-43.8	-0.84	20% load degradation from maximum load resistance in push to south

* visual observation

Load-Displacement:

The load-displacement hysteresis curves for the preliminary and primary tests for Specimen 5 are shown in Figure 4.42. All major events were marked on the load-displacement curve and are presented in Table 4.32 with their corresponding lateral displacement and load values at a specific point during the scan. . The initial yielding of the extreme tensile reinforcement (ε_y = 0.00225 in./in.) occurred at 50% of the peak load level in the preliminary test in the push direction and near the end of the preliminary test in pull direction. Critical masonry strain was attained early at $1\Delta_y$ in the pull direction and at $2\Delta_y$ in the push direction. The peak lateral load was defined at the cycle peaks of $2\Delta_y$ and $3\Delta_y$ in the pull and push directions, respectively. The 20% load degradation was reached in the second cycles of $3\Delta_y$ and $4\Delta_y$ in the pull and push directions, respectively. The wall strength degraded more rapidly in the pull direction following attainment of the peak lateral load.

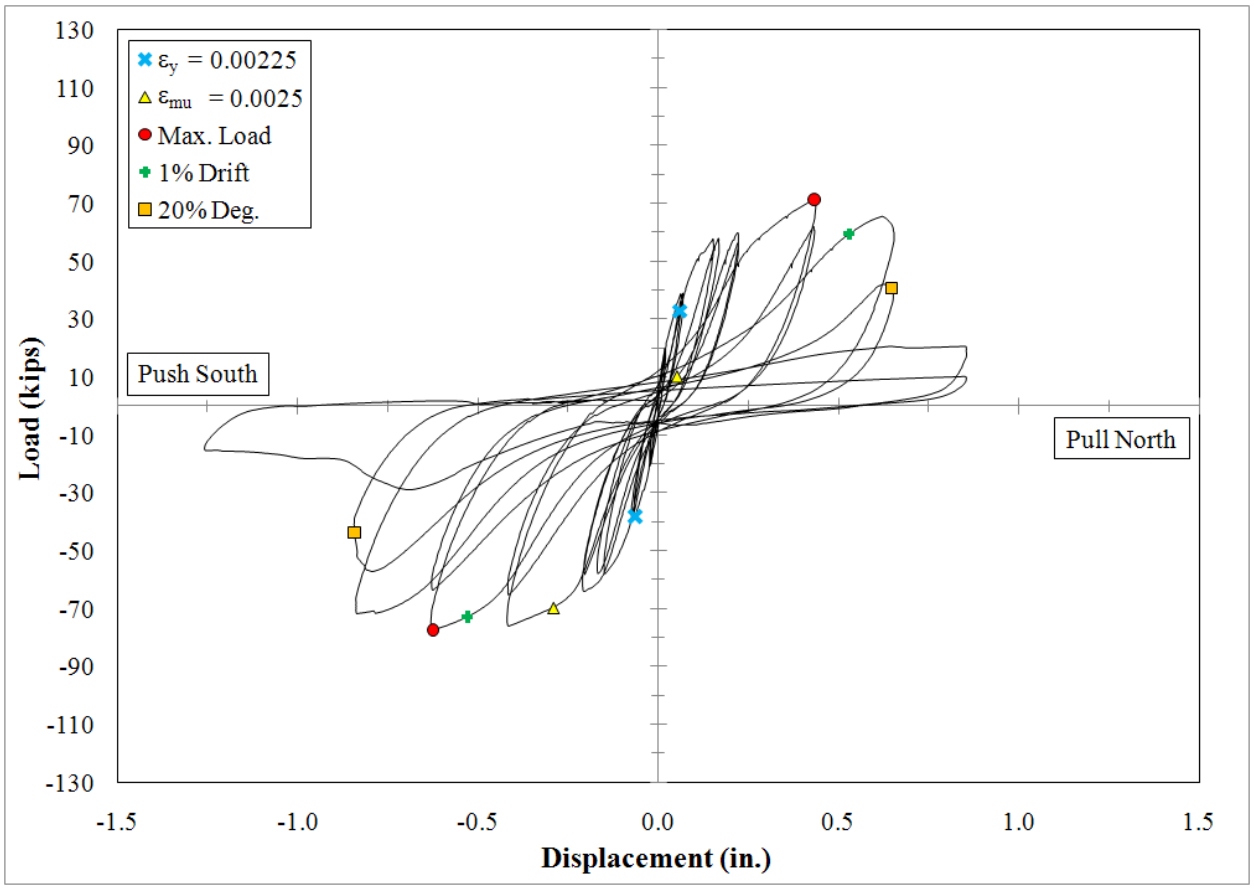

Figure 4.42 Specimen 5: Load-Displacement Hysteresis Curve

Components of Displacements and Drifts:

Load-displacement curves for each component of displacement and the total displacement are presented in Figure 4.43. Average drift contributions from sliding, shear, and flexural deformations and total drift at three limit states, including critical masonry strain, peak lateral load, and failure are given in Table 4.33. Specimen 5 was dominated by flexural deformations, with small levels of shear deformations occurring near failure in both loading directions. There were significant (~21% of total displacement) sliding deformations near failure.

Table 4.33 Specimen 5: Component Percentages of Total Drift

Limit State	Total Drift (%)	Sliding (% Total)	Shear (% Total)	Flexural (% Total)
ε_{mu}	0.3	4.7	9.0	86.3
Peak Load	0.9	14.7	14.2	71.1
Failure	1.3	20.8	11.5	67.6

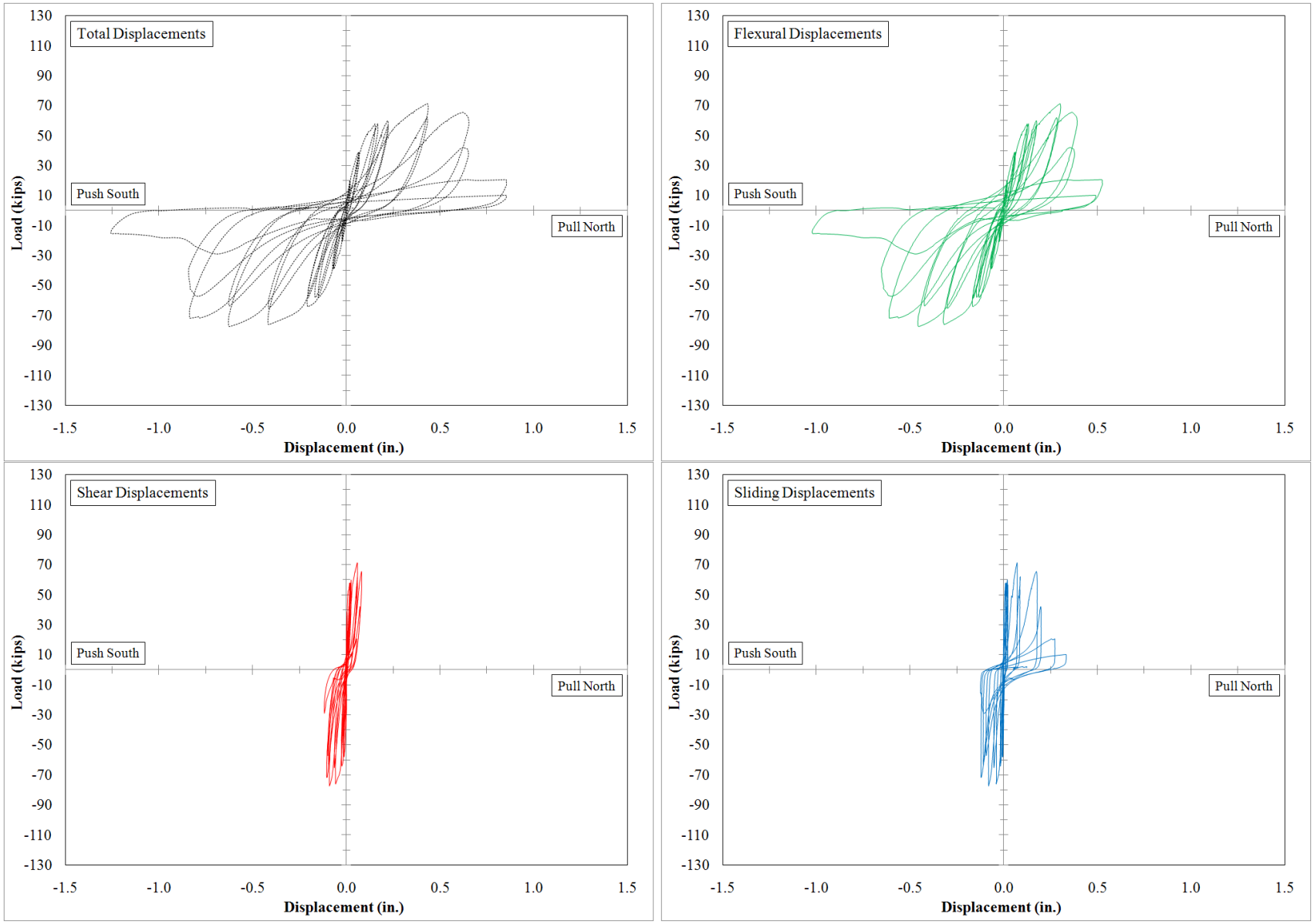

Figure 4.43 Specimen 5: Displacements from Associated Components

Wall Curvatures:

A plot of curvature along the wall height of Specimen 5 is shown in Figure 4.44. Curvatures along the wall height of Specimen 5 were symmetric about its center line (mid-length of wall) until $4\Delta_y$ in the push direction. The ultimate curvature was defined at the 20% load degradation of the peak load for both directions. The curvatures at the second level height (~12 in. above the footing) were approximately zero.

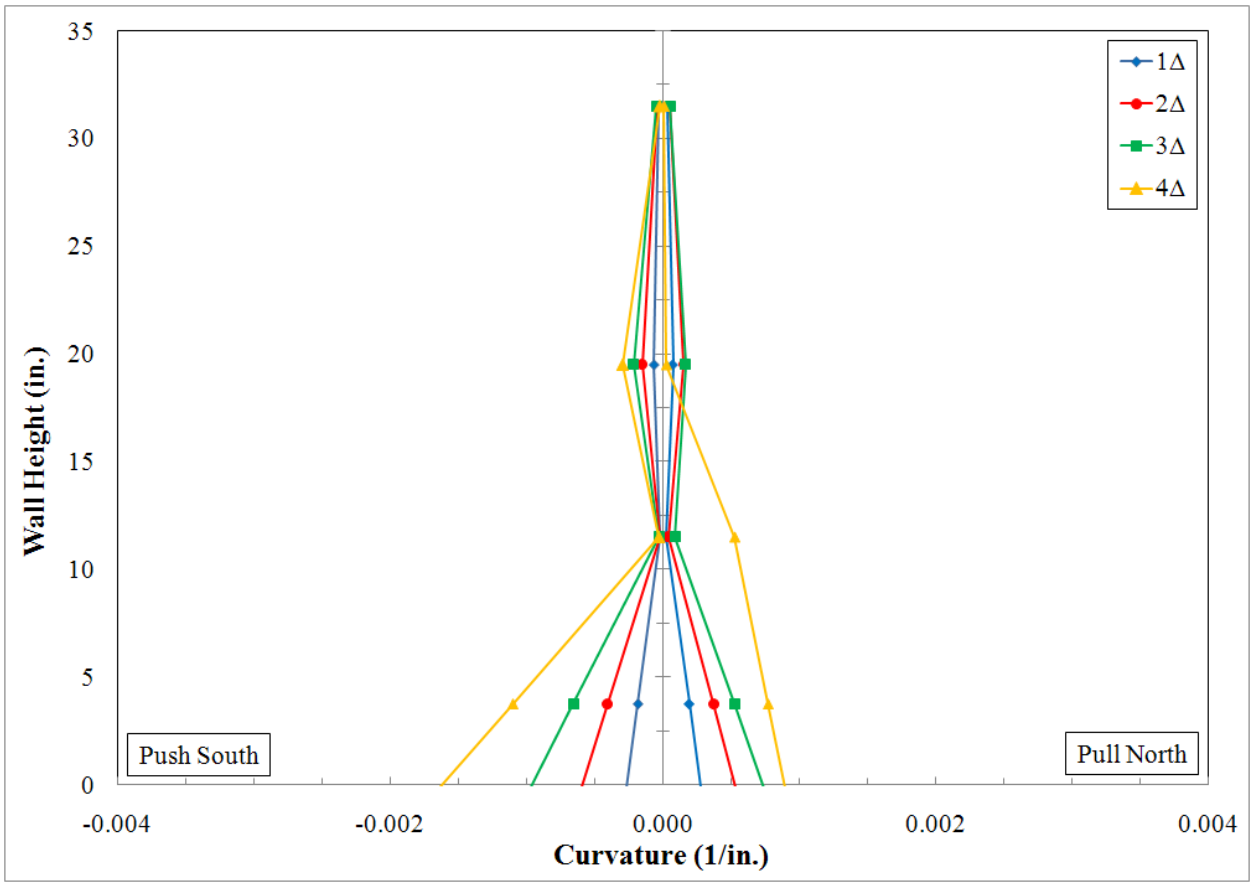

Figure 4.44 Specimen 5: Wall Curvature

Ductility:

The displacement ductility for Specimen 5 is presented in Table 4.34 for both loading directions along with the average value. The total drift obtained at 20% load degradation (with Δ_u = 0.74 in.) was 1.3%.

Table 4.34 Specimen 5: Displacement Ductility

Direction of Load	Displacement					
	P'_y (kips)	Δ'_y (in.)	Δ_u (in.)	P_y (kips)	Δ_y (in.)	μ_Δ
Push South	-38.1	-0.06	-0.84	-67.4	-0.11	7.4
Pull North	32.7	0.06	0.65	60.6	0.11	5.8
Average	35.4	0.06	0.74	64.0	0.11	6.6

The curvature ductility for Specimen 5 is presented in Table 4.35 for both loading directions along with the average value.

Table 4.35 Specimen 5: Curvature Ductility

Direction of Load	Curvature					
	M'_y (kip-in.)	ϕ'_y (in.$^{-1}$)	ϕ_u (in.$^{-1}$)	M_y (kip-in.)	ϕ_y (in.$^{-1}$)	μ_ϕ
Push South	-2118	-0.00006	-0.0014	-3610	-0.00011	13.1
Pull North	1821	0.00004	0.0005	3383	0.00008	6.1
Average	1970	0.00005	0.0010	3496	0.00010	10.1

Height of Plasticity and Equivalent Plastic Hinge Length:

The height of plasticity and equivalent plastic hinge length for both loading directions and their averages are given in Table 4.36. The ratio of the average plasticity zone height to the wall length and the equivalent plastic hinge length to the wall length are also tabulated.

Table 4.36 Specimen 5: Height of Plasticity & Equivalent Plastic Hinge Length

Direction of Load	Height of Plasticity Zone (in.)	Plastic Hinge Length (in.)
Push South	29.1	11.4
Pull North	29.5	31.8
Average	29.3	21.6
(L_p or l_p)/L_w	41.0%	30.2%

Energy Dissipation:

The total energy dissipated by Specimen 5 through the displacement level at which failure occurred in both loading directions was 199 kip-in.

4.9 Specimen 6

Specimen 6 had an aspect ratio of 0.78, No. 4 flexural reinforcement spaced 8 in. on center with a 16-in. long splice at the wall base, two No. 4 shear bars spaced 8 in. on center, and an axial load of 86 kips. Specimen 6 had a predicted capacity of 105 kips from the 2008 MSJC Code and 113 kips from the XTRACT analysis. The horizontal reinforcement located in the first course did not yield during testing. The extreme vertical reinforcement yielded in the footing for Specimen 6.

Test Observations:

A yield displacement (Δ_y) of 0.14 in. was obtained from the preliminary test. The specimen was then loaded to displacements of ±1, 2, 3, 4, 6, 8, and 10 times the yield displacement for the primary test. The entire specimen and north and south toe regions of the wall at test completion are presented in Figures 4.45 and 4.46. Test observations along with corresponding lateral displacements and loads follow. Wall behavior was dominated by flexure, but diagonal shear cracks were evident in every course. Flexural cracks developed at $1\Delta_y$, and moderate crushing and spalling of both toes occurred in the first and second courses later in testing. Vertical splitting was observed on the end faces of the wall at $6\Delta_y$.

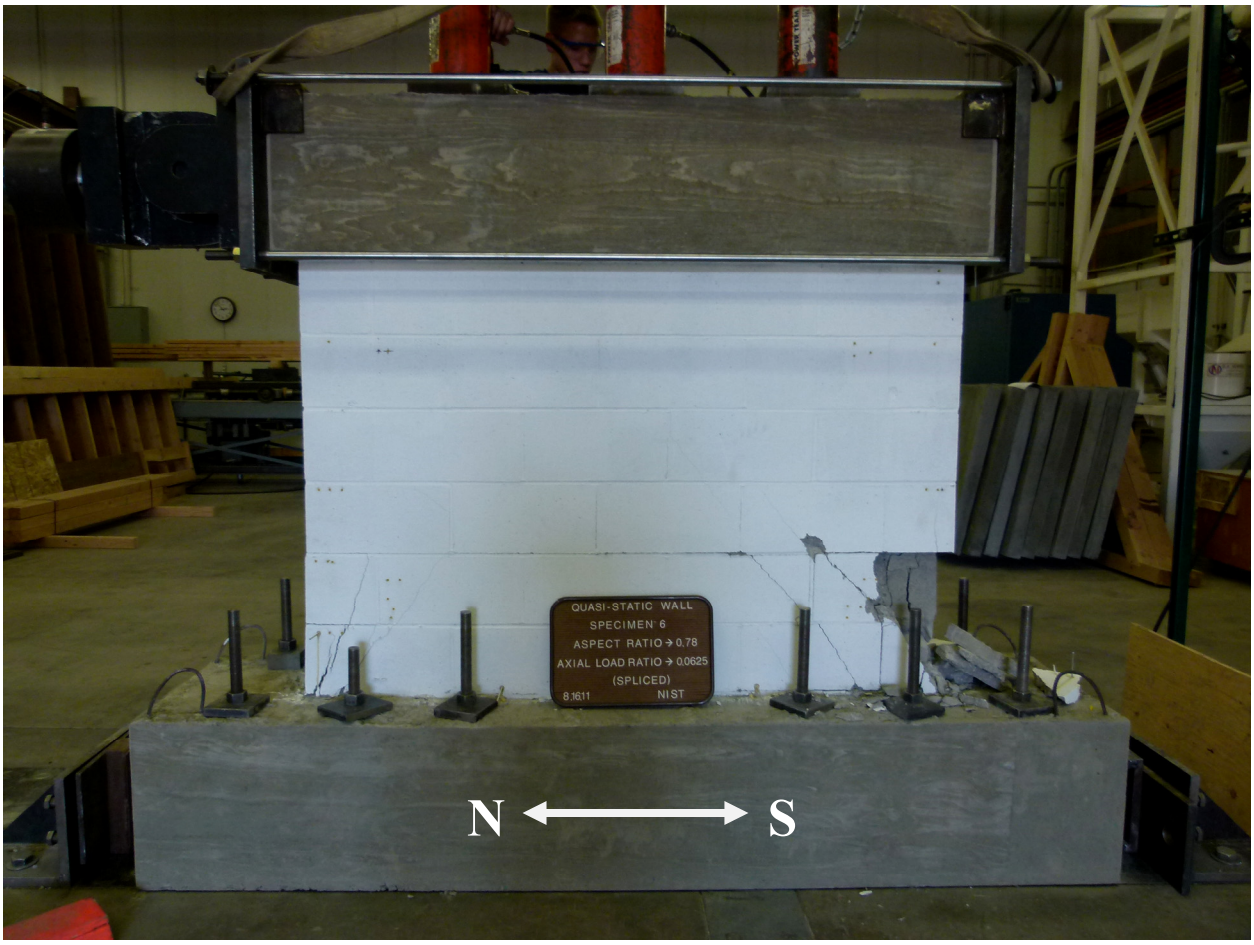

Figure 4.45 End-of-Test Picture of Entire Specimen 6

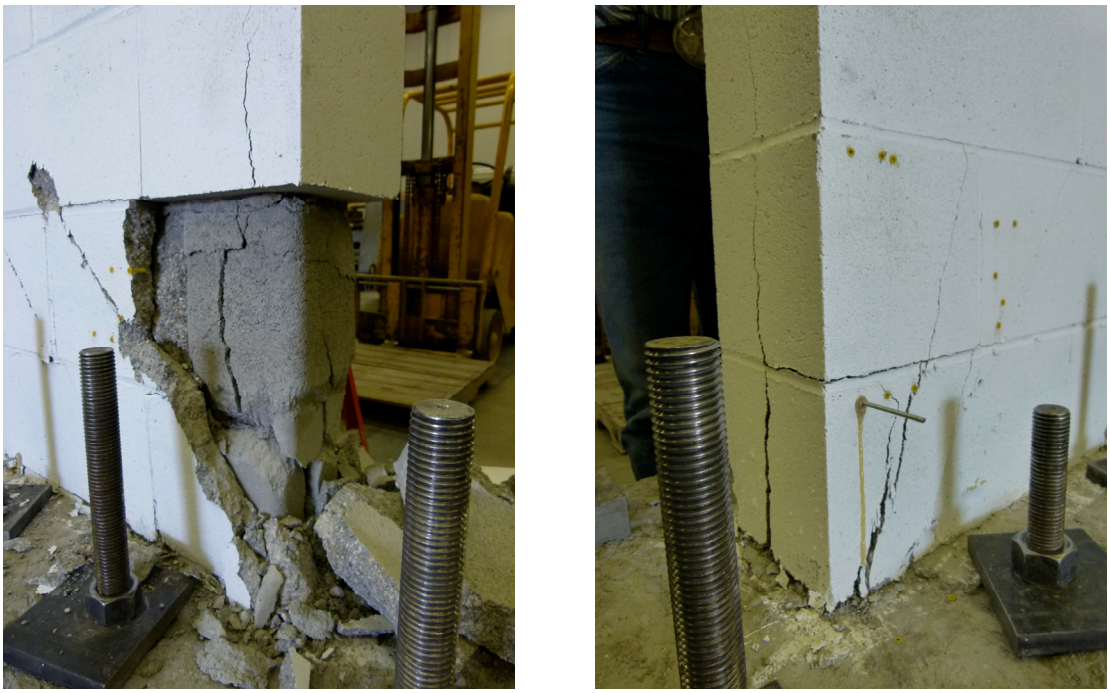

Figure 4.46 End-of-Test Pictures for Specimen 6: South Toe (left) and North Toe (right)

Table 4.37 Specimen 6 Test Observations

Load (kips)	Disp. (in.)	Test Observation
-79.6	-0.08	1st Yield of extreme vertical reinforcement bar in south toe (push)
80.6	0.08	1st Yield of extreme vertical reinforcement bar in north toe (pull)
74.6	0.13	Critical masonry strain in north toe (pull)
-95.4	-0.14	*Flexural cracking in north toe (push)
85.7	0.15	*Flexural cracking in south toe (pull)
-112.2	-0.23	Critical masonry strain in south toe (push)
-125.8	-0.40	Maximum load resistance in push to south
119.8	0.42	Maximum load resistance in pull to north
104.3	0.53	1% Drift in pull to north
-118.0	-0.53	1% Drift in push to south
-118.0	-0.53	*Onset of toe crushing in south toe (push)
92.2	0.55	20% load degradation from maximum load resistance in pull to north
83.7	0.84	*Onset of toe crushing in north toe (pull)
-95.8	-1.10	20% load degradation from maximum load resistance in push to south

* visual observation

Load-Displacement:

The load-displacement hysteresis curves for the preliminary and primary tests for Specimen 6 are shown in Figure 4.47. All major events were marked on the load-displacement curve and are presented in Table 4.37 with their corresponding lateral displacement and load values at a specific point during the scan. The initial yielding of the extreme tensile reinforcement (ε_y = 0.00225 in./in.) occurred near the end of the preliminary test in both loading directions. Critical masonry strain was attained preceding the cycle peak of $1\Delta_y$ in the pull direction and near the cycle peak of $2\Delta_y$ in the push direction. The wall reached the peak load at $3\Delta_y$ of the primary tests in both loading directions. Toe crushing (illustrated in Figure 4.48) occurred at the first cycle of $4\Delta_y$ and $6\Delta_y$ in the push and pull directions, respectively. The 1% drift was reached near the cycle peak of $4\Delta_y$. The 20% load degradation was defined at the second cycle of $4\Delta_y$ in the pull directions and the first cycle of $8\Delta_y$ in the push direction. This

wall exhibited rapid load degradation following the peak load in the pull direction, and slow load degradation in the push direction until the second cycle of $8\Delta_y$.

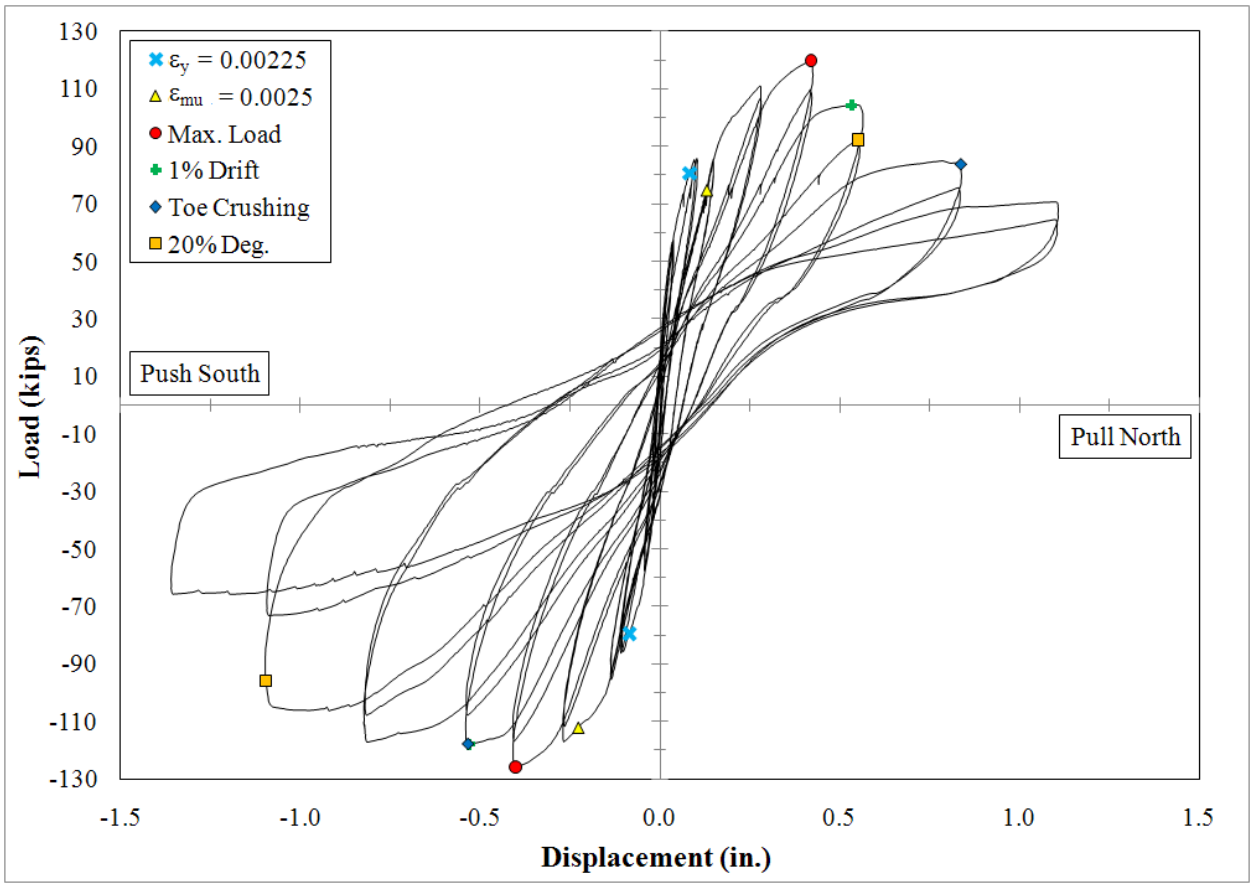

Figure 4.47 Specimen 6: Load-Displacement Hysteresis Curve

Figure 4.48 Onset of Toe Crushing for Specimen 6: South Toe (left) and North Toe (right)

Components of Displacements and Drifts:

Load-displacement curves for each component of displacement and the total displacement are shown in Figure 4.49. Average drift contributions from sliding, shear, and flexural deformations and total drift at the three limit states of critical masonry strain, peak lateral load, and failure are given in Table 4.38. Specimen 6 was dominated by flexural deformations, with small levels of shear and sliding deformations occurring near failure.

Table 4.38 Specimen 6: Component Percentages of Total Drift

Limit State	Total Drift (%)	Sliding (% Total)	Shear (% Total)	Flexural (% Total)
ε_{mu}	0.3	0.4	11.0	88.5
Peak Load	0.7	5.5	14.0	80.6
Failure	1.5	4.8	10.1	85.1

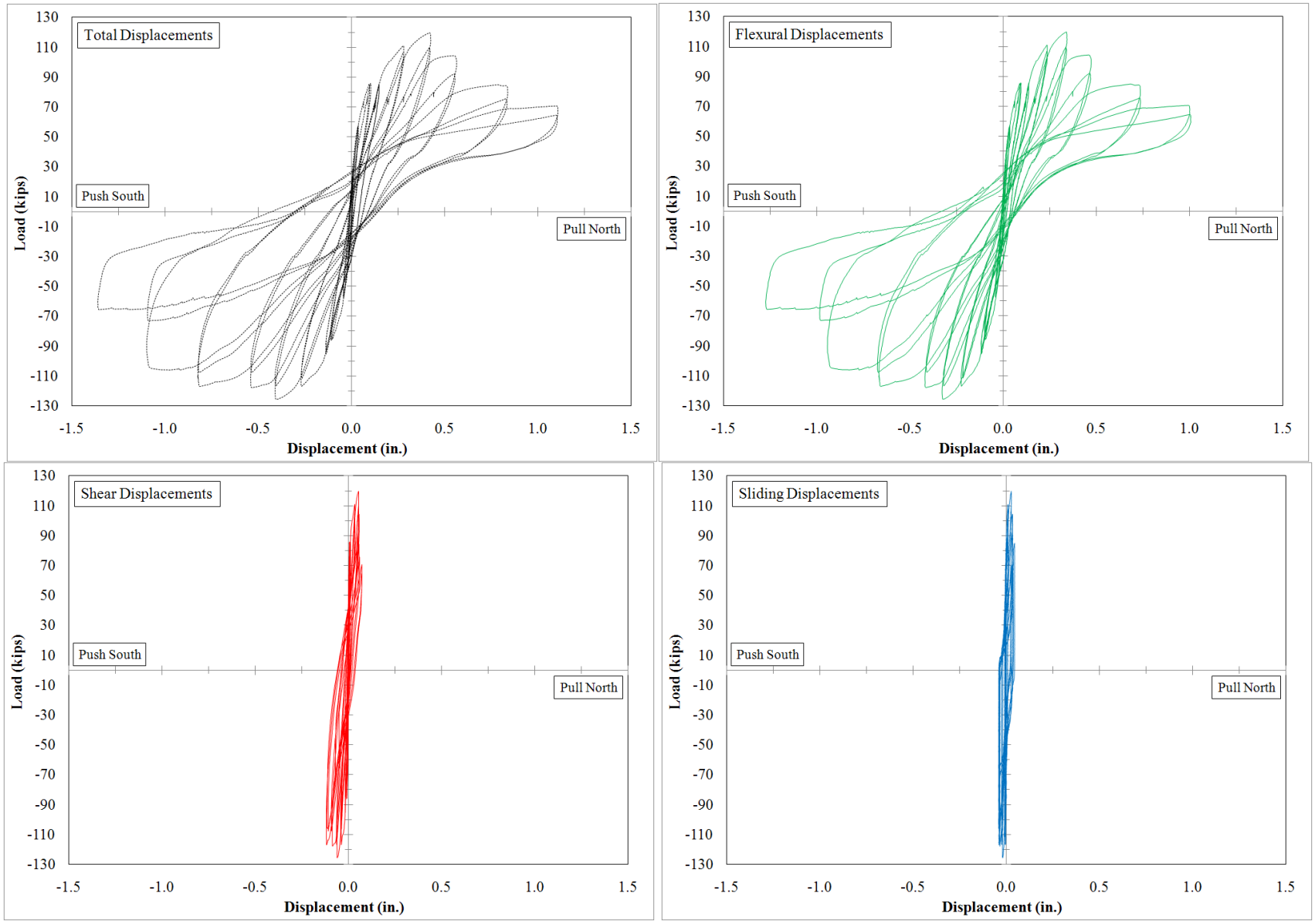

Figure 4.49 Specimen 6: Displacements from Associated Component

Wall Curvatures:

A plot of curvature along the wall height of Specimen 6 is shown in Figure 4.50. Curvatures along the wall height of Specimen 6 were symmetric about its center line (mid-length of wall) up to $8\Delta_y$ in both directions. The ultimate curvature was defined at the 20% load degradation of the peak load in both directions. The curvatures at the second level height (~12 in. above the footing) were approximately zero.

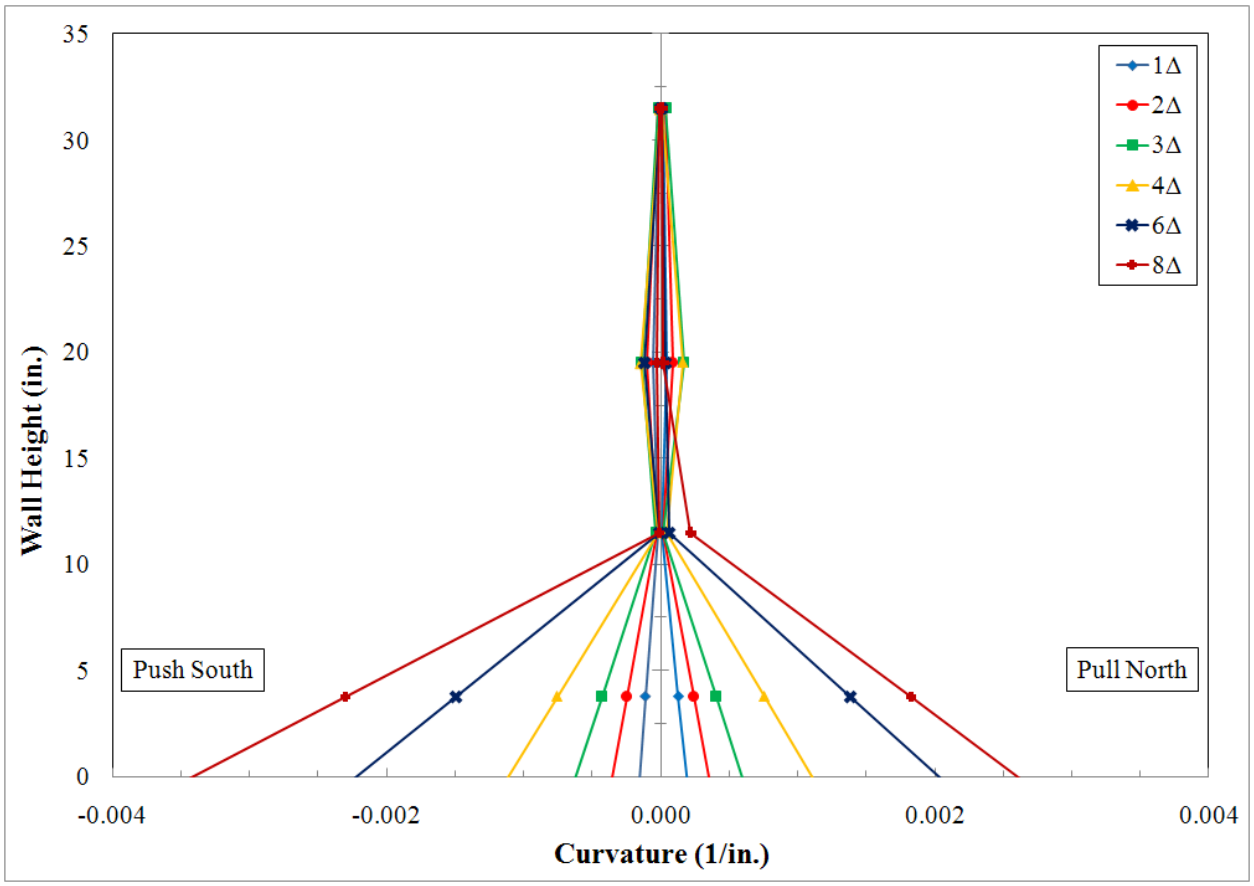

Figure 4.50 Specimen 6: Wall Curvature

Ductility:

The displacement ductility for Specimen 6 is presented in Table 4.39 for both loading directions along with the average value. The total drift obtained at 20% load degradation (with Δ_u = 0.82 in.) was 1.5%.

Table 4.39 Specimen 6: Displacement Ductility

Direction of Load	Displacement					
	P'_y (kips)	Δ'_y (in.)	Δ_u (in.)	P_y (kips)	Δ_y (in.)	μ_Δ
Push South	-79.6	-0.08	-1.10	-114.1	-0.12	9.1
Pull North	80.6	0.08	0.55	107.1	0.11	5.0
Average	80.1	0.08	0.82	110.6	0.12	7.1

The curvature ductility for Specimen 6 is presented in Table 4.40 for both loading directions along with the average value.

Table 4.40 Specimen 6: Curvature Ductility

Direction of Load	Curvature					
	M'_y (kip-in.)	ϕ'_y (in.$^{-1}$)	ϕ_u (in.$^{-1}$)	M_y (kip-in.)	ϕ_y (in.$^{-1}$)	μ_ϕ
Push South	-4426	-0.00007	-0.0023	-6334	-0.00009	24.3
Pull North	4486	0.00007	0.0008	5959	0.00009	8.7
Average	4456	0.00007	0.0016	6146	0.00009	16.6

Height of Plasticity and Equivalent Plastic Hinge Length:

The height of plasticity and equivalent plastic hinge length for both loading directions and their averages are given in Table 4.41. The ratio of the average plasticity zone height to the wall length and the equivalent plastic hinge length to the wall length are also tabulated.

Table 4.41 Specimen 6: Height of Plasticity & Equivalent Plastic Hinge Length

Direction of Load	Height of Plasticity Zone (in.)	Plastic Hinge Length (in.)
Push South	11.3	8.8
Pull North	11.3	13.0
Average	11.3	10.9
(L_p or l_p)/L_w	15.8%	15.2%

Energy Dissipation:

The total energy dissipated by Specimen 6 through the displacement level at which failure occurred in both loading directions was 508 kip-in.

4.10 Summary

This chapter presented results from tests performed on eight concrete masonry shear walls including test observations, load-displacement measurements, components of displacement and drifts, curvature measurements, displacement and curvature ductility, height of plastic and equivalent plastic hinge length, and energy dissipation. Photos of each specimen at the end of testing, the onset of toe crushing, the load-displacement hysteresis curves, and curvature along wall height were provided. Test observations, components of wall drift, displacement and curvature ductility, the height of plasticity, and the equivalent plastic hinge lengths were tabulated for each specimen.

CHAPTER 5

ANALYSES AND COMPARISONS OF WALL PERFORMANCE

5.1 Introduction

This chapter evaluates the effects that key design and wall parameters have on the performance of the reinforced masonry shear walls as presented in the preceding chapters. Performance is evaluated with respect to predicted load capacities, drift, displacement ductility, height of plasticity, equivalent plastic hinge length, and energy dissipation. The effects of lap splices in the vertical reinforcement in the plastic-hinge zone of shear walls on wall performance are also evaluated. Finally, wall performances obtained in this study are compared to previous studies.

5.2 Theoretical Predictions

The ratios of average experimental-to-predicted capacities for the peak lateral load and their associated capacities are given in Table 5.1. The XTRACT analysis, which produces moment-curvature results for a monotonic push test, typically underestimated the lateral capacity by about 10%. However, the XTRACT analysis slightly overestimated the lateral capacity for the specimens with zero axial stress. On average, theoretical predictions based on the MSJC Code underestimated the lateral capacity by about 23% for all axial load levels. The XTRACT results were less conservative than those based on the MSJC Code because strain hardening of the vertical reinforcement is accounted for in XTRACT. In an earlier study, Vaughan (2010) reported that the predicted load capacities underestimated experimental capacities by about 7%.

Table 5.1 Comparison of Predicted and Experimental Capacities

Specimen	Aspect Ratio	$P/(f'_m A_g)$	Predicted Capacity (kips)		Average Experimental Capacity (kips)	V_{exp}/V_{MSJC}	V_{exp}/V_{XTRACT}
			MSJC 2008[a]	XTRACT			
1A[b]	2.00	0.0625	34	38.1	41.1	1.21	1.08
1B	2.00	0.0625	34	38.1	45.1	1.33	1.19
2A[b]	2.00	0.125	30	31.6	37.3	1.24	1.18
2B	2.00	0.125	30	31.6	37.8	1.26	1.20
3	1.00	0	49	59.7	59.4	1.21	0.99
4	1.00	0.0625	81	88.2	98.9	1.22	1.12
5	0.78	0	63	76.7	74.4	1.18	0.97
6	0.78	0.0625	105	113	123	1.17	1.08

[a]Compression reinforcement was considered in strength calculations
[b]No lap splice in vertical reinforcement

5.3 Wall Drifts

The 2008 MSJC Code defines failure in a reinforced concrete masonry shear wall when the masonry strain reaches a critical value of 0.0025. However, the test results in this study indicate that the critical masonry strain was attained several displacement levels prior to reaching wall failure, defined in this study as a 20% load degradation from the peak lateral load. The average total wall drifts for each specimen are given in Table 5.2 at the three limit states of critical masonry strain, peak lateral load, and failure. The ratios of average total wall drifts at peak load to those at critical masonry strain and the ratios of drifts at failure to those at critical masonry strain are provided. All specimens experienced average total drift levels at the peak and failure limit states that were significantly higher than those at the code-specified failure of critical masonry strain. This indicates that much larger drift capacities can be achieved at actual wall failure than is implied by the MSJC Code.

Specimen 4 was the only wall that experienced a total drift less than 1.0% at failure, which resulted in the lowest ratio of total drift at failure to critical masonry strain. Total drift at the critical masonry strain limit state ranged from 0.2% to 0.6%, with the larger drifts attained in

the walls with aspect ratios of 2.0. The walls with an aspect ratio of 2.0 also attained larger total drifts at the limit states of peak lateral load and wall failure, with drifts ranging from 0.9% to 2.8% at failure. Eikanas (2003) reported drifts from 1.4% to 6.0% at failure and Snook (2005) reported drifts from 2.0% to 3.2% at failure. The lower range of drifts in this study is likely due to the larger axial loads that were applied during testing.

Table 5.2 Total Wall Drift at Three Limit States

Specimen	Aspect Ratio	P/ ($f'_m A_g$)	Vertical Reinf.	Total Drift @			Peak/ ε_{mu}	Failure/ ε_{mu}
				ε_{mu}	Peak Load	Failure		
1A[a]	2.00	0.0625	#6 @ 8in.	0.5%	1.1%	2.8%	2.3	5.7
1B	2.00	0.0625	#6 @ 8in.	0.4%	1.5%	2.1%	3.5	5.0
2A[a]	2.00	0.125	#4 @ 8in.	0.6%	0.8%	2.3%	1.4	4.0
2B	2.00	0.125	#4 @ 8in.	0.5%	0.9%	1.5%	1.9	3.2
3	1.00	0	#4 @ 8in.	0.2%	0.7%	1.0%	3.6	5.5
4	1.00	0.0625	#4 @ 8in.	0.4%	0.7%	0.9%	1.8	2.5
5	0.78	0	#4 @ 8in.	0.3%	0.9%	1.3%	3.1	4.3
6	0.78	0.0625	#4 @ 8in.	0.3%	0.7%	1.5%	2.3	4.6

[a]No lap splice in vertical reinforcement

Drift contributions from sliding, shear, and flexural deformations and total drift at wall failure are given in Table 5.3. All of the walls experienced contributions from flexural deformations greater than 67%, indicating that the responses in all of the walls were dominated by flexure. The walls with aspect ratios of 1.0 and 0.78 exhibited shear deformations between 10% and 16% of the total displacements. These were significantly higher than the walls with an aspect ratio of 2.0 which ranged from 4% to 7%. Specimen 3 exhibited the largest shear deformations at 16% of the total. Specimen 5, with a wall aspect ratio of 0.78 and no axial load, exhibited the largest sliding deformations at 21% of the total.

Table 5.3 Components of Wall Drifts at 20% Load Degradation

Specimen	Aspect Ratio	$P/(f'_m A_g)$	Vertical Reinf.	Total Drift (%)	Sliding (% Total)	Shear (% Total)	Flexure (% Total)
1A[a]	2.00	0.0625	#6 @ 8in.	2.8	5.3	7.4	87.3
1B	2.00	0.0625	#6 @ 8in.	2.1	1.6	5.3	93.1
2A[a]	2.00	0.125	#4 @ 8in.	2.3	0.0	4.9	95.3
2B	2.00	0.125	#4 @ 8in.	1.5	1.3	4.4	95.5
3	1.00	0	#4 @ 8in.	1.0	7.2	15.5	77.2
4	1.00	0.0625	#4 @ 8in.	0.9	2.1	11.9	86.0
5	0.78	0	#4 @ 8in.	1.3	20.8	11.5	67.6
6	0.78	0.0625	#4 @ 8in.	1.5	4.8	10.1	85.1

[a]No lap splice in vertical reinforcement

5.4 Displacement Ductility

The average yield displacement, ultimate displacement, and calculated displacement ductility for each wall are given in Table 5.4. The average yield displacements ranged from 0.11 in. to 0.41 in., with larger values attained in the specimens with an aspect ratio of 2.0. Walls with aspect ratios of 1.0 and 0.78 attained average ultimate displacements less than 1 in. Walls with an aspect ratio of 2.0 attained average ultimate displacements that ranged from 1.23 in. to 2.20 in. Displacement ductility varied with design and wall parameters and is discussed further in Section 5.7.

Table 5.4 Average Yield and Ultimate Displacements, & Displacement Ductility

Specimen	Aspect Ratio	$P/(f'_m A_g)$	Vertical Reinf.	Yield Displacement, Δ_y (in.)	Ultimate Displacement, Δ_u (in.)	Displacement Ductility, μ_Δ
1A[a]	2.00	0.0625	#6 @ 8in.	0.41	2.20	5.3
1B	2.00	0.0625	#6 @ 8in.	0.35	1.68	4.8
2A[a]	2.00	0.125	#4 @ 8in.	0.25	1.80	7.1
2B	2.00	0.125	#4 @ 8in.	0.25	1.23	5.0
3	1.00	0	#4 @ 8in.	0.15	0.75	4.9
4	1.00	0.0625	#4 @ 8in.	0.13	0.64	4.8
5	0.78	0	#4 @ 8in.	0.11	0.74	6.6
6	0.78	0.0625	#4 @ 8in.	0.12	0.82	7.1

[a]No lap splice in vertical reinforcement

5.5 Height of Plasticity and Equivalent Plastic Hinge Length

The ratios of average height of plasticity and equivalent plastic hinge length to the wall length, and their associated values, are given in Table 5.5. The height of plasticity typically exceeded the equivalent plastic hinge length. The ratio of height of plasticity to wall length ranged from 16% to 75%, and the ratio of equivalent plastic hinge length to wall length ranged from 15% to 64%. Eikanas (2003) reported ratios of plastic hinge length to wall length that ranged from 25% to 48%. Shedid (2010) reported ratios of height of plasticity to wall length that ranged from 43% to 78%, and ratios of equivalent plastic hinge length to wall length that ranged from 17% to 37%.

Table 5.5 Height of Plasticity and Equivalent Plastic Hinge Length and the Ratios to Wall Length

Specimen	Aspect Ratio	$P/(f'_m A_g)$	Vertical Reinf.	Height of Plasticity, L_p (in.)	Equivalent Plastic Hinge Length, l_p (in.)	L_p/L_w (%)	l_p/L_w (%)
1A[a]	2.00	0.0625	#6 @ 8in.	25.7	15.7	65	40
1B	2.00	0.0625	#6 @ 8in.	11.0	11.1	28	28
2A[a]	2.00	0.125	#4 @ 8in.	29.7	25.4	75	64
2B	2.00	0.125	#4 @ 8in.	25.9	10.2	65	26
3	1.00	0	#4 @ 8in.	29.1	16.3	41	23
4	1.00	0.0625	#4 @ 8in.	14.9	12.4	21	17
5	0.78	0	#4 @ 8in.	29.3	21.6	41	30
6	0.78	0.0625	#4 @ 8in.	11.3	10.9	16	15

[a]No lap splice in vertical reinforcement

5.6 Energy Dissipation

The total energy dissipated by each wall through the displacement level at which failure occurred in both loading directions is given in Table 5.6. The total energy ranged from 110 kip-in. to 529 kip-in., with the largest energy dissipated in Specimen 1A and the least in Specimen 3. Specimen 1A attained the largest ultimate displacement at failure of 2.20 in., which is likely what caused the large total energy. Specimen 6, which attained the largest ultimate displacement

and loads compared to the walls with aspect ratios of 1.0 and 0.78, dissipated the most energy between these four specimens.

Table 5.6 Total Energy Dissipation

Specimen	Aspect Ratio	$P/(f'_m A_g)$	Vertical Reinforcement	Total Energy Dissipation (kip-in.)
1A[a]	2.00	0.0625	#6 @ 8in.	529
1B	2.00	0.0625	#6 @ 8in.	356
2A[a]	2.00	0.125	#4 @ 8in.	363
2B	2.00	0.125	#4 @ 8in.	155
3	1.00	0	#4 @ 8in.	110
4	1.00	0.0625	#4 @ 8in.	195
5	0.78	0	#4 @ 8in.	199
6	0.78	0.0625	#4 @ 8in.	508

[a]No lap splice in vertical reinforcement

5.7 Effects of Key Parameters

Key parameters and their effects on wall performance are discussed in Sections 5.7.1 to 5.7.4.

5.7.1 Aspect Ratios

The effects of aspect ratio on wall performance were evaluated through testing Specimens 3, 4, 5, and 6. The relevant parameters for these four specimens are given in Table 5.7. All of these specimens contained lap splices.

Table 5.7 Evaluation of Aspect Ratios

Specimen	Vertical Reinforcement	Axial Compressive Stress (psi)	Aspect Ratio
3	#4 @ 8 in. (spliced)	0	1.0
5			0.78
4		156	1.0
6			0.78

Figure 5.1 gives the load-displacement envelopes for Specimens 3, 4, 5, and 6. These plots illustrate that Specimens 5 and 6 exhibited greater initial stiffness than did the comparable

Specimens 3 and 4. Specimen 5 attained less displacement at failure than Specimen 3 for the pull direction, but more in the push direction. This was also observed in Specimens 6 and 4. On average, the total wall drift decreases with an increase in aspect ratio at the peak-load and failure limit states (Table 5.2). This was likely due to the larger sliding deformations that occurred in the walls with the lower aspect ratios presented in Table 5.3. The contributions from sliding deformations increased from 7.2% to 21% between Specimens 3 and 5, respectively. Specimen 4 exhibited sliding deformations at 2.1% of the total, while Specimen 6 exhibited 4.8% of the total. Studies by Eikanas (2003), Snook (2005), and Vaughan (2010) show similar trends of increasing drift capacity with increasing aspect ratios.

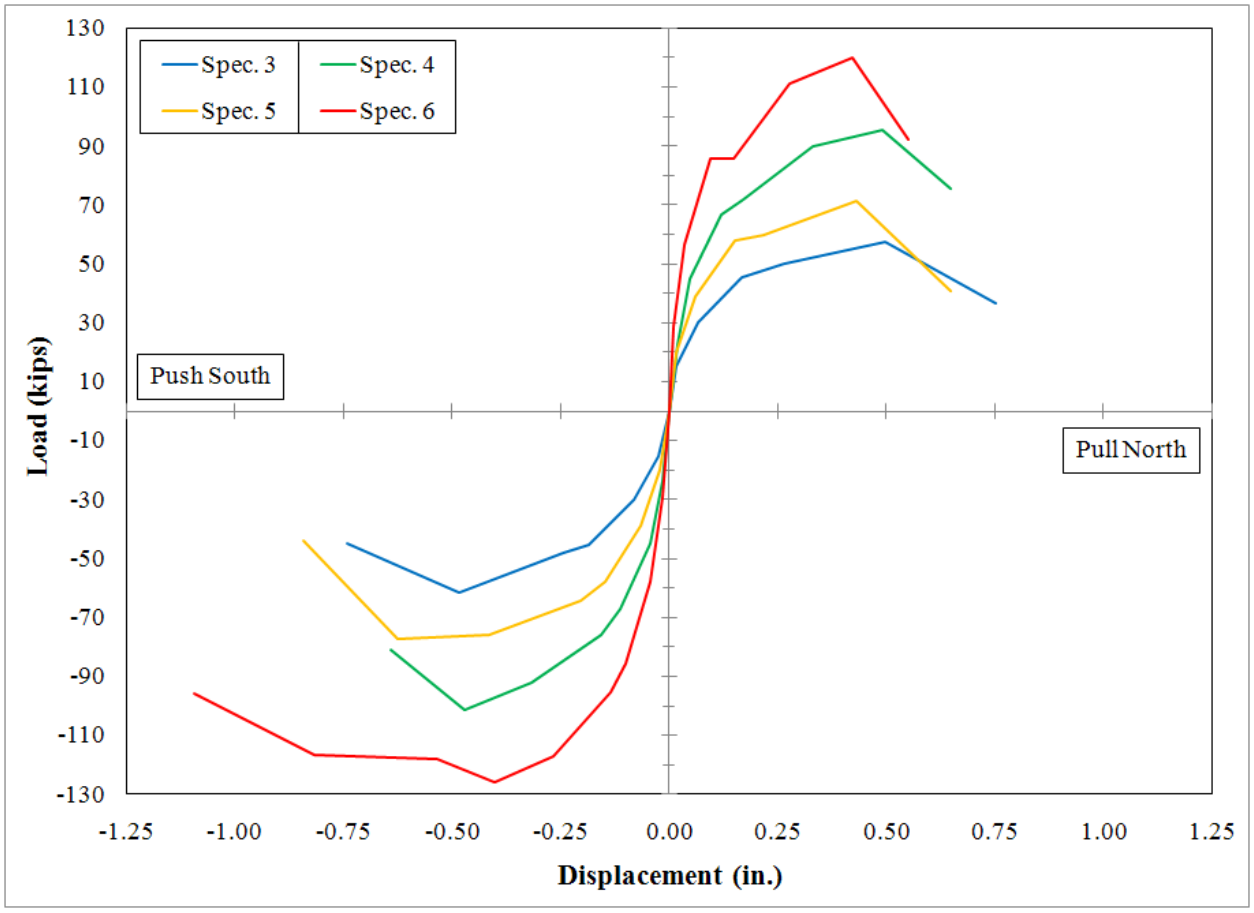

Figure 5.1 Load-Displacement Envelopes for Specimens 3, 4, 5, and 6

There is an increase in average yield displacements of the elastoplastic approximation from the load-displacement envelopes with increasing aspect ratio (Table 5.4); this is similar to findings by Shedid (2010). Larger yield displacements and smaller average ultimate displacements depicted in Figure 5.1 for the specimens with larger aspect ratios correlate to a reduction in displacement ductility. Specimen 4 had a displacement ductility of 4.8, while Specimen 6 had a displacement ductility of 7.1. Theoretical predictions by Paulay and Priestley (1992) and results from previous studies (Priestley, 1986; Vaughan, 2010) also found a reduction in displacement ductility with increasing aspect ratios. Eikanas (2003) concluded that the plastic hinge lengths decreased with increasing aspect ratios. Paulay and Priestley (1992) also found smaller plastic hinge lengths at larger aspect ratios. However, aspect ratios do not have a significant effect on the plastic hinging for the walls evaluated in this study (presented in Table 5.5) and also those in a study by Shedid (2010). Specimens 3 and 4 dissipated less energy than their respective counterparts that had the lower aspect ratios (Specimens 5 and 6).

5.7.2 Axial Compressive Stresses

Variations in the axial compressive stress were present in all eight specimens. The relevant parameters for all eight specimens are given in Table 5.8. All of these specimens incorporated lap splices expect for Specimens 1A and 2A.

Table 5.8 Evaluation of Axial Compressive Stresses

Specimen	Aspect Ratio	Axial Compressive Stress (psi)
1A	2.0	156
2A		313
1B	2.0	156
2B		313
3	1.0	0
4		156
5	0.78	0
6		156

The load-displacement envelopes for all eight specimens are given in Figure 5.2. The walls with the lower axial compressive stresses are generally less stiff than their counterparts. Except in the comparison of Specimens 5 and 6, the rest of the specimens exhibited higher displacements at failure for the walls with lower axial compressive stresses.

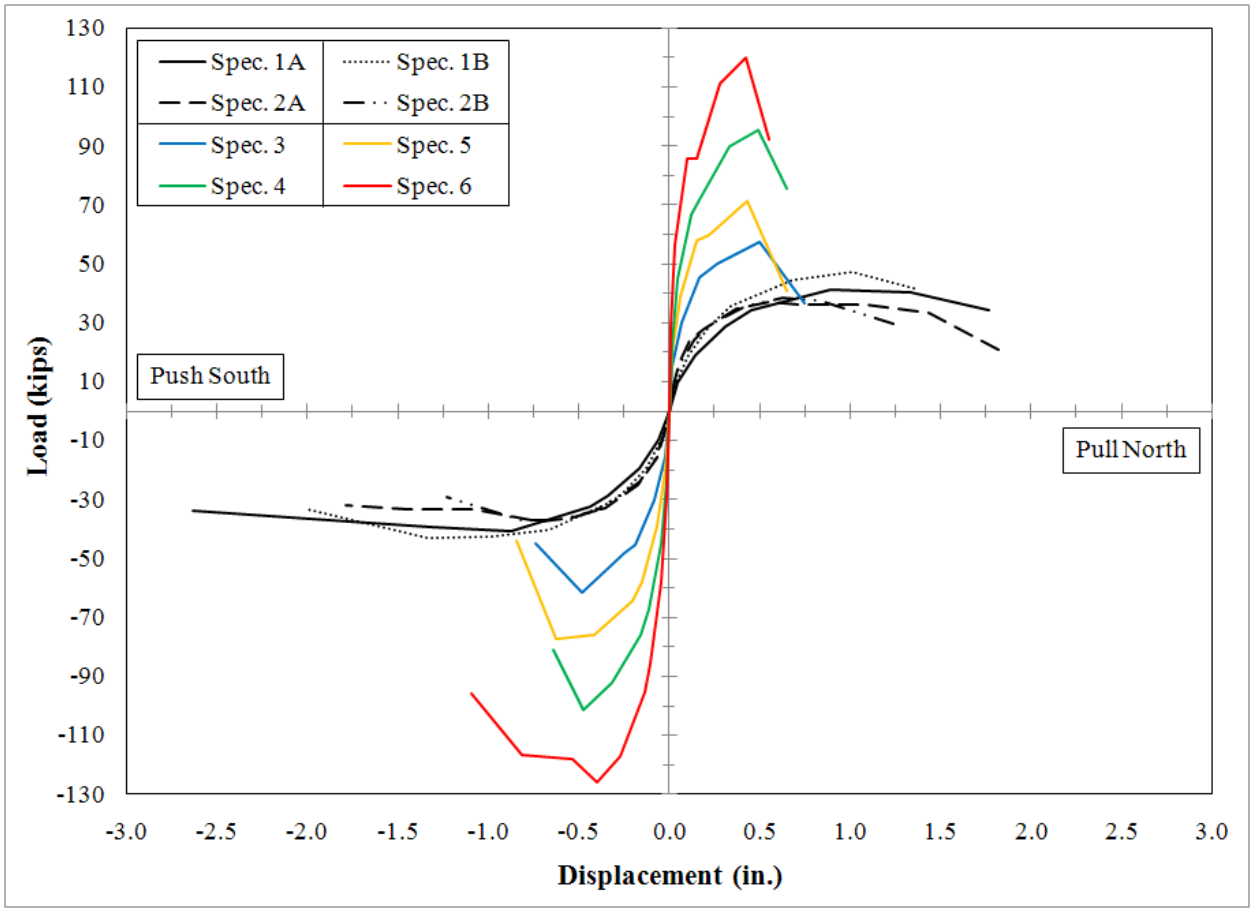

Figure 5.2 Load-Displacement Envelopes for All Specimens

Drift contributions from sliding and shear deformations are larger with lower axial loads, as shown in Table 5.3. Specimens 3 and 5 had the largest contributions from sliding and shear because they had no axial compressive stress to help resist these deformations. Vaughan (2010) concluded that the low levels of axial compressive stress that were evaluated in his study showed no significant effects on drift. However, the walls in this study experienced axial compressive stresses typically 1.6 times larger than the walls evaluated by Vaughan. Axial compressive

stresses have no evident effects on displacement ductility (Table 5.4). However, previous studies (Priestley, 1986; Shing, 1990; Shedid, 2008) reported a decrease in displacement ductility with increasing axial loads. The reason for this difference is likely due to the limited number of varying levels of axial load evaluated in this study. There is a consistent trend in Specimens 3, 4, 5, and 6 of an increase in the height of plasticities and equivalent plastic hinge lengths with decreasing axial compressive stresses (Table 5.5). However, this trend is contradicted in comparing results for Specimens 1A and 1B with lower axial loads to their respective counterparts of Specimens 2A and 2B. There are no consistent trends from the effects of axial compressive stress on average total drift and energy dissipation.

5.7.3 Reinforcement Ratios

The vertical reinforcement ratios varied between Specimens 1A, 1B, 2A, and 2B. The relevant parameters for these four specimens are given in Table 5.9. Specimens 1A and 2A contained no lap splices, and Specimen 1B and 2B contained 33-in. and 16-in. long splices, respectively.

Table 5.9 Evaluation of Reinforcement Ratios

Specimen	Aspect Ratio	Vertical Reinforcement Ratio
1A	2.0	0.0072
2A		0.0033
1B	2.0	0.0072
2B		0.0033

The four specimens were designed with the maximum allowed vertical reinforcement (ρ_{max}) with Specimens 1A and 1B equal to 107% of ρ_{max} and Specimens 2A and 2B equal to 183% of ρ_{max}. Figure 5.3 gives the load-displacement envelopes for Specimens 1A, 1B, 2A, and 2B. The walls with the larger vertical reinforcement ratios are initially less stiff, but they

generally exhibit larger loads and displacements at failure. Specimens 1A and 1B also had larger peak capacities than their respective counterparts Specimens 2A and 2B.

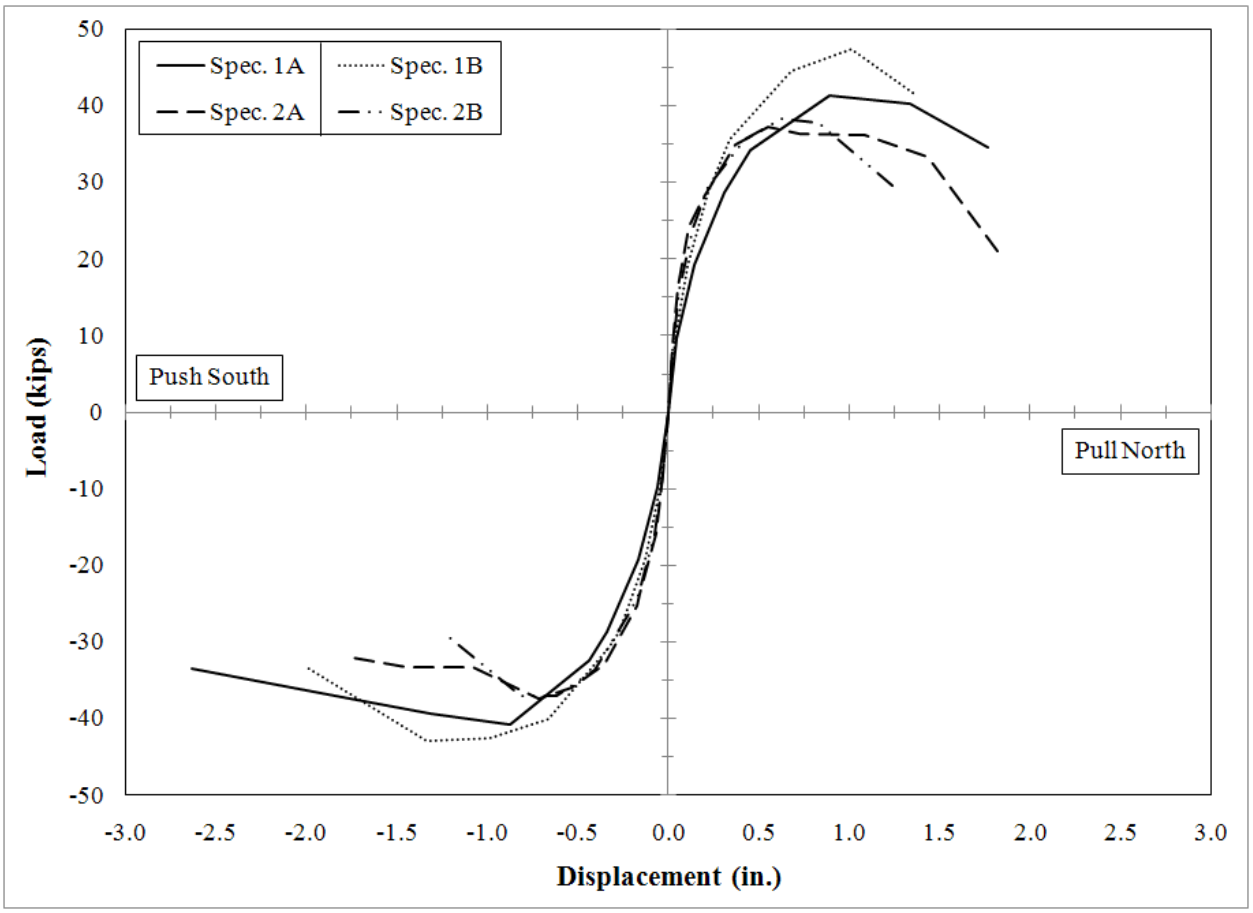

Figure 5.3 Load-Displacement Envelopes for Specimens 1A, 1B, 2A, and 2B

The drift contributions from flexural deformations in Specimen 1A were less than Specimen 2A because of the larger contributions from sliding and shear deformations occurring in Specimen 1A (see Table 5.3). This trend is also observed in Specimens 1B and 2B. Larger yield displacements of the elastoplastic approximation from the load-displacement envelopes are determined in walls with larger vertical reinforcement ratios (Table 5.4). Shedid (2008) found a similar trend. Although the increased vertical reinforcement ratio from Specimen 1A exhibited larger yield and ultimate displacements than Specimen 2A, the displacement ductility is reduced with increasing vertical reinforcement ratios. This also occurred between Specimens 1B and 2B.

Previous studies by Vaughan (2010) and Shedid (2008) also found a similar trend. On average, larger vertical reinforcement ratios reduce the height of plasticity and equivalent plastic hinge length; this trend corresponds to that obtained in a previous study by Shedid (2010). Reinforcement ratios have no significant effects on energy dissipation (see Table 5.6).

5.7.4 Lap Splices

The effects of lap splices in the vertical reinforcement were evaluated in Specimens 1A and 2A, which had no splices, and Specimens 1B and 2B, which contained 33-in. and 16-in. long splices, respectively. The load-displacement envelopes of Specimens 1A, 1B, 2A, and 2B are presented in Figure 5.3. On average, the spliced Specimens 1B and 2B were stiffer than their non-spliced counterparts (Specimens 1A and 2A). Specimen 1B exhibited higher load capacity, but lower displacements at failure than Specimen 1A. Specimens 2A and 2B had similar load capacities, but Specimen 2A experienced an ultimate displacement of 1.80 in. at failure compared to 1.23 in. in Specimen 2B. The larger ultimate displacements in the non-spliced specimens resulted in an average increase of 26% in displacement ductility compared to the spliced specimens as presented in Table 5.4. Specimen 1A had larger contributions from sliding and shear deformations than did Specimen 1B (Table 5.3). Specimens 2A and 2B had similar contributions from flexural deformations.

Specimen 1B exhibited a height of plasticity and equivalent plastic hinge length that were significantly less than those for Specimen 1A (see Table 5.5). Referencing Figure 4.16, there was essentially no curvature in Specimen 1B above the instrumentation point 12 in. above the footing due to increased stiffness from the lap splice. This was illustrated by concentrated separation of the mortar joint at the wall base of Specimen 1B rather than a gradual decrease of separation over the wall height, as observed in the non-spliced Specimen 1A (Figure 5.4). The rapid decline

of curvature between the wall base and the 12-in. height resulted in a significantly lower height of plasticity. This observation occurred at the instrumentation point 12 in. above the footing for the other spliced walls because of the shorter, 16-in. lap splices. The equivalent plastic hinge lengths for the spliced Specimens 1B and 2B were lower than for their counterparts Specimens 1A and 2A. Specimens 1B and 2B had ultimate displacements that were typically 28% less than Specimens 1A and 2A due to the lap splices; this resulted in lower values for the equivalent plastic hinge lengths.

Figure 5.4 Separation of Mortar Joints in Specimens 1A (left) and 1B (right) at Respective Lateral Displacements of 0.88 in. and 1.0 in.

The lap splices in Specimens 1B and 2B resulted in less energy dissipation than in Specimens 1A and 2A (Table 5.6). This is illustrated by narrower hysteresis curves following toe crushing (see Figure 4.13 and Figure 4.25). Spliced Specimen 2B exhibited early onset of toe crushing following the peak lateral load compared to the non-spliced Specimen 2A. The lap

splices in Specimens 1B and 2B caused a rapid load degradation following toe crushing when compared to Specimens 1A and 2B, respectively.

Overall, lap splices of walls with vertical reinforcement perform more poorly than walls without lap splices. Priestley (1986) concluded that lap splices should be avoided in the plastic hinge zone of masonry shear walls. However, this would cause some difficulties with the construction of masonry structures. It is recommended that the effects of lap splices be further evaluated considering additional design and wall parameters beyond those considered in this study.

5.8 Summary and Conclusions

This chapter evaluated the effects that design and wall parameters, including aspect ratio, axial compressive stress, reinforcement ratios, and lap splices, have on the performance of concrete masonry shear walls under in-plane loading. Performance was evaluated with respect to theoretical predictions, drift, displacement ductility, height of plasticity, equivalent plastic hinge length, and energy dissipation. All walls experienced flexural failure mechanisms and on average exceeded their anticipated lateral load capacity for both the MSJC Code and XTRACT analysis. However, the XTRACT analysis slightly overestimated the lateral capacity for the walls with zero axial stress. The predicted capacities from the XTRACT program were less conservative than those obtained using the MSJC Code because the program considers strain hardening in the vertical reinforcement.

Lower aspect ratios result in increased sliding deformations and displacement ductilities. Increased axial compressive stresses correspond to decreased contributions from sliding and shear deformations. The only significant conclusion in this study that did not coincide with previous research was that axial compressive stresses have no effect on displacement ductility;

this was likely due to the limited number of varying levels of axial load used in this study. Larger drift capacities can be achieved at actual wall failure than is implied by the MSJC Code, even for walls that exceeded the maximum amount of permitted vertical reinforcement. Larger vertical reinforcement ratios cause a reduction in the displacement ductility, height of plasticity, and equivalent plastic hinge length. The specimens with lap splices experienced a reduction in wall performance in comparison to the non-spliced specimens.

CHAPTER 6

SUMMARY, CONCLUSIONS AND FUTURE RESEARCH

6.1 Summary

This research was conducted in collaboration with researchers from the University of California at San Diego and the University of Texas at Austin and was funded by the National Institute of Standards and Technology (NIST). The objective of the broader project is to quantify the seismic performance of reinforced masonry shear-wall structures for use in developing improved design procedures. The research presented in this thesis will increase the current database for reinforced masonry shear walls to better understand their seismic performance.

The primary objective of this study is to evaluate the effects of key design and wall parameters on the performance of concrete masonry shear walls under in-plane loading. A secondary objective is to evaluate the effects that splicing of the vertical reinforcement has on wall performance. Eight, fully grouted, cantilever concrete masonry shear walls were constructed in accordance with the 2008 MSJC *Building Code Requirements for Masonry Structures*. The walls were subjected to cyclic, in-plane lateral loads that were applied at the top of the walls under a constant axial stress. Wall aspect ratios of 0.78, 1.0, and 2.0 were included along with a variation in axial compressive stresses of 0, 156, and 313 psi to evaluate their effects. Two pairs of walls with varying vertical reinforcement ratios were used to evaluate the effects of lap splices in the vertical reinforcement.

Wall response was monitored using a load cell located within a hydraulic actuator, string displacement potentiometers, and strain gages. The measurements were converted into load, displacements, drifts, curvature, ductility, plastic hinging, and energy dissipation. Visual observations of wall behavior were made during testing. Lateral loads were plotted against in-

plane lateral displacements to develop hysteresis curves. The amount of energy dissipated from each wall was determined based on the area under the hysteresis curves. Components of displacements and drifts from shear, sliding, and flexural deformations were separated from total in-plane displacements. Wall heights were plotted against curvatures and used to establish curvature ductilities and height of plasticity zones. Displacement ductilities and equivalent plastic hinge lengths were calculated based on the test results.

The test results were analyzed to evaluate the effects that key design and wall parameters, including aspect ratio, axial compressive stress, and amounts of reinforcement, have on wall performance. Theoretical predictions of wall load capacities were compared with experimental results. Total wall drift and components of drift from shear, sliding, and flexural deformations were examined. Displacement ductility, plastic hinging, and energy dissipation were evaluated. The effects of lap splices in the vertical reinforcement in the plastic-hinge zone of masonry shear walls were also evaluated. Results of the wall performance obtained in this study were compared to previous studies.

6.2 Conclusions

Results from tests of the eight concrete masonry shear walls in this study generally followed expected trends from previous studies. Predicted lateral load capacities were obtained from the 2008 MSJC Code and a cross-sectional analysis program, XTRACT. The XTRACT analysis typically underestimated the lateral load capacity by 10%. Predicted lateral capacities based on the MSJC Code underestimated the lateral load capacity by about 23%. The XTRACT results were less conservative than those based on the MSCJ Code because strain hardening of the vertical reinforcement is accounted for in XTRACT. All eight walls exhibited a flexural response with contributions from flexural deformations greater than 67%. There are no

consistent trends from the effects of axial compressive stresses and reinforcement ratios on energy dissipation at failure.

Effects of Aspect Ratios: Walls with lower aspect ratios exhibit greater initial stiffness than walls with larger aspect ratios. Walls with larger aspect ratios exhibit larger deformations from sliding. Larger aspect ratios also increase yield displacements of the elastoplastic approximation, but decrease the ultimate displacements at failure. These comparisons correlate to a reduction in the displacement ductility for the specimens with larger aspect ratios. Although the plastic hinge length was found to be dependent on aspect ratios in previous studies, this study showed no significant effects. Walls with larger aspect ratios generally dissipate less energy than walls with lower aspect ratios.

Effects of Axial Compressive Stresses: Walls with larger axial loads are generally stiffer than their comparable walls that have lower axial loads. Nearly all of the specimens with lower axial loads attained larger displacements at failure than their counterparts. Walls with lower axial loads exhibit larger contributions from sliding and shear deformations. The specimens with no axial loads experienced the largest contributions from sliding and shear deformations because there was no axial load to help resist them. Axial compressive stresses have no evident effects on displacement ductility. This does not correspond with results from previous studies, perhaps because of the limited number of varying levels of axial load evaluated in this study. There are no consistent trends in relation to axial compressive stress and plastic hinging.

Effects of Reinforcement Ratios: Walls with larger vertical reinforcement ratios are initially less stiff than their counterparts, but generally exhibit larger loads and displacements at failure. At actual wall failure, walls with the maximum allowed vertical reinforcement exhibit total drift levels significantly higher than the drift associated with the code-specified failure. This

indicates that much larger drift capacities can be achieved at actual wall failure than is implied by the MSJC Code, even for the walls with reinforcement that exceeds the maximum amount permitted by the Code. Walls with larger vertical reinforcement ratios experience larger contributions from sliding and shear. Displacement ductility is reduced in walls with larger vertical reinforcement ratios. On average, larger vertical reinforcement ratios reduce the height of plasticity and equivalent plastic hinge length.

Effects of Lap Splices: Walls with lap splices in the vertical reinforcement exhibit a stiffer response than walls with no splices. Larger displacements at failure were attained in the walls with no splices, which also increased the displacement ductility compared to the spliced walls. The most significant effect from the lap splices on wall performance was wall curvature, which was used to interpret curvature ductility, height of plasticity, and equivalent plastic hinge length. There was essentially no measured curvature in the spliced walls at the instrumentation point 12 in. above the footing due to increased stiffness. Most of the mortar joint separation occurred at the wall base with no gradual decrease in separation over the wall height of the spliced walls as was observed in the non-spliced walls. This causes a reduction in the wall curvature and in effect reduces the height of plasticity and equivalent plastic hinge length of spliced walls compared to non-spliced walls. Walls with no splices exhibit more energy dissipation than spliced walls. Less energy dissipation is illustrated by more pinched hysteresis curves in the specimens with splices. Spliced walls also experience rapid load degradation following toe crushing. Walls with lap splices experience a reduction in wall performance.

6.3 Future Research

The conclusions made in this thesis are constrained by the number of specimens evaluated in this study. Additional research is recommended to expand the variation of design

parameters such as wall aspect ratio, axial compressive stress, and reinforcement ratios and compare them with similar parameters of wall performance evaluated in this study. Such work is ongoing. The effect of lap splices on the performance of concrete masonry shear walls should be further evaluated considering additional design and wall parameters. Future research is currently in progress to compare the walls reported in this study with other parameters such as confining boundary elements and concentrated reinforcement at wall ends. The results from the walls in this study contribute to a larger on-going study developing an innovative performance-based design methodology for masonry structures.

REFERENCES

Eikanas, I.K. (2003). "Behavior of Concrete Masonry Shear Walls with Varying Aspect Ratio and Flexural Reinforcement." M.S. Thesis, Department of Civil and Environmental Engineering, Washington State University, Pullman, WA.

Massone, L. M. and Wallace, J.W. (2004). "Load-Deformation Responses of Slender Reinforced Concrete Walls." *ACI Structural Journal*, Vol. 101, No.1, pp. 103-113.

Paulay, T. and Priestley, M.J.N. (1992). Seismic Design of Reinforced Concrete and Masonry Buildings. New York: Wiley-Interscience.

Priestley, M.J.N. (1986). "Seismic Design of Concrete Masonry Shearwalls." *ACI Structural Journal*, Vol. 83, No. 1, pp. 58-68.

Priestley, M.J.N. (1993). "Myths and Fallacies in Earthquake Engineering – Conflicts Between Design and Reality." *Bulletin NZNSEE*, Vol. 26, Iss. 3, pp 329-341.

Priestley, M.J.N.; Calvi, G.M.; and Kowalsky, M.J. (2007). Displacement-Based Seismic Design of Structure. (1st ed.). Pavia, Italy: IUSS Press..

Shedid, M.T.; Drysdale, R.G.; and El-Dakhakhni, W.W. (2008). "Behavior of Fully Grouted Reinforced Concrete Masonry Shear Walls Failing in Flexure: Experimental Results." *Journal of Structural Engineering*, Vol. 134, No. 11, pp. 1754-1767.

Shedid, M.T.; Drysdale, R.G.; and El-Dakhakhni, W.W. (2010). "Seismic Performance Parameters for Reinforced Concrete-Block Shear Wall Construction." *Journal of Performance of Contructed Facilities*, Vol. 24, No. 1, pp. 4-18.

Shing, P.B.; Schuller, M.; and Hoskere, V.S. (1990). "In-Plane Resistance of Reinforced Masonry Shear Walls." *Journal of Structural Engineering*, Vol. 116, No. 3, pp. 619-640.

Shing, P.B.; Schuller, M.; Hoskere, V.S.; and Carter, E. (1990). "Flexural and Shear Response of Reinforced Masonry Walls." *ACI Structural Journal*, Vol. 87, No. 6, pp. 646-656.

Snook, M.K. (2005). "Effects of Confinement Reinforcement on the Performance of Masonry Shear Walls." M.S. Thesis, Department of Civil and Environmental Engineering, Washington State University, Pullman, WA.

Vaughan, T.P. (2010). "Evaluation of Masonry Wall Performance Under Cyclic Loading." M.S. Thesis, Department of Civil and Environmental Engineering, Washington State University, Pullman, WA.

Voon, K.C. and Ingham, J.M. (2006). "Experimental In-Plane Shear Strength Investigation of Reinforced Concrete Masonry Walls." *Journal of Structural Engineering*, Vol. 132, No. 3, pp. 400-408.